CRASHWORTHINESS OF VEHICLE-TO-POLE COLLISIONS USING A HYBRID III 3-YEAR-OLD CHILD DUMMY

by

VID KRZNARIC

Bachelor of Engineering, Ryerson University

Toronto, Canada

October 2003

A thesis

Presented to Ryerson University

In partial fulfillment of the

Requirements for the degree of

Master of Applied Science

In the Program of Civil Engineering

Toronto, Ontario, Canada, 2006

AUTHOR'S DECLARATION

I herby declare that I am the sole author of this thesis.

I authorize Ryerson University to lend this thesis to other institutions or individuals for the purpose of scholarly research.

Vid Krznaric

I further authorize Ryerson University to reproduce this thesis by photocopying or by other means, in total or in part, at the request of other institutions or individuals for the purpose of scholarly research.

Vid Krznaric

ABSTRACT

Title: Crashworthiness of vehicle-to-pole collisions using a Hybrid III 3-year-old child dummy

Author: Vid Krznaric, B.Eng., Civil Engineering, Ryerson University, Canada, October 2003

Program: Master of Applied Science, In the Program of Civil Engineering, Ryerson University Canada, 2006

To date, statistics indicate that motor vehicle crashes are one of the leading causes of death and injury for children despite improved crashworthiness of vehicles and child restraint systems, since children are at risk for devastating head and neck injuries due to their fragile physiology. Thus, this thesis focused on minimizing child injuries experienced during frontal vehicle-to-pole collisions by improving on the safety and energy absorption of existing traffic pole structures. A finite element computer model, using LS-DYNA software, was used to simulate crash events in order to determine the influence of pole structural and material characteristics on the injury parameters of a 3-year-old child dummy occupant. It was concluded that the anchored base support, and the embedded pole in soil systems provide desirable crashworthy results. In addition, it is recommended to mandate traffic protection devices in all areas with poor energy absorbing characteristics that resemble non-deformable objects.

ACKNOWLEDGEMENTS

My profound thanks goes to my supervisors, Dr. Khaled Sennah and Dr. Michael Chapman, for providing me with all the support and guidance I needed to effectively complete my research objectives. My sincere thanks and gratitude goes out to Dr. William Altenhof from the University of Windsor for providing me with the guidance and expertise to effectively use the LS-DYNA software, along with providing the child dummy model for this research.

I would also like to offer my sincere gratitude for the financial support provided by the Canadian Network of Centers of Excellence of the 21st Century Automobile, NCE Auto 21, and the Transport Canada. I would like to offer my special thanks to Ahmed Elmarakbi for helping me develop the finite element models used in this study and for his timely advice. In addition, I would like to acknowledge the research assistantship received from Dr. Sennah's NCE AUTO 21 funding, Ryerson Post-Graduate Scholarship, and all the staff and faculty members from the civil engineering department who directly and indirectly helped me towards the completion of my thesis.

Lastly I would like to acknowledge all the help and support provided by my family, and especially all the help and assistance given to me from my brother.

TABLE OF CONTENTS

LIST OF TABLES

LIST OF FIGURES

LIST OF ACRONYMS

AIS	Abbreviated Injury Scale
CHBDC	Canadian Highway Bridge Design Code
CREST	Child Restrain System for Cars
CRS	Child Restraint Systems
EU	European Union
FMVSS	Federal Motor Vehicle Safety Standards and Regulations
HIC	Head Injury Criteria
FMVSS	Federal Motor Vehicle Safety Standards and Regulations
LS-DYNA	Livermore Systems – Dynamic Analysis
LSTC	Livermore Software Technology Corporation of California
NCHRP	National Cooperative Highway Research Program
NHTSA	National Highway Safety Administration
NTBRC	National Transportation Biomechanics Research Center
PRV	Protection Reference Values
SAE	Society of Automotive Engineers
SMT	Standards, Measurements and Testing Program
UMTRI	University of Michigan Transportation Research Institute

LIST OF ABBREVIATIONS

C.A. -'X'	Chest Acceleration 'X' (g)
C.A. -'Z'	Chest Acceleration 'Z' (g)
H.A.- 'X'	Head Acceleration 'X' (g)
H.A. -'Z'	Head Acceleration 'Z' (g)
HIC 15	Head Injury Criteria 15 ms
HIC 36	Head Injury Criteria 36 ms
M.I.E	Maximum Internal Energy (kJ)
R.L.N.F	Resultant Lower Neck Force (N)
R.L.N.M.	Resultant Lower Neck Moment (N·m)
R.P.F.S	Rigid Pole Fixed Support
R.U.N.F	Resultant Upper Neck Force (N)
R.U.N.M	Resultant Upper Neck Moment (N·m)
T.0.V.	Time of 0 Velocity (ms)
T.M.H.X.	Time of Max Head Acceleration 'X' (ms)

CHAPTER 1

INTRODUCTION

1.1 General

In 2000, Sachs and Tombrello [1] determined that each year in the United States, 1,400 children under the age of 14 are killed in vehicle collisions and over 280,000 are injured. In March of 2002, the U.S. National Centre for Statistics and Analysis reported that everyday in North America approximately 6 children between the ages of 0-14 years are killed and 797 are injured [2].

To date, statistics indicate that motor vehicle crashes are one of the leading causes of death and injury for children, despite improved crashworthiness of vehicles and child restraint systems (CRS). In a study released by the University of Michigan Transportation Research Institute (UMTRI) [3], Weber determined that young children are at risk for devastating head and neck injuries due to their fragile physiology. To compare the differences in child deaths due to vehicle crashes, the number of child fatalities per capita was calculated for Sweden, Canada, and the United States for 2003 [4,5,6]. It was estimated that for every child that dies in Sweden, approximately 4.5 and 9.25 children die every year in Canada and the United States, respectively. Such statistics bring serious doubts into the current child safety system designs, which can partly be explained by the cervical vulnerability and the physical immaturity in younger

passengers. Studies indicate that during a collision, children develop injury patterns, which are not fully understood. These child injury patterns are different from those experienced by adults due to the changes in weight, height, and body proportions. Infants are particularly vulnerable because of a disproportionately large head, a higher centre of gravity, and a weaker neck structure resulting in relatively poor head support.

Currently, researchers have been investigating child safety from various perspectives in conjunction with new and improved CRS. The focus is shifting towards designing energy absorbing mechanisms, which will effectively absorb the kinetic energy during a vehicle collision and, thus, minimize the injury potential. To enhance the child safety, and effectively develop such energy absorbing mechanisms, researchers are currently developing advanced computer models that create real-life testing situations without harm to children and/or material resources.

1.2 Research Objectives

The main objective of the research focuses on minimizing child injuries experienced during frontal vehicle-to-barrier collision by improving the safety and energy absorption of existing roadside structures, particularly laminar traffic poles. By using a computer model, simulations will be modified to reconstruct the crash scenario in order to

effectively analyze and further understand the various parameters affecting injury development. The main goal of the research is to understand what can be done to prevent injury and/or lessen the severity during a vehicle collision involving a child occupant.

During a vehicle-to-pole collision, the motion (kinetic) energy plays a vital role influencing the injury experienced by the child occupants. The aim of the current research is to produce an energy-absorbing vehicle-to-pole system that will effectively reduce the kinetic energy absorbed by the vehicle, and in conjunction will stay upright minimizing any further injury and damage to the public and/or property.

The crashworthiness of a particular vehicle-to-pole scenario in terms of child safety will be determined using the guidelines provided through the National Highway Safety Administration (NHTSA) [7,8], and the European Commission through the Child Restrain System for Cars (CREST) project [9,10]. A 3-year-old child dummy will be incorporated into the computer analysis and the injury assessment will be performed on the child model by taking into consideration various parameters such as the head injury criterion, neck moments and forces, induced accelerations, energy absorption characteristics, and deflection profiles. Based on the results, improvements and recommendations to the existing safety aspects of traffic pole structures can be effectively evaluated and improved.

1.3 Arrangements of Contents of the Thesis

The following summary outlines the six chapters contained within this thesis.

- Chapter 1: The research objectives and the need for research are addressed.
- Chapter 2: Literature review pertaining to finite element research for crashworthiness and injury evaluation is presented.
- Chapter 3: Finite element modeling and its associated theory are explained.
- Chapter 4: Techniques used in the analyses and the extraction of occupant injury criteria in terms of crashworthiness are presented.
- Chapter 5: The results of finite element analysis including child dummy injury criteria is presented.
- Chapter 6: Lastly, based on the finite element modeling and analyses, the conclusions and recommendations for future research are presented in this chapter.

CHAPTER 2

LITERATURE REVIEW

2.1 Crashworthiness

The standard definition of crashworthiness is the resistance to the effects of a collision [11]. From an engineering perspective, crashworthiness is the ability of the vehicle to prevent occupant injuries in the event of an accident. The major principal governing crashworthiness is; given the injury mechanisms of an accident, and typically some measure of its severity, could the occupants of the vehicle have fared better than they did? Was some feature lacking in the vehicle, and/or the surrounding environment, which could have reduced the injury and should have been there based on some form of theory [12]?

A typical list of crashworthiness features include air bags, seat belts, crumple zones, side impact protection, interior padding and head rests. All of these items have been available since the early 1970's, yet some are still not found in vehicles currently driven on our roads, even though some are mandated by Federal Motor Vehicle Safety Standards and Regulations (FMVSS) to one degree or another [13]. Gradually, standards are being upgraded to include all of the items listed above as well as other features long known to be required for occupant safety.

Over the past decade researchers have been shifting their primary focus away from the standard definition of crashworthiness, which included the vehicle, and are now focusing more on the surrounding environments, which influence injury development during a vehicle collision with roadside objects such as traffic poles, jersey barriers, energy absorbing attenuators.

In the past researchers have used field-testing to study and improve on the aspects of crashworthiness during vehicle collision, however, the disadvantage of using such field tests is the associated costs per test. To overcome this disadvantage computer modeling, namely finite element analysis, is being increasingly used to perform crash simulations at a fraction of the cost. Currently, crashworthiness has seen its major advancements in North America and the European Union using computer simulations and finite element modeling.

2.2 Finite Element Modeling

LS-DYNA [14] software is used in this study as a general-purpose finite element code for analyzing the large deformation and dynamic response of structures. The main solution methodology is based on explicit time integration. LS-DYNA uses contact-impact algorithms that allow difficult contact problems to be easily treated. A variety of element formulations are available for each element type. Specialized capabilities for airbags, sensors, and seatbelts have tailored LS-DYNA for applications in the automotive

industry. LS-DYNA currently contains approximately two hundred material models and ten equations to cover a wide range of material behavior.

The history of LS-DYNA dates back to the 1960's, where initial research on highway vehicle impact simulations began, and resulted in limited versions of computer programs. The initial versions were not easy to use and because of computer hardware limitations of that period many simplifying assumptions were required. The number of elements that could be used in a model was very limited, as the vehicle was represented by lumped masses, and the interactions between the impacting structures were very approximate in form.

Extensive advances in computational power, and significant funding increases to the military, aerospace and automotive industries allowed for substantial improvements using finite element modeling. Of the commercially available finite element software, LS-DYNA is developed by Livermore Software Technology Corporation of California, and was created to perform finite-element impact analysis using explicit, geometric and material nonlinear codes for dynamic response. To date LS-DYNA is amongst the more popular non-linear explicit finite element codes used for studying crashworthiness and for modeling crash problems.

2.3 Past Research in Crashworthiness and Occupant Protection

The current research available to the public to date studying crashworthiness, namely vehicle-to-traffic pole simulations, is very limited. Most of the published research to date mainly focuses on finite element modeling to assess crashworthiness in terms of energy absorption without the use of actual crash test dummies. The main focus of the research was to design and analyze structures on the basis that material properties and geometrical shapes intended to absorb the impact energy. The safety regulations and the limiting criteria were analyzed using theoretical approaches to predict the safety of passengers. The researchers did not have validated dummy models that could be used for finite element modeling and were forced too use arbitrary points throughout the car to evaluate and correlate to occupant response and injury criteria.

Sennah et. al [16, 17, 18] have conducted significant finite element analysis into the investigation of the energy absorption characteristic for different traffic pole support types and conditions, including the anchored base support and embedded pole to soil support condition. Their research has provided valuable results and insights into the investigation of crashworthiness for traffic poles and their recommendations have provided the need for future research, including the research objectives contained within this thesis. The main shortfall their research lacked was the injury assessment in terms of actual dummy models that should be used in order to effectively assess the injury criteria during a particular crash scenario. The validated dummies at that time were not

available, and the researches were forced to use more direct theoretical methods to evaluate the effectiveness of each simulation considered. In terms of occupant injury assessment using dummy models, very few researchers to date have published analytical results involving human occupants, particularly involving children, because the current models were not validated with experimental verification and most were not available to the general public.

Turchi et. al [6] were one of the few researchers who offered meaningful insight into occupant crashworthiness using a hybrid 3-year-old child dummy. They performed simulations using finite elements and investigated the injury potential of children under a five-point child restraint system (CRS) by comparing and correlating their analytical findings to real experimental results. The main purpose of their research was to design an effective CRS system that would perform as well as the experimental model of the child and would effectively correlate to human injury predicament. The research compared the head, and chest accelerations to the experimental findings, in order to verify numerical observations, which were observed to offer reasonable correlation between the data that existed. Comparison of both qualitative and quantitative observations from the numerical simulations and experimental test has illustrated an acceptable correlation and has indicated that the numerical model can simulate the experimental sled test with an acceptable level of predictability. However, their research was geared from a mechanics perspective, and was aimed to design a child restraint system that would effectively perform as well as real life models, and did not include crashworthiness in terms of improvements to the designs of transportation infrastructure.

Based on the current research available today, the goal of the enclosed thesis was to combine the structural analysis in terms of crashworthiness and occupant safety, with respect to a finite element 3-year-old child dummy model, and to effectively correlate the child injury potential vs. a particular traffic pole support system design.

2.4 Traffic Poles

Currently in North America, traffic poles are offered in lengths from 2.5 to 12 m and are used because they accept a wide range of design configurations. These poles are available in many forms including wood, concrete and metal configurations. However, based on current research into crashworthiness involving poles, a number of utilities are being installed on metal poles due to their many advantages over wood or concrete poles.

Traffic poles in old cities are made of wood material, which is known to offer very little deformation during a vehicle collision, and is not considered effective in terms of crashworthiness. Hollow round concrete poles reinforced with pre-stressed wires or strands are also commonly used in both urban and rural areas. However, this type of pole structure is very brittle and often fails with very little impact force as shown in Figures 2.1, and 2.2 of this chapter. These types of materials can create serious damage to a crowded downtown area and can be a hazard and further inflict injury to surrounding pedestrians.

The ideal pole design should offer high-energy absorption characteristics and should deform properly so that it can offer the greatest amount of energy absorption, without failing and creating further damage to the surrounding environment. This desirable internal deformation helps to dissipate the vehicles kinetic energy involved during a collision, and minimizes the internal forces experienced by the vehicle's occupants. In addition, the ideal pole needs to be designed to the minimum yield strength of the material with an adequate factor of safety to withstand the dead loads of the structure as well as the specified wind loads, as outlined through the Canadian Highway Bridge Design Code [18]. Pole failure should only be designed into the system when the forces exceed the critical limits known to cause severe injury and/or a fatal collision. A good illustration of an improperly designed pole structure is illustrated in Figure 2.3. From this figure it is clearly evident that the pole structure deformed very little during the collision causing the majority of the impact energy to be dissipated within the vehicle, thus offering less chance of survival to the vehicles occupants. Such pole designs should be avoided at all costs, and a lot more research is required into transportation infrastructure to prevent such serious accidents, which could have been prevented if the structures were designed properly.

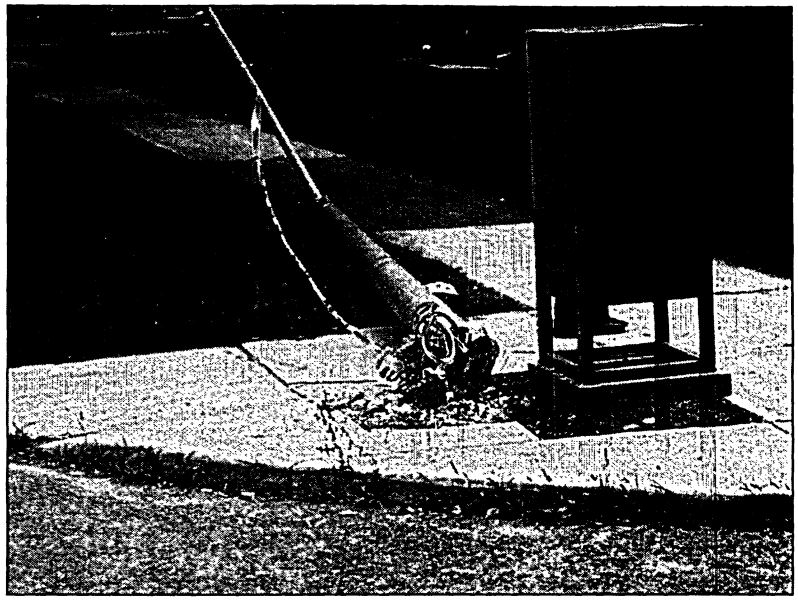

Figure 2.1 **View of a pre-stressed concrete light pole after a minor vehicle collision**

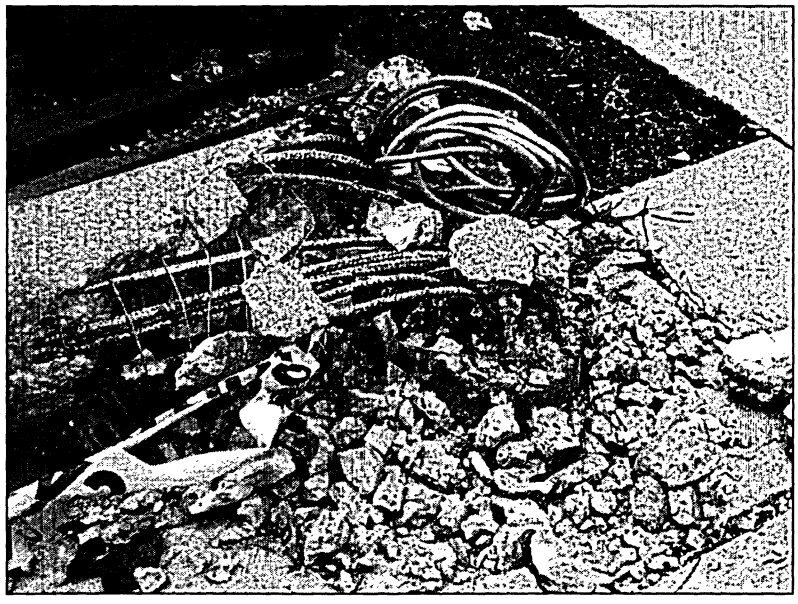

Figure 2.2 **Close up view a of pre-stressed concrete light pole after a brittle failure**

Figure 2.3 **Image of a severe vehicle collision with a traffic pole improperly designed**

2.5 Child Dummy Protection Reference Values

The main difference in the anatomy between children and adults is the proportion of the total mass in the head. At birth the head comprises of 30% of body weight while the adult head makes up only 6% of body weight. Lengthwise, an infants head is ¼ the total length, while an adults head is 1/7 the total height [8]. The skull structure in children is also notably different from adults. At birth, an infant's skull is flexible, and consists of six sections called fontanelles that eventually grow and fuse together [8]. The infant skull can deform more easily under load, which might make it less susceptible to fracture; however other mechanisms of injury may be possible. Thus, these features make the

rigid skull assumption used in adult dummies incorrect in terms of injury criteria used for a child dummy.

Similar to the head, the neck region also behaves in a different fashion compared to the adult. At birth the neck vertebrae consist of three different bones joined by cartilage. They typically grow together during the third year, however, the atlas C1 and the C2 do not finish developing until age 25 [20]. Atlas C1 and C2 are the first two vertebrae in the spinal cord from the head. In addition to the differences in cervical spine structure, the infant neck muscles are not well developed, and most children cannot hold up their heads until about three months. As the child's muscles begin to develop in the neck region, they have a relatively bigger head to support thus allowing for greater potential of neck injuries during vehicle collisions if not properly supported. Another injury found in children, which most likely results from the difference in neck structure, is spinal cord stretch injury [20]. Under impact, a child's flexible vertebral can displace more without fracture, but allow the spinal cord to stretch. For this reason, the children can have spinal cord injuries without vertebral damage, which is rarely found in adults. Another difference in neck injuries between adults and children is the point where most cervical spine fractures occur. About 60-70% of paediatric cervical fractures occur at C1 or C2, compared to about 16% of adult cervical spine fractures. This occurs because the natural neck pivot of children is at C2 or C3, while in adults it occurs near C6 (6^{th} vertebra from neck) [20].

Many more notable distinct differences exist for the child as compared to an adult, however it becomes quite clear that adult protection reference values cannot be scaled down proportionally for children because the two bodies act distinctively different in most regions of the body.

Thus, to effectively develop child protection reference values, mechanical properties of biological tissues, such as modulus of elasticity, ultimate strength, and percent elongation are useful in both determining the child dummy design characteristics and aiding in the scaling of different reference values. A review of injuries received by children in automotive accidents helps to show which dummy measurements may be most representative of the actual crash scenario. Currently, there is no single method or set of data standards set out clearly as the best choice for development of protection reference values because actual biomechanical data is insufficient and of limited applicability. Both biomechanical and accident reconstruction testing is needed to provide more information about the injury criteria and protection reference values (PRV).

To date two leading agencies exist who have devoted extensive research into the development of the child protection reference values, namely; the National Highway and Traffic Safety Administration, NHTSA, situated in North America, and the Crest Project funded through the European Community Under the Standards, Measurements and Testing (SMT) programme. Currently, the NHTSA has more extensive databases into the development of improved injury criteria, however, the European Union in terms of statistics has safer and improved crashworthy transportation infrastructure [21].

2.5.1 Child Dummy Protection Reference Values – NHTSA

The National Highway and Traffic Safety Administration (NHTSA) is North America's leading agency in terms of traffic safety and state of art injury criteria assessment. Many researchers from around the world have contributed to the current database of knowledge into the biomechanics involved during a vehicle collision for the NHTSA. The NHTSA has actively pursued research into the safety of automotive occupants for decades. Current issues and experimental results are presented every year at international conferences dedicated to biomechanics research.

During developing stages of the proposed injury criteria, the NHTSA's National Transportation Biomechanics Research Center (NTBRC) has drawn extensively from existing published research. Existing data from human cadavers, animal subjects, and to a limited degree live volunteers have been extensively analyzed during the process of developing the proposed injury criteria. In March of 2000, the NHTSA has published revised injury criteria for the assessment of advanced Automotive Restraint Systems, which will be used extensively in this thesis. The summary of the child dummy protection reference values is presented in Table 2.1 below [7, 8].

Table 2.1 NHTSA recommended child protection reference values [7, 8]

Injury Criteria	NHTSA 3YO – Child Protection Reference Value – Injury Criteria
Chest Acceleration 'X'	55 g's
Chest Acceleration 'Z'	55 g's
Upper Neck Force	2120 N
Lower Neck Force	2120 N
Upper Neck Moment	27 N·m
Lower Neck Moment	68 N·m
Head Injury Criteria – 15ms	570
Head Injury Criteria – 36ms	570

2.5.2 Child Dummy Protection Reference Values - The Crest Project

The Crest Project is funded through the European Community under the SMT programme. It consists of a group of manufacturers, university laboratories, and European research centres working together to improve on the existing child injury criteria and to provide effective child restraint systems on the market that are reliable, comfortable, and easy to use.

The European Crest Project was formed in1996, and incorporated the analysis of numerous types of injuries sustained in different kinds of accident scenarios that involves children varying in age from 0 to 12 years. Nearly 400 accident cases had been gathered by six European teams based in four countries (France, Italy, Germany, and United Kingdom). For laboratory reconstruction purposes, the accidents selected included a sufficient number of precise elements such as speed, type of impact, state of the vehicles after the accident, nature of the injuries, exact position of the children, etc. The data was

collected using a precise methodology designed to determine how injuries are related to the mechanics involved in a particular scenario.

Their initial findings indicated that restraint systems designed for young passengers which, on the basis of tests, should provide effective protection in 70% to 80% of accidents cases, only offer real protection in 30% to 50% of cases [9, 10]. The CREST team needed to make tests more reliable, particularly, by improving the reliability of the dummies used in the tests, as the lack of bio-fidelity of the child dummies, and insufficient biomechanical knowledge on injury mechanisms hampered effective designs in the past.

Through the analysis of accidents involving children, CREST revealed that CRS in compliance with current regulations give highly contrasted levels of protection in real world accidents [22]. Such a low effectiveness of child restraint systems is partly explained by the greater cervical vulnerability and morphological immaturity associated with child passengers. Unlike for adults, child impact tolerances or behaviours cannot be determined directly by experiments on human bodies. The main sources of data up to the creation of CREST come from child free-fall studies, aircraft field investigations, animal testing, scaling from adults and very few post mortem experiments on human subjects.

The method employed by CREST was to collect data from accident case investigations and to form constructed crash tests in order to determine the physical parameters such as forces, accelerations and deformations on the child occupants that correspond to the

various child injury mechanisms. Injury risk curves were established following studies into injuries of restrained children according to the body segment on which they occurred. Selections were performed according to the Abbreviated Injury Scale 3+ (AIS3+) from Table 2.2, meaning cases with Serious to Un-Survivable sustained injuries.

Table 2.2 Standard Abbreviated Injury Scale

AIS Score	Injury
1	Minor
2	Moderate
3	Serious
4	Severe
5	Critical
6	Un-survivable

For head, thorax and pelvis, the analysis was done directly by comparing AIS levels of injuries with measurements. For example, head accelerations or HIC, parameters were associated in relation with head AIS. For the neck, a more detailed analysis of injury mechanisms was made in order to associate the good physical parameters to each kind of injury. All results of reconstructions and sled tests were analyzed and used to construct injury risk curves. Since accident cases concern several ages, data were scaled to 3 years old, using geometrical and material failure factors.

The graphs for the level of Neck Injury in relation with Neck Moments (My) corrected for 3 years old were in refinement stages for the definition of injury risk curves, in

particular, cases with injury. Based on the findings provided through the CREST project for the limiting moments (My) in the neck region, CREST can only state that a large amount of cases without injury demonstrate My values under 30 N·m.

In conclusion, the CREST project offers an alternative approach to the more conventional NHTSA child protection reference values. Although, the results are currently in the refinement stages, nevertheless the initial findings will be taken into consideration during the analysis stages of this report. However, the NHTSA reference values will be used as a standard for child protection values throughout this thesis.

CHAPTER 3

FINITE ELEMENT MODELING

3.1 General

As described in the pervious chapter LS-DYNA version 970, revision number 5434a [14], is used in this study on a personal Intel Pentium (R), 1.80 GHz computer, with 1.00 GB of RAM. Originally, the 256 MB of RAM used was not enough to handle the complexity of the simulations considered in this study. A total of 69 different simulations were performed using the upgraded hardware. The total time to complete ranged between 65 to 128 hrs based on the model complexity described in the following sections of this chapter.

The main goal of the proposed finite element models is to study, provide confidence, and enhance the energy absorption characteristics in transportation infrastructure involved in vehicle crash accidents. Crash tests are complex events that are not easily replicated because of difficulties in controlling critical test conditions such as speed, angle, and condition of test vehicle, the vehicle occupants, and the sometimes random and unstable behavior of dynamic crush and fracture mechanisms. The National Cooperative Highway Research Program, NCHRP 350 [23], testing procedures was followed during the modeling stages of the vehicle and pole/support interaction in this thesis. The goal of using NCHRP 350 was to enhance the precision of the analysis, and to stay consistent with most commonly followed practice. The 'S3' sign convention was used during the

validation stages of the child dummy model, and this sign convention is followed throughout this thesis described in Table 3.1.

Table 3.1 Modeling sign convection

	S3
Length	Millimeter (mm)
Mass	Kilogram (kg)
Force	kiloNewton (kN)
Time	Millisecond (ms)
Stress	kiloPascal ($kN \cdot mm^{2}$)
Density	($kg \cdot mm^{-3}$)
Moment	($kN \cdot mm$)

The design procedure for each simulation design using LS-DYNA software follows a five-step finite element modeling procedure briefly outlined below:

1. Modeling: In this stage the model is created and meshed using appropriate methods related to each design.
2. Material: Material properties are assigned to each material type in LS-DYNA standard card format, and input variables are dependent on the unique properties of each material type.
3. Property: Finite element sectional properties are defined in this step, and depend on the characteristics of the material type defined and the desired output characteristics.
4. Contact: Contact impact algorithms are defined in this section and depend on the type of interaction between the impacting entities. i.e. CONSTRAINED _NODES_ TO _ SURFACE deals with welded elements that are coupled via a

fixed connection, AUTOMATIC_NODES_TO_SURFACE is defined for impacting entities, and the AUTOMATIC_SINGLE_SURFACE is defined for the general interaction between the various components within the vehicle.

5. Boundary Conditions: The boundary option provides a way of defining imposed motions on boundary nodes. This final step is required in order to effectively create unique environments of each simulation. In this study the boundary conditions are applied to the ground using fixed nodes, are used to set appropriate vehicle velocities, and are used to provide appropriate seatbelt tensioning of the child dummy model after the impact.

After the model has been properly designed following the five steps outlined above, the appropriate control options were set in order to control the desired output databases for post-processing. The results were analyzed using the standard LS-DYNA post-processing software, LS-PRE/POST v1.0.

The next sections of this chapter describe the fundamental finite element theory used by LS-DYNA software, the modeling characteristics considered in this study, along with a description of the major design variations considered. For an in-depth review of LS-DYNA software, please refer to LS-DYNA manuals referenced in this thesis [25].

3.2 Theory

To simulate the impact scenario, LS-DYNA uses the explicit finite element time integration method. The explicit method solves the equilibrium at time t by direct time integration using the central difference method summarized below:

$$m \cdot \ddot{x}_t + c \cdot \dot{x}_t = F_t - (F_s)_t \tag{3.1}$$

$$\dot{x}_t = \frac{x_{t+\Delta t} - x_{t-\Delta t}}{2\Delta t} \tag{3.2}$$

$$\Delta t < 2\frac{\sqrt{1+\zeta^2} - \zeta}{\varpi_{max}} \tag{3.3}$$

$\ddot{x}_t$ = Acceleration

$\dot{x}_t$ = Velocity

m = Diagonal mass matrix

c = Diagonal damping matrix

Δt = Time step for the time integration

ϖ_{max} = The maximum eigen frequency of the system

ζ = The fraction of critical damping of the highest mode

For the explicit, central difference method, dynamic equilibrium is considered at a time t to evaluate the solution at time $t+\Delta t$. This explicit methods mandates a small Δt, however this results in equations requiring relatively little computational effort to solve. The explicit time integration method is conditional stable, when the time step, Δt, is subjected to a limitation via Equation 3.3. Thus, the maximum time step for an explicit conditionally stable integration scheme is determined by the stability limit provided from Equation 3.3. With the use of the central difference method, the time step has been chosen such that Δt is smaller than the critical unstable value, and in turn means that Δt will be small enough to obtain accuracy in the integration of all 'n' equations of dynamic equilibrium.

The calculation cost of the explicit solution procedure is directly proportional to the size of the finite element model. This is a major disadvantage compared to the implicit method, where the calculation cost is proportional to the square of the matrix bandwidth of the mesh for very large models. The diagonalized mass matrix allows the explicit method to use a very fine mesh at any location without taking the increase of wave front into consideration [24].

Due to non-linear nature of problems, an iteration procedure is used to ensure equilibrium. Depending upon the procedure chosen, each iteration process requires the formation and solution of the linear system of equations. With the increase of size of problems (e.g. 3D solids), this system of equation can become very large and the computational cost of solving this system may dominate the total CPU time. Due to the

iterative nature of the solution procedure, a successful solution requires the satisfaction of convergence criterion at each incremental step. Generally, the convergence speed is quite problem dependent and failure to converge results in premature termination of the analysis [24].

3.3 Vehicle Modeling

A finite element model for a midsize sedan vehicle was obtained from the National Crash Analysis Centre (http://www.ncac.gwu.edu/vml/models.html/, 2004) and has been used in the enclosed research for frontal impact crash scenarios.

The vehicle model is based on a 2000 Ford Taurus 4-door designed for frontal impact by the FHWA/NHTSA. The front-end components from bumper to A-pillar were modeled with a fine mesh, Figure 3.1, with the rear half of the vehicle model having a fairly coarse mesh density. Components such as the bumper, front rail, upper load path beams, radiator, engine cradle, etc., shown in Figure 3.2, were modeled to capture all significant geometric imperfections such as holes, beads and crush initiators which play a vital role in the overall crash characteristics of the vehicle.

The major characteristics of the complete FE vehicle model can be summarized as follows:

- 71,063 elements in total

- 28, 714 shell elements
- 291 beam elements and 183 Rigid Bodies
- 136 material cards, defining the material models employed, including steel, rubber, honeycomb, and glass
- 16 Accelerometers
- Automatic single surface contact from A-pillar to rear bumper
- Tied nodes to surface contact between the columns and the plates
- Automatic nodes to surface contact between the bumper and the columns
- Conventional spot weld, and rigid body nodal constraints
- Discrete springs, discrete dampers, and discrete masses.

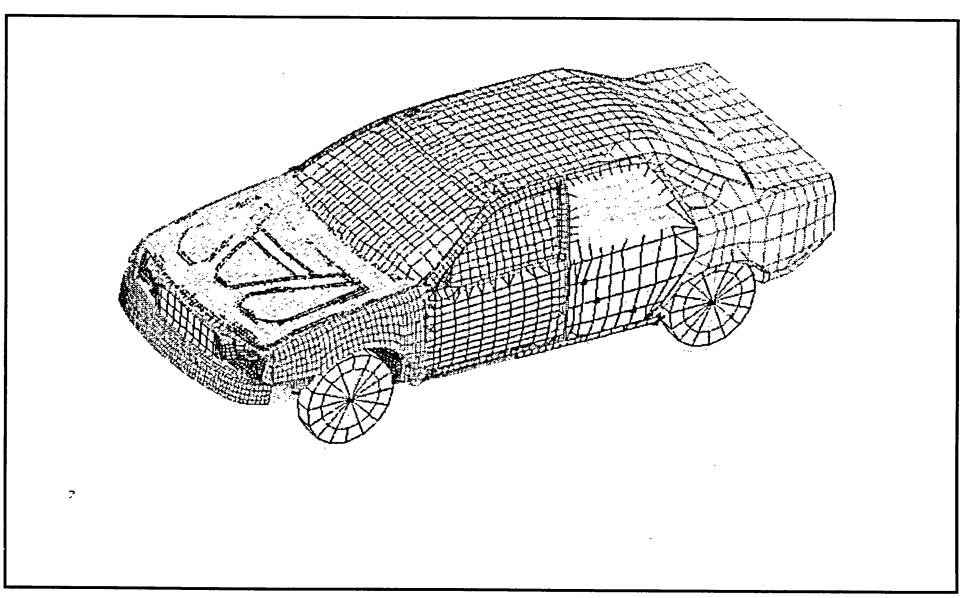

Figure 3.1 Top view of a 4-door Ford Taurus finite element model

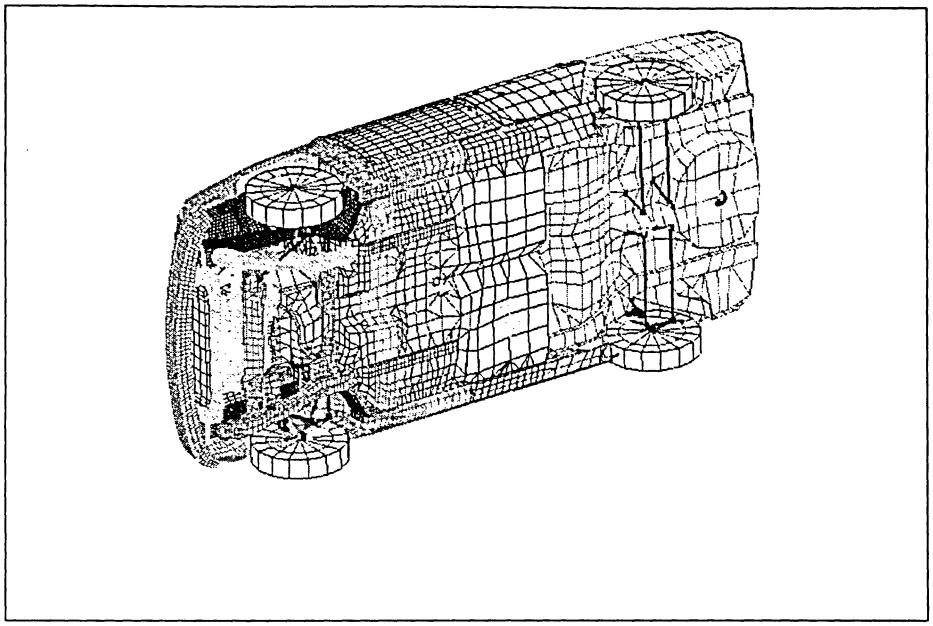

Figure 3.2 Bottom view of a 4-door Ford Taurus finite element model

3.4 Hybrid III - 3-Year-Old Dummy - Model Development

The numerical model of the Hybrid III 3-year-old dummy, version 2.3-2, used in this report was originally created and developed by First Technology Safety Systems and Ove Arup & Partners Detroit Limited.

The Hybrid III 3-year-old dummy model is comprised of 12,172 elements, 11,698 nodes and consists of a completely deformable finite element mesh. Beam elements and nodes are strategically located in specific areas of the body in order to provide numeric response required for the extraction of occupant injury criteria. The load cells and accelerometers

are positioned throughout the child dummy model as per the coordinate system specified through the Society of Automotive Engineers (SAE J211, 2003) [25], and the locations were identical to the experimental sled testing procedures recommended by the Federal Motor Vehicle Safety Standards and Regulations (FMVSS 213) [26]. Detailed model information of the child dummy can be found in reference [27] of this thesis.

The child restraint system was developed and validated by Turchi et. al [6] in accordance to experimental testing procedures outlined by FMVSS 213 [27] based on a convertible five point forward/rearward facing CRS. The CRS is only validated for the forward facing orientation since many simplifying assumption were made which are briefly described below. Figure 3.3 illustrates the child dummy model and the child restraint system used in this study.

The child safety seat was modeled using a rigid material model, material type 20 in LS-DYNA, as the deformation of the child restraint system was observed to be negligible during the experimental sled testing as compared to the displacements associated with the child limbs. Values for the density, elastic modulus, and Poisson's ratio were all required because of the contact algorithm between the CRS and the child dummy model and were specified 900 kg/m^3, 1.2 GPa, and 0.3, respectively, which are typical polypropylene CRS material properties [6]. The seat belt was modeled to fit around the Hybrid III 3-year-old dummy in a similar fashion as the experimental set up outlined through FMVSS 213 [27]. Element edge lengths associated with the seat belt were not greater than 8.9 and were not less than 4.8 mm. *MAT_FABRIC was used to simulate the material

characteristics of the seat belt webbing. The density, elastic modulus, and Poisson's ratio was specified as 911.8 kg/m^3, 6.27 GPa , and 0.3 respectively [6]. A foam pad, which is inserted between the polypropylene shell and the seat fabric of the CRS, was also incorporated into the FE model of the CRS. Density and stress/strain relationship for the foam were experimentally determined and values for the elastic modulus and density of the material were assigned as 50.2 kg/m^3, and 5.52 MPa, respectively [6].

Based on the simplifying assumptions and the characteristics described above, the results from reference [6] of this thesis closely resembled frontal impact sled test results from which the model was derived. The model is only valid for approximating the injury response for frontal impact simulation and technically is not acceptable to be used in any other position, especially the rearward facing position.

The integration of the 3-year-old child dummy model into the Ford Taurus vehicle model was accomplished using the LS-DYNA Finite Element Model Builder, eta/FEMB-PC version 27 [14]. The sign convention was kept consistent with the 'S3' units previously described in the beginning of this chapter. The child and the vehicle were both faced in the negative 'X' direction as per the procedure outlined in the validation stages of the CRS system [6]. The child model, including the seat were incorporated into the LS-DYNA using the *CONSTRAINED_RIGID_BODIES option. This option allows the child including the seat to be directly integrated into the vehicle model in the absence of a back seat. This option was the best alternative available because the back section of the Ford Taurus model has a fairly coarse mesh, and by joining the seat to the vehicle via a

rigid body between the two entities, the crash pulse was effectively transferred into the child. This procedure allowed for effective extraction of child injury response parameters during the crash pulse.

The model was now ready to perform crash simulations as the child and the vehicle were effectively combined into one. The total number of elements of the two joined bodies is now approximately 83,200 elements. Detailed vehicle models of approximately 240,000 elements were also available for analysis purpose, but due to computer performance limitations, it become quite impossible to effectively analyze the crash scenario using these vehicle models.

The simulations were analyzed for time duration of 150 ms and the control options were set in accordance to FTSS Hybrid III 3 Year Old Child Dummy Manual [27]. The only difficulties experience while running the analysis was the *CONTROL_TIMESTEP option which created negative element volumes in the seat belt because the standard time step scale factor was set to a factor of 0.9 the original value. Since the seat belt elements were relatively thin compared to the contacting environment of the child dummy and the CRS system, they usually wrapped in around each other, and created negative volumes in and around the loops and buckles of the CRS system during a severe collision. This problem was fixed by decreasing the time step scale factor on a trial and error basis until a stable simulation was achieved. For the more sever crash impact case the time step had to be decreased down to a factor of 0.80 in order to achieve stable results. On average the time step scale factor of 0.85 was adequate to cover most of the analysis performed.

However, each reduction in the time step scale factor had a significant increase to the computational time for each simulation adjusted.

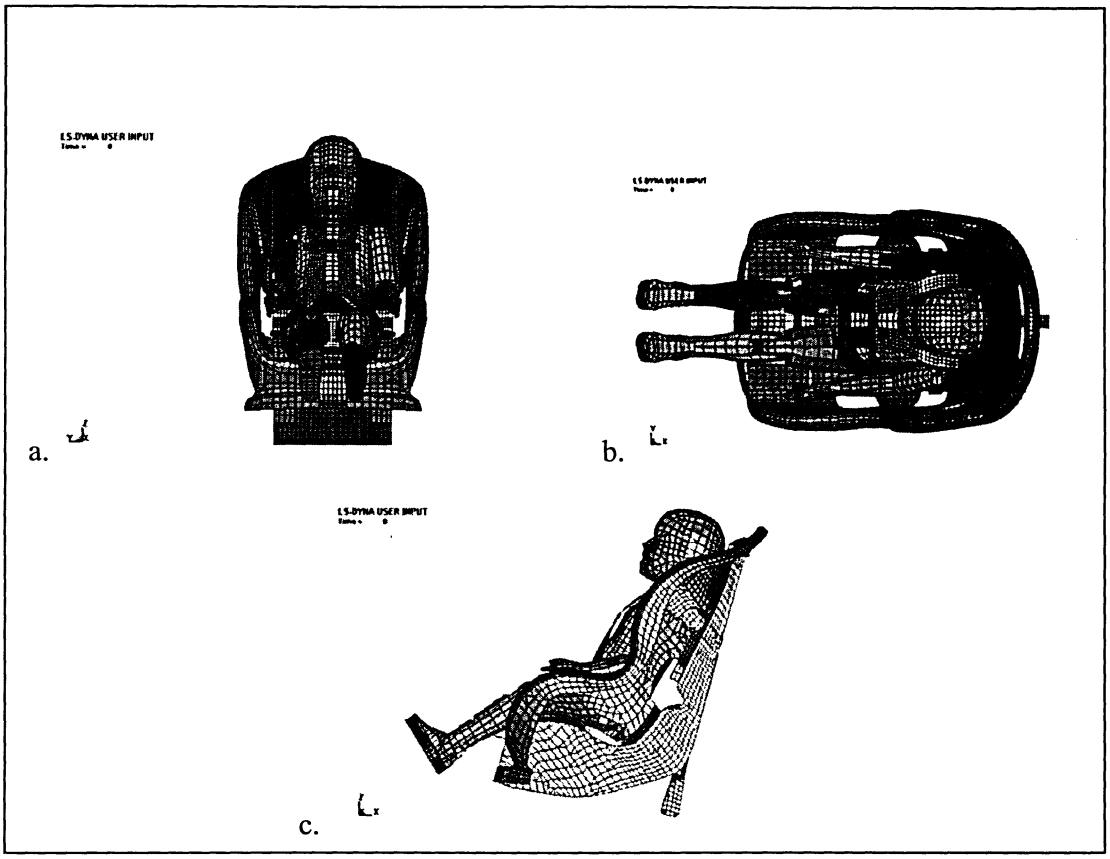

Figure 3.3 Hybrid III 3-year-old dummy model restrained in a five-point-restraint in a forward facing position illustrated in (a) front, (b) top, (c) side views.

3.5 Modeling of Laminar Traffic Poles and Pole Support Systems

In this study the steel and aluminum pole structures were modeled in terms of five different support conditions, namely; the fixed support, anchored base support, springs/anchored base support, rubber/fixed base support, and embedded pole-soil support system. The shell thickness of the pole structures was also analyzed in terms of thickness variations and all designs were correlated against three different impact velocities; namely 64, 48, and 40 km/hr in accordance to the National Cooperative Highway Research Program.

The Canadian Highway Bridge Design Code (CHBDC, 2000) [18] was followed in the designs stages of the pole structures which states that poles are to be designed to the minimum yield strength of the material with an adequate factor of safety that will withstand the dead loads of the structure as well as the specified wind loads.

3.5.1 Traffic Light Pole

A typical 10.4 m high octagonal traffic pole described in the literature review of this thesis is used in this study with a bottom diameter of 0.30 m and the top diameter of 0.133 m. The pole is modeled using the Bleytschko-Lin-Tsay shell element with five through-the-thickness integration points. Such a shell element is based on a combined co-rotational and velocity strain formulations. The Belytschko-Lin-Tsay shell elements are more efficient and require 725 mathematical operations as compared to the 4066

operations for the under-integrated Hughes-Liu element, and 35,367 mathematical operations for the fully integrated Hughes-Liu element [24, 28]. Table 3.2 of this chapter illustrates the remarkable efficiency of the Belytschko-Tsay element compared to fully integrated shells. A total of 800 quad plate elements were utilized during the modeling stages of the pole structure.

The steel pole shaft considered in this study is normally fabricated from hot rolled commercially available carbon steel. The following steel material properties were used during the modeling phases of the analysis:

- Density: $\rho = 78.3$ kN/m^3
- Young's Modulus: E = 207 GPa
- Yield Stress: $\sigma = 215$ MPa
- Poisson's Ratio: $\upsilon = 0.28$

The material properties used in this study for the aluminum poles, Grade 6005-T5 is as follows:

- Density: $\rho = 27.0$ kN/m^3
- Young's Modulus: E = 69 GPa
- Yield Stress: $\sigma = 240$ MPa
- Poisson's Ratio: $\upsilon = 0.33$

Table 3.2 Efficiency of Shell Element formulations in LS-DYNA compared to the Computer time of Bleytschko-Lin-Tsay [24, 28]

Type	Element Name	Nodes	CPU efficiency compared with Element Type 2
1	Hughes-Liu	4	3.5
6	SRI Hughes-Liu	4	20
7	Fast SRI Hughes-Liu	4	10
2	Bleytschko-Lin-Tsay	4	1
10	Bleytschko-Wong-Chiang	4	1.1
8	Belytschko-Levianthan	4	1.3
16	FI-ANS (Bathe-Devorkin)	4	3.5

3.5.2 Modeling of Traffic Pole Support

Five different cases of pole supports were analyzed in this study as shown in Figure 3.4. The first case of the support system consists of anchored bolts embedded directly into a rigid foundation, such as a concrete island or walkway as per Figure 3.4 (a). The steel anchored bolts are fabricated from hot rolled steel bars with high yield strength. The threaded end is galvanized with a minimum of 30 mm diameter and each bolt is furnished with two flat washers and two hex nuts. Eight-node solid elements were implemented to model the anchors and the anchor's head. The base plate is constrained to the bottom of the pole using CONSTRAINED _NODES_ TO _ SURFACE option and the thickness of the plate is set at 30 mm. The material properties of the anchored bolts and the steel base plate are summarized as follows:

- Density: $\rho = 78.3$ kN/m^3
- Young's Modulus: E = 207 GPa

- Yield Stress: $\sigma = 215$ MPa
- Poisson's Ratio: $\upsilon = 0.28$

The second pole support system considered in this thesis contains springs between the nuts and bolts over and under the steel plate and the arrangement is similar to the anchored bolts system described above, Figure 3.4 (b). Springs were given a stiffness value of 50 N/m and represent the stiffness currently available for a 30 mm diameter bolt that is equivalent to approximately 5 kg in force. Their purpose is to act similar to shock absorbers, and absorb as much of the impact energy as possible in this situation.

The third pole support system considered in this study is similar to the second support system, however instead of using springs between the nuts and the base plate, dampers are used to represent rubber rings in order to dissipate the impact energy. The rubber material is similar to the material properties considered for the vehicle tire and the damping coefficient considered is set at 10 N·s/m.

The fourth pole support type considered in this study is comprised of a cylindrical rubber base connecting the pole base to the foundation via a fixed connection. The base plate is designed to carry and transfer the entire force of impact into the ground. Anchored bolts and nuts are also used to strengthen the bond between the plate and the ground as per Figure 3.4 (c), of this section. The solid rubber base pole is comprised of a similar material type to the damper previously discussed and the material properties are as follows:

- Density: $\rho = 10.63$ kN/m^3
- Young's Modulus: E = 2.46 GPa
- Yield Stress: $\sigma = 24.7$ MPa
- Poisson's Ratio: $\upsilon = 0.323$

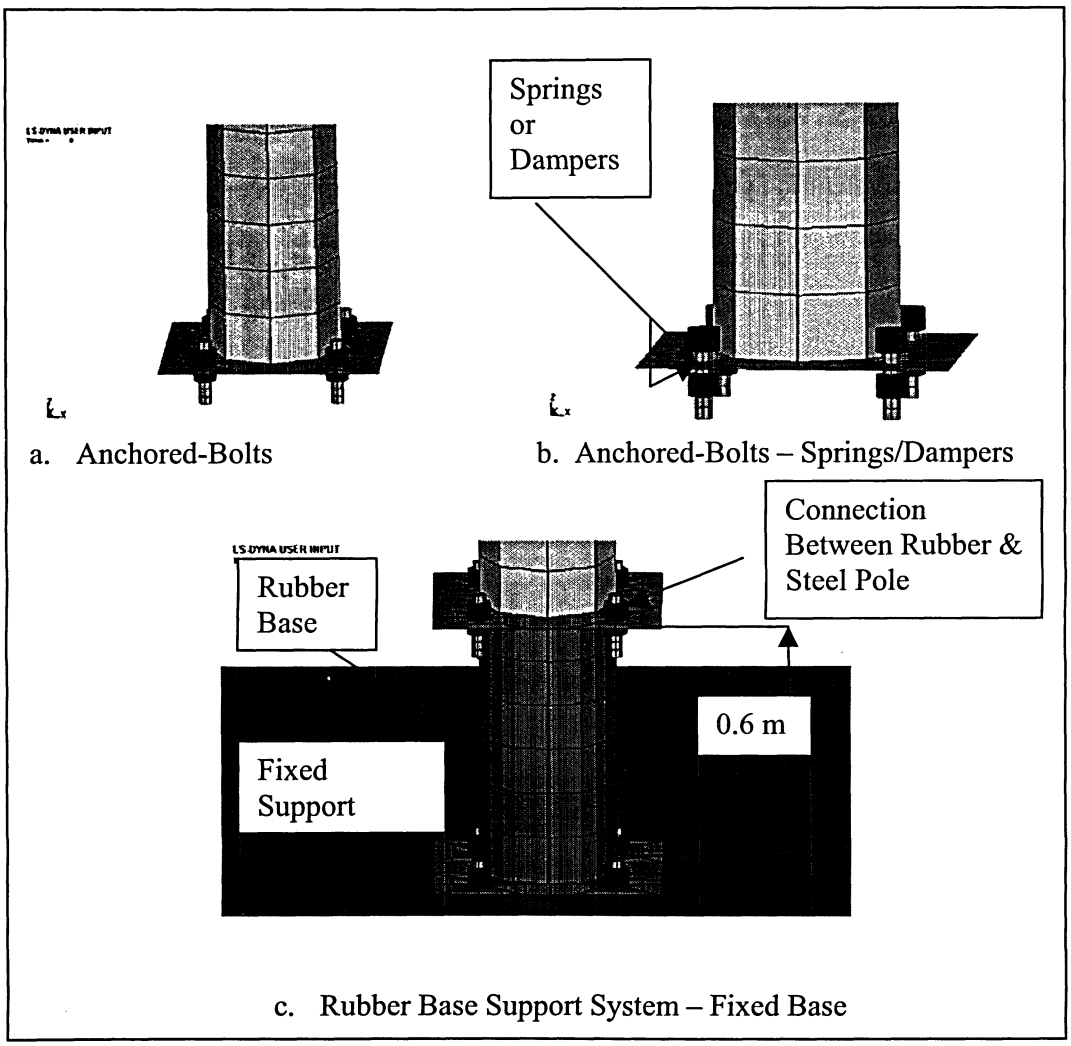

Figure 3.4 Different Pole Support Systems Considered in this study.

The last pole support design employed compares poles embedded at different depths for clayey and sandy soil conditions. The soil conditions were represented using horizontal

springs set to act in compression only via the LS-DYNA defined material Type 8, using the *MAT_SPRING_INELASTIC standard card definition. With this material type, an inelastic compression is provided using a user defined arbitrary Force vs. Displacement load curve and is used to represent the lateral bearing capacity of the soils. The loading values used to represent the soil conditions are described in detail in the following section.

3.5.3 Soil-Pole Interaction Modeling

Two different soil materials are considered in this study to study the effects of the embedment depths, namely: clayey and sandy soils. Eight springs are used to represent the lateral resistance of the soil that are identified to act in the horizontal direction at each of the node levels of the embedded portion of the poles shown in Figure 3.5. The frictional resistance of the soil was represented by springs in the vertical direction at selected node levels of the embedded part of the pole structure shown below, and are defined at 10% of the lateral bearing capacity values for the soil type under consideration [29].

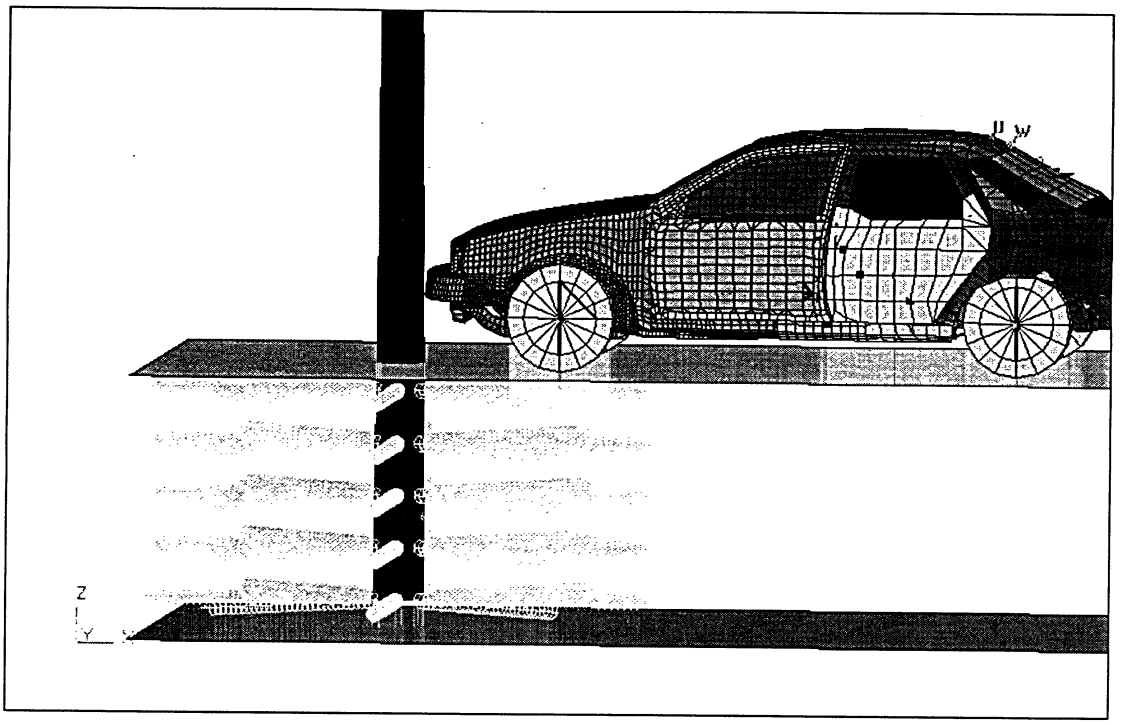

Figure 3.5 Schematic representation of the springs used to define the lateral bearing capacity of the soils

To model the soil-pole interaction, Hudson Matlock's theory was used where correlations were developed for design of laterally loaded piles in soils [29]. A program of research on laterally loaded piles for offshore structures had included in field tests with an instrumented pile, laboratory modal testing, and development of correlations for the design of the lateral bearing values represented via Force vs. Displacement graphs. The goal of the research was aimed in designing laterally loaded piles that would effectively withstand service loading conditions from winds and waves resulting from severe storm occurrences such as hurricanes.

The following subsections explain the methodology used to model the soil-pole interaction and summarize the equations from which the spring constants were obtained.

The springs were defined to act in compression only since pole separation is possible under lateral loads. The force vs. displacement (p-u)defined for clayey and sandy soils are based on the soil properties and the lateral bearing characteristics.

3.5.3.1 Lateral Bearing Capacity for Clay

A series of lateral load tests on instrumented piles in clay [29] were used to produce the p-u relationship for piles in soft to medium clays [30] in the form for a wedge failure near ground surface.

The actual lateral resistance of soil subjected to lateral loads was determined from the relationship

$$P = 0.5 \cdot P_u \cdot \left(\frac{y}{y_c}\right)^{\frac{1}{3}} \tag{3.4}$$

P = the actual lateral resistance of soil

y = the actual lateral deflection and P_u is the ultimate resistance, given by the smaller

$$P_u = \left(3 + \frac{y'}{c} \cdot x + \frac{J}{D} \cdot x\right) \cdot c \cdot D, \qquad x < x_{cr} \tag{3.5}$$

for a wedge failure near ground surface, and

$$P_u = 9 \cdot c \cdot D, \qquad x \geq x_{cr} \text{ for a flow failure at a certain depth.} \tag{3.6}$$

y' = effective unit weight of clayey soil = 60 lb/ft^3 (961 kg/m^3)

c = shear strength of soil = 5 lb/in^2 (24.5 kN/m^2)

J = dimensionless empirical constant = 0.25 (for medium dense clay)

D = pole diameter = 0.3 m

x = depth below soil surface

y_c = the lateral displacement at one-half the ultimate resistance, given by

$$y_c = 2.5 \cdot \varepsilon_c \cdot D \tag{3.7}$$

ε_C = Strain at 50% of the ultimate strength from laboratory stress/strain = 0.01

The depth at which the failure transitions from wedge, Equation 3.5 to flow type, Equation 3.6, is

$$x_{cr} = \frac{6 \cdot c \cdot D}{y' \cdot D + J \cdot c} \tag{3.8}$$

Figures 3.6 and 3.7 illustrate the force vs. deformation characteristics of the horizontal springs representing the bearing capacity of the soft to medium clay soil type at different

soil depths. The characteristics of vertical springs representing the frictional resistance are considered 10% of the horizontal values presented below.

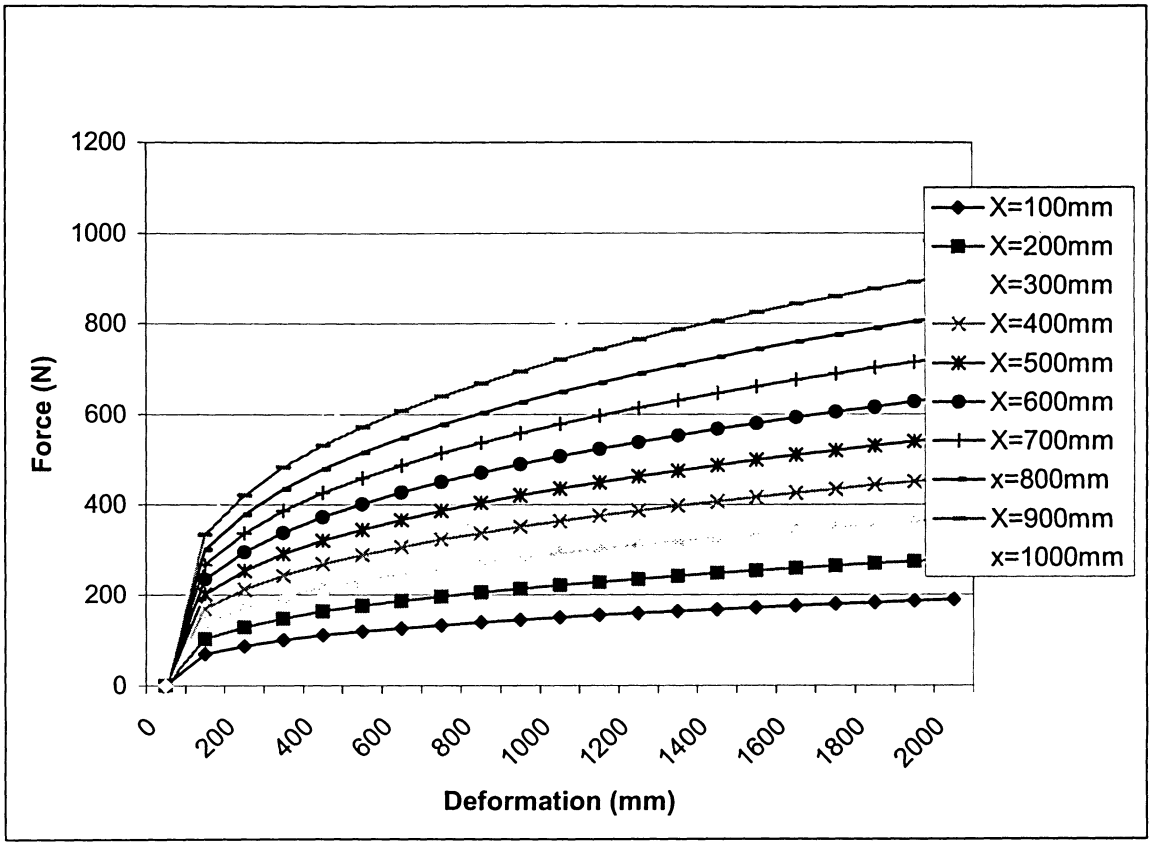

Figure 3.6 Force vs. Deformation characteristics for a soft to medium clay soil type for embedment depths between 100 to 1000 mm

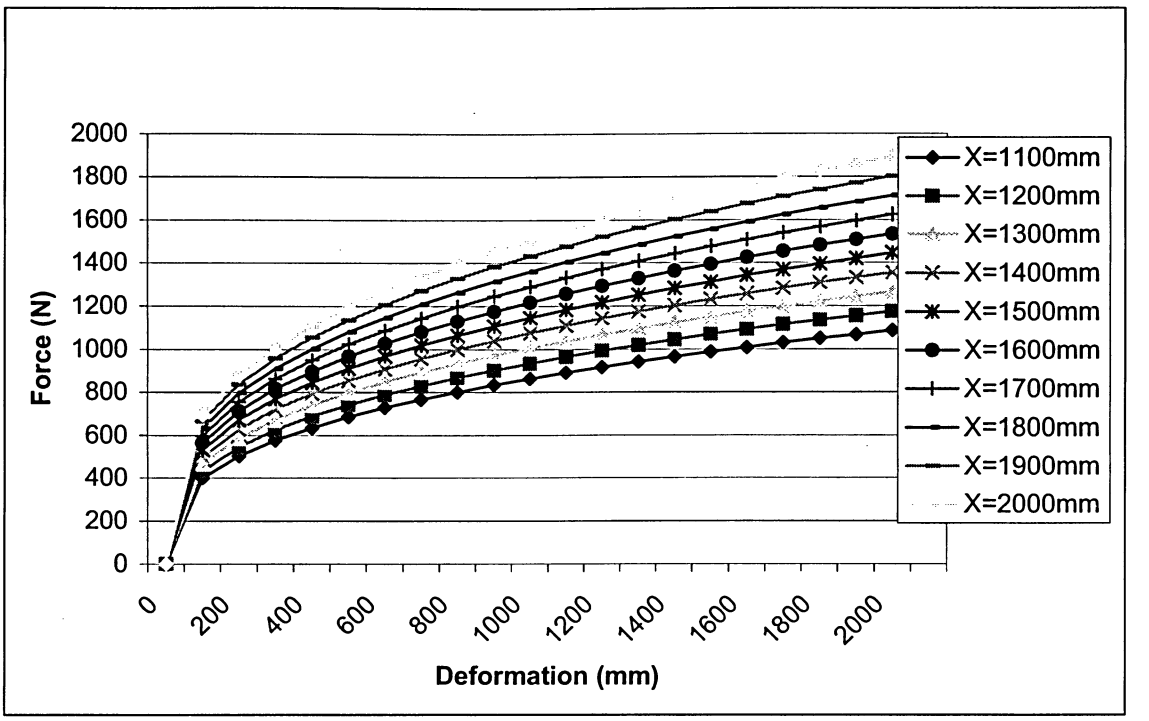

Figure 3.7 Force vs. Deformation characteristics for a soft to medium clay soil type for embedment depths between 1100 to 2000mm

3.5.3.2 Lateral Bearing Capacity of Sand

The ultimate lateral bearing capacity for sand was found to vary from a value at shallow depths determined by Equation 3.9 to a value at deep depths determined by Equation 3.10 [16]. At a given depth the equations summarized below that give the smallest value of P_u should be used as the ultimate bearing capacity, where P_u is the ultimate resistance (s = shallow, d = deep).

$$P_{us} = (C_1 \cdot x + C_2 \cdot D) \cdot y' \cdot x \qquad (3.9)$$

$$P_{ud} = C_3 \cdot D \cdot y' \cdot x \tag{3.10}$$

y' = Effective unit weight of sandy soil 65 lb/ft^3 (1040 kg/m^3)

C_1, C_2, C_3 = Are coefficient function of ϕ and are equal to 3, 3.5, 54, respectively

ϕ = Angle of internal friction = 35^0

The lateral soil resistance-deflection relationship for sand is a non-linear relationship. The following expression is used for lateral resistance at depth 'x' [16]:

$$P = n \cdot A \cdot P_u \tanh\left(\frac{k \cdot x \cdot y}{n \cdot A \cdot P_u}\right) \tag{3.11}$$

P_u = The ultimate lateral soil resistance

k = The initial modulus of sub grade reaction = 80 lb/in^3 (21,720 kN/m^3)

n = The geometry factor, 1

$$A = 3 - 0.8\left(\frac{x}{D}\right) \geq 0.9 \tag{3.12}$$

x = Embedded pole depth

D = Pole Diameter

Figures 3.8 and 3.9 illustrate the force vs. deformation characteristics of the horizontal springs at different depths for loose sand. These values are directly substituted into the LS-DYNA load curve format and are used to define the non-linear spring behavior based on the desired embedment depths. The characteristic values of the vertical springs representing the frictional resistance are considered 10% of the horizontal values [16].

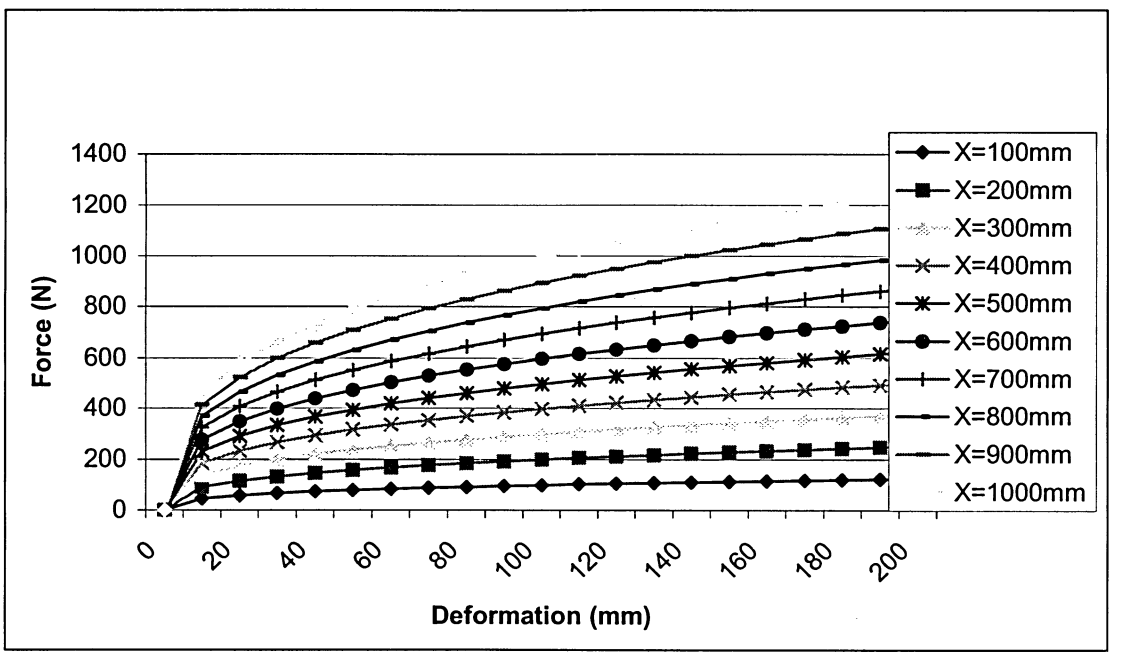

Figure 3.8 Force vs. Deformation Characteristics for a loose sandy soil type for embedment depths between 100 to 1000 mm

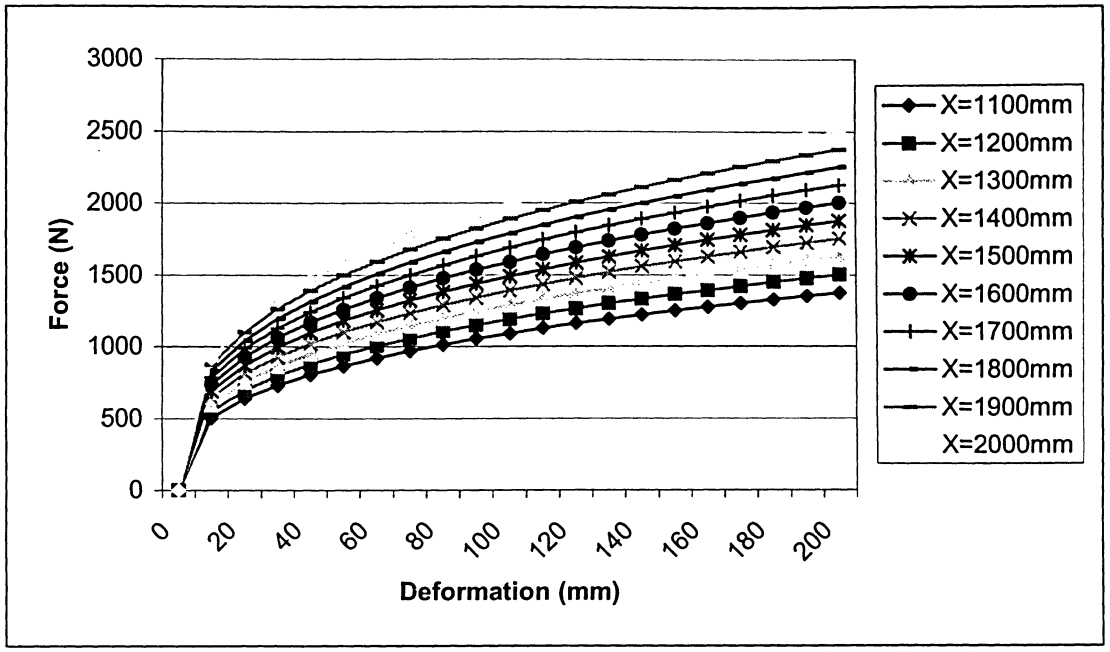

Figure 3.9 Force vs. Deformation Characteristics for a loose sandy soil type for embedment depths between 1200 to 2000 mm

CHAPTER 4

ANALYSES AND INJURY CRITERIA EXTRACTION

This chapter explains the techniques used in the extraction of Occupant Injury Criteria (OIC) and crashworthiness analyses for a simulated 3-year-old child dummy involved in vehicle crash events with a traffic light pole using the LS-DYNA software.

4.1 Extraction of Occupant Injury Criteria

As mentioned in the literature review, in March of 2000, The National Traffic Safety Administration, NHTSA [8], had improved their previously developed occupant injury criteria in their report titled "*Supplement: Development of Improved Injury Criteria for the Assessment of Advanced Automotive Restraint Systems II*". Based on their research on advanced airbags, NHTSA proposed a comprehensive set of injury criteria for evaluating the potential for injury to the head, neck, chest and lower extremities for the various dummy sizes, ranging from the 1-year-old-child to the 50^{th} percentile male. The recommended injury criteria used in this study for a 3-year-old child dummy is summarized below in Table 4.1 of this chapter.

All of the results were obtained and filtered in accordance to the Society of Automotive Engineers standards (SAE J211, October 1988) [25] outlined in Table 4.2 of this section. Based on these criteria, a high output interval is required. In LS-DYNA a high output frequency in achieved in the database control section by setting the output option to compute a point every 1.0×10^{-5}s.

Table 4.1 – Summary of recommended injury criteria for a 3 year old child dummy (NHTSA) [8]

Occupant Injury Criteria	Limiting Threshold Value
Head Injury Criteria (HIC 15)	570
Head Injury Criteria (HIC 36)	570
Thoracic Criteria: Chest Acceleration	55 g's
Neck Criteria: Tension/Compression Force	2120 N
Neck Criteria: Flexion Moment	68 N·m
Neck Criteria: Extension Moment	27 N·m

4.1.1 Head Accelerations, Head Injury Criteria, and Chest Accelerations

The Head Injury Criteria is a commonly used in frontal impact evaluation criteria that has been is place for decades as a standard to assess the level of head injury risk in frontal collisions. Normally, for an average adult, an HIC of 1000 is conventionally considered to represent the threshold where linear skull fractures will begin to appear [31]. However, for child passengers as discussed in previous chapters, these values are considerably less due to their physical immaturity and higher level of injury development. Based on NHTSA, an HIC value of 570 is recommended to be the tolerant reference threshold value where serious injury development is highly likely.

To determine the level of HIC, first the head acceleration was measured using the standard LS-DYNA accelerometer with respect to local coordinate systems as defined through the SAEJ 211 [25] in three perpendicular axes. For the crash problem investigated in the study, local x-axis and z-axis were positioned to correspond with the local plane of motion.

To determine the head acceleration value, LS-DYNA directly integrates the velocities over time at this particular location illustrated in Figure 4.1. The resultant head acceleration is computed using Equation 4.1 and than is further transformed using Equation 4.2 to determine the HIC value.

$$a_{resultant} = \sqrt{a_x^{\,2} + a_y^{\,2} + a_z^{\,2}} \tag{4.1}$$

$$HIC_{t2-t1} = \left[\frac{1}{t2-t1} \int_{t1}^{t2} a_{resultant} \cdot dt \right]^{2.5} \cdot (t2-t1) \tag{4.2}$$

t1 = beginning of the evaluation interval is sec

t2 = end of the evaluation interval in sec

a = the instantaneous resultant acceleration of the head in g's

In Equation 4.2 the resultant acceleration is expressed as a multiple of local accelerations due to gravity. Since the resultant acceleration is expressed using a discrete number of data points, Equation 4.2 can be further simplified using the trapezoidal rule of integration.

From the above equations the head injury is related to the magnitude and the time duration of the acceleration. Normally, the head can sustain high accelerations if the

loading is relatively short and lesser accelerations if the time duration is relatively long. Thus, the time interval, t2-t1, must be chosen such that the difference is less than 36 msec for HIC 36 and less than 15 msec for HIC 15. In all cases, the HIC values under investigation need to be less than the NHSTA recommended of HIC 570 for a 3 year old child occupant in order to sustain non-life threatening injuries to the region of the head. In graphical terms, HIC is related to the quantity $\Delta V/\Delta t$ that represents the slope curve on a velocity time history graph. As a general rule of thumb, larger slopes will result in larger values of the HIC.

Chest accelerations are computed in a similar fashion by a way of a chest accelerometer illustrated in Figure 4.1 and are located in accordance to the local coordinate systems defined through the SAEJ 211 [25] in three perpendicular axes. Normally, chest accelerations are used for assessing the risk of thoracic injury in conjunction with chest deflection profiles. However, for reference purpose only the peak values of the chest accelerations will be analyzed in this study. During the validation stages of the FTSS Hybrid III 3 Year Old Child Dummy Model Version 2.3, the developers of the Child Restraint System were only successful in obtaining similar peak values of the chest accelerations [6]. The relationship of the acceleration profile was slightly different from the experimental observation, and it was determined that the current model requires further modification to the CRS system in order to obtain satisfactory results. Accordingly, NHTSA recommends a value of 55 g's as a limiting threshold before any serious injury is expected to develop in comparison to a 3-year-old child.

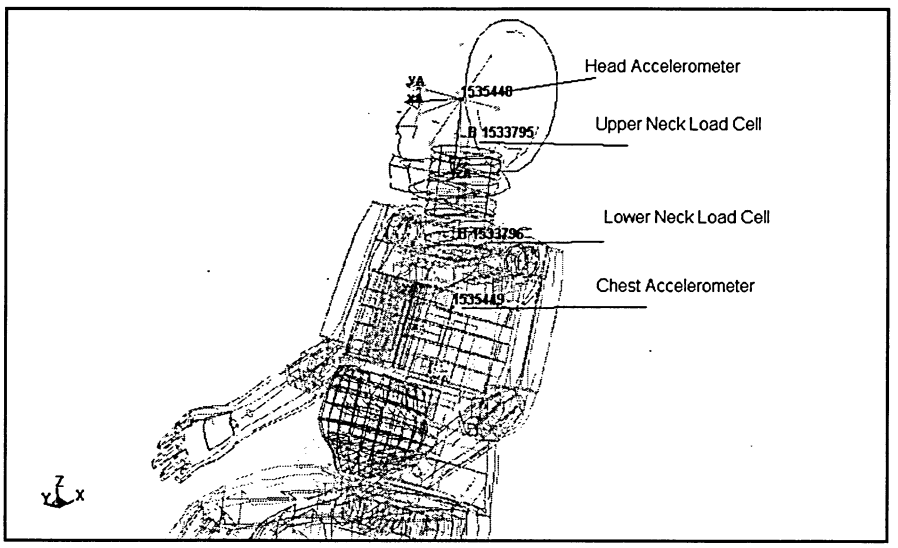

Figure 4.1 Accelerometer and load cell locations of the Hybrid III 3-year old dummy model

4.1.2 Upper/Lower Neck Forces and Moments

The upper/lower neck forces and moments are calculated based on the guidelines provided through the SAE J211 [25] and are located in the Hybrid III 3-year old dummy as per Figure 4.1, where the x, y, z axes are the local coordinate systems located at each neck location.

In LS-DYNA forces and moments are computed using load cells. Load cells are defined as zero length beams using LS-DYNA material Type 66 (linear elastic discrete beam) element that acts as a stiff translational and rotational spring. These load cells provide six output channels – three forces and three moments. Forces and moments are computed in three mutually perpendicular directions and are filtered based on the criteria provided in SAE J211 [25] as illustrated in Table 4.2. Two numerical load cells are located within

the neck region of the child dummy and are refereed to as the upper and lower neck load cells respectively.

The following equations are used to determine the upper/lower neck forces and moments resultants respectively.

$$F_{resultant} = \sqrt{F_x^2 + F_y^2 + F_z^2} \tag{4.3}$$

Fx = Axial force resultant

Fy = Shear force resultant

Fz = Shear force resultant

$$M_{resultant} = \sqrt{M_x^2 + M_y^2 + M_z^2} \tag{4.4}$$

Mx = Moment 'X' direction

My = Moment 'Y' direction

Mz = Torsional 'Z' direction

In this study, the values obtained above will be used as a reference value only since the NHTSA is currently working on developing the neck Injury (N_{ij}) criteria for a 3-year old child dummy model defined below in Equation 4.5.

According to NHTSA the maximum limiting value for force component in both tension and compression is set at 2120 N. The limiting maximum moment component is set at 68

N·m and 27 N·m for Flexion and Extension, respectively. As a general rule of thumb, values above this limit will cause greater potential for injuries the longer the neck is subjected to this limiting load value.

With respect to the neck injury criteria, the N_{ij} is computed using the following equation:

$$N_{ij} = \left(\frac{F_z}{F_{zc}}\right) + \left(\frac{M_Y}{M_{YC}}\right) \tag{4.5}$$

Fz = Axial neck load in the local z-axis direction (tension and compression)

Fzc = Critical threshold value of 2120 N for both tension and compression

My = Moment about the local y-axis

Myc = Critical threshold value of 68 N·m and 27 N·m in flexion and extension, respectively

The N_{ij} represents a linear combination of the normalized neck axial load (tension or compression) in the local z direction and the normalized neck moment about the local y-axis.

4.2 Energy Absorption Criteria

The energy absorption characteristics of the pole and support structure during a motor vehicle collision plays a vital role during the injury development of the occupants involved in the collision. It becomes very important to take into consideration the kinetic energy of the impacting vehicle and the way this energy is absorbed by the pole and support system.

For the crash scenario of this study, the total kinetic energy can be summarized as follows:

$$E = \frac{1}{2} m \cdot v^2 \tag{4.6}$$

E = Total kinetic energy

m = Mass of vehicle including the occupants

v = Velocity of the vehicle

For the vehicle of this study, the total mass including the back seat and the 3 year old child dummy, is 1403 kg, and for a velocity of 17.77 mps (64kmphr), the total kinetic energy of the system using equation 4.6 is expected to be E = 214.3 KJoules.

This kinetic energy is balanced during the impact by the various material components of vehicle and the pole support structure in terms internal energy form the sum of the plastic and elastic strains of the individual material properties.

The goal during the design stages of the traffic pole and support structure is to design a system that will effectively absorb the above mentioned kinetic energy to high degree thus minimizing the vehicles own energy absorption, and theoretically will effectively minimize the occupant injury potential.

CHAPTER 5

RESULTS & DISCUSSION

5.1 General

A total of 69 crash simulations were analyzed in this study and are described in Table 5.1. The major focus considering such variances was to investigate how injury potential develops and the major factors in design that come into affect during critical injury prevention. To take into consideration current traffic design conditions, velocities were selected from 64 km/hr (40 mph) to 40 km/hr (25 mph), and were chosen to represent the average vehicle speeds on North American roads. During these speeds, vehicles are most likely exposed to roadside structures such as traffic poles at roads and intersections not protected by traffic safety devices such as guide rails, temporary energy attenuators, etc...which are designed to protect the occupants in excessive speeds. To study the variations in traffic pole designs with respect to injury patterns, the pole supports, pole material types, and shaft thickness were all varied with respect to each simulation to determine the effect of each parameter on a 3-year old child dummy occupant. To keep parameters consistent in the finite element simulation, all models were designed to impact the pole structure at approximately 4 ms. This common parameter allowed for synchronization of the occupant time history response curves and allowed for effective evaluation and comparison of the injury risk criteria.

The analyses from the impact scenarios are described in detail in the following sections of this chapter. At the end of the chapter the results are summarized with respect to design variations and the injury potential in terms of the most effective design.

Table 5.1 Configurations and variances considered in current finite element analysis

Support Type	Pole Material	Pole Thickness	Vehicle Speeds	# of Simulations
Fixed Support	Rigid Pole	3.05 mm	64, 48, 40 km/hr	3
Anchored Base	Steel, Aluminium	6.35, 5.05, 4.80, 3.05 mm	64, 48, 40 km/hr	10
Fixed Support	Steel, Aluminium	3.05 mm	64 km/hr	2
Anchored Damper Base	Steel, Aluminium	4.80, 3.05 mm	64, 48, 40 km/hr	6
Anchored Spring Base	Steel, Aluminium	4.80, 3.05 mm	64, 48, 40 km/hr	6
Rubber Base	Rubber/Steele	Solid Rubber/ 3.05mm Steel	64, 48, 40 km/hr	3
Clay - 1.2 m Deep	Steel, Aluminium	5.05, 4.20, 4.05 mm	64, 48, 40 km/hr	9
Clay - 1.5 m Deep	Steel, Aluminium	5.05 mm	64, 48, 40 km/hr	6
Clay - 1.8 m Deep	Steel, Aluminium	5.05 mm	64, 48, 40 km/hr	6
Sand - 1.2 m Deep	Steel, Aluminium	5.05 mm	64, 48, 40 km/hr	6
Sand - 1.5 m Deep	Steel, Aluminium	5.05 mm	64, 48, 40 km/hr	6
Sand - 1.8 m Deep	Steel, Aluminium	5.05 mm	64, 48, 40 km/hr	6

5.2 Fixed Pole Rigid Support

In this section, the collision analysis is modeled to represent the worst-case scenario. The traffic pole is modeled out of rigid non-deformable material with a fixed support system yielding absolutely no deflection during the collision. This design was arranged to allow for maximum vehicle damage in order to cause the greatest injury potential to the child dummy occupant. The main purpose of the "fixed pole-rigid support" analysis was to determine baseline results, which assisted in determining the effectiveness of the pole structure and support system designs as outlined in Table 5.1 of this chapter. Normally, in real life situations, the worst-case scenario usually occurs when the vehicle impacts a highly non-deformable object such as a tree and/or a very dense structure with very little yield and/or energy absorbing characteristics.

The summaries of the results are displayed in Table 5.2 and were modeled with three different vehicle impact velocities, namely 64, 48, and 40 km/hr. From the results, it is clear that at speeds greater than 48 km/hr the child occupants sustained critical non-survivable injuries, especially to the head.

The HIC response is very severe for the 64 km/hr impact scenario with the value being 411% higher than the allowable threshold value of 570 g's. With respect to the neck and chest limiting criteria, the child occupants also sustained critical injuries to this region with the limiting values being exceeded with a range of 111 to 219%. For the 48 km/hr scenario, the child occupant has a slightly higher chance of surviving with the HIC 36

being at 105% of the limiting value. Although the chances for survival at this speed are slightly improved, the chance of a fatal injury is also still very likely.

The graphical results for the head accelerations in the 'X' & 'Z' directions are illustrated in Figures 5.1 and 5.2, respectively, for the three impact speeds. From the figures, it is evident that the time of maximum head acceleration occurs at approximately 90 ms for the 64 km/hr, which is approximately 10 to 15 ms sooner than the 48 and 40 km/hr speeds. For the 48 and 40 km/hr speeds, the maximum head acceleration response occurs at approximately 100 ms and 105 ms, respectively. In most cases, the time of maximum head extension along with the time duration of maximum response is directly related to maximum values obtained from the critical head injury criteria. Figure 5.3 schematically illustrates this critical time parameter experienced by the child occupant by comparing the actual deflections of the child limbs at 92 ms of the simulation for the 3 vehicle speeds under consideration. From this figure, one can clearly see that the child occupant reaches maximum head and limb extensions at 92 ms for the 64 km/hr simulation. For the 48 and 40 km/hr speeds, the extension of the limbs and the head is less severe and occurs at a later time, Table 5.2. During this critical time of maximum extension, the internal organs of an occupant continue to travel forward until they strike internal tissue, bone matter and/or are stopped by connecting tissue. In the case of the 64 km/hr simulation, the brain of the child occupant has sustained sever damage during this point in time from either a rupture and/or organ damage, which is directly reflected by the high HIC value recorded in Table 5.2.

In terms of neck injury, the upper and lower neck region has exceeded the respective limiting criteria for all speeds considered. The neck injuries involved during a 48 km/hr impact speeds are less severe than the 64 km/hr case and closely resemble the sled impact test simulation that the child model was derived from. Normally, if the neck injury is slightly over the limit, the child occupant will survive the impact, however the HIC levels need to be below their respective limits, since the injury to the head is less forgiving.

Based on the results alone, it is recommended to mandate traffic protection devices in all areas with poor energy absorbing characteristics that resemble non-deformable objects. If such traffic protection structures are not available due to site conditions, the posted speeds shall not be greater than 40 km/hr (25mph) for these sections of the road.

Table 5.2 Maximum values from time history results of rigid pole fixed support simulation

	Rigid Pole Fixed Support									
Description	**H.A.- 'X'**	**H.A. -'Z'**	**C.A. -'X'**	**C.A.-'Z'**	**R.U.N.F.**	**R.L.N.F.**	**R.U.N.M**	**R.L.N.M.**	**HIC 15**	**HIC 36**
Limitation (NHTSA)			**55**	**55**	**2120**	**2120**	**27**	**68**	**570**	**570**
Sled Test Sim.	**-34**	**45**	**-63**	**-39**	**1300**	**1300**	**35**	**104**	**175**	**324**
R.P.F.S -64 km/hr	-41.7	87.5	-72.6	33.6	2357	2378	43.9	148.7	784.8	2342
% of Limit			**132%**	**61%**	**111%**	**112%**	**163%**	**219%**	**138%**	**411%**
R.P.F.S - 48km/hr	-28.1	47.7	-51.1	-27	1410	1352	36.4	104.9	199.5	598
% of Limit			**93%**	**49%**	**67%**	**64%**	**135%**	**154%**	**35%**	**105%**
R.P.F.S - 40km/hr	-30.5	38.8	-33.4	-18.5	1180	1173	31.5	103.9	126.4	378.4
% of Limit			**61%**	**34%**	**56%**	**55%**	**117%**	**153%**	**22%**	**66%**

	RIGID POLE	
Vel. - Thickness	**T.0.V**	**T.M.H.X.**
64km/hr - Rigid	80	90
48km/hr - Rigid	84	100
40km/hr - Rigid	90	105

H.A.- 'X'= Head Acceleration 'X' (g)
H.A. -'Z'= Head Acceleration 'Z' (g)
C.A. -'X'= Chest Acceleration 'X' (g)
C.A. -'Z'= Chest Acceleration 'Z' (g)
R.U.N.F= Resu. Upper Neck Force (N)
R.L.N.F= Resu.Lower Neck Force (N)
R.U.N.M= Res.Upper N. Moment (N·m)
R.L.N.M.=Resu.Lower N. Moment (N·m)
HIC 15= Head Injury Criteria 15ms
HIC 36= Head Injury Criteria 36ms
M.I.E= Max.Internal Energy (kJ)
(for Pole and Support System)
T.0.V.=Time of 0 Velocity (ms)
T.M.H.X.=Time of Max H.A.-'X' (ms)

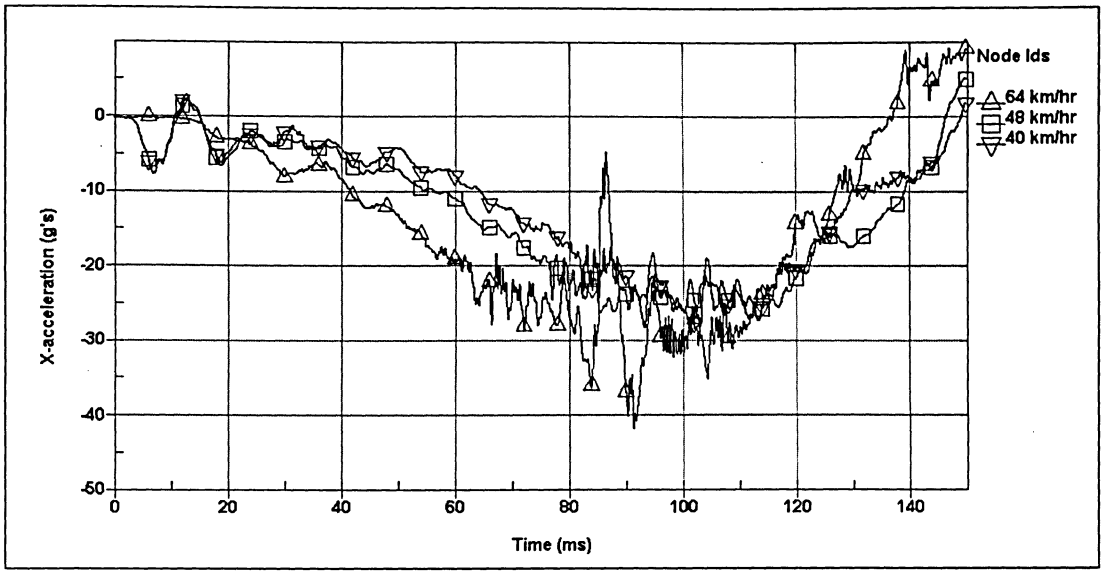

Figure 5.1 Head acceleration time history profile in 'X' direction – fixed support – Rigid pole – 64, 48, 40 km/hr

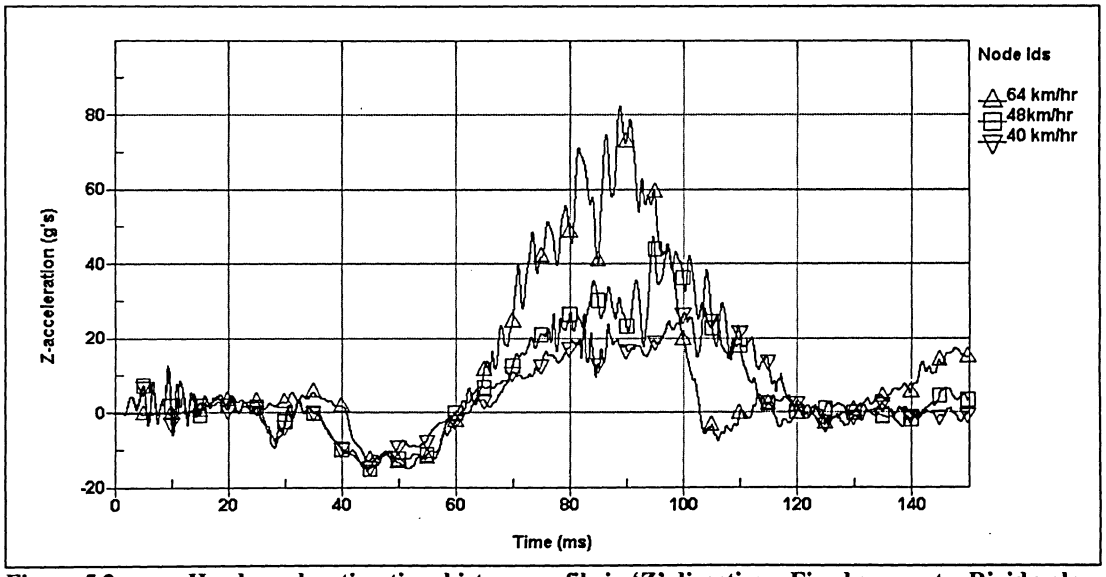

Figure 5.2 Head acceleration time history profile in 'Z' direction - Fixed support – Rigid pole – 64, 48, 40 km/hr

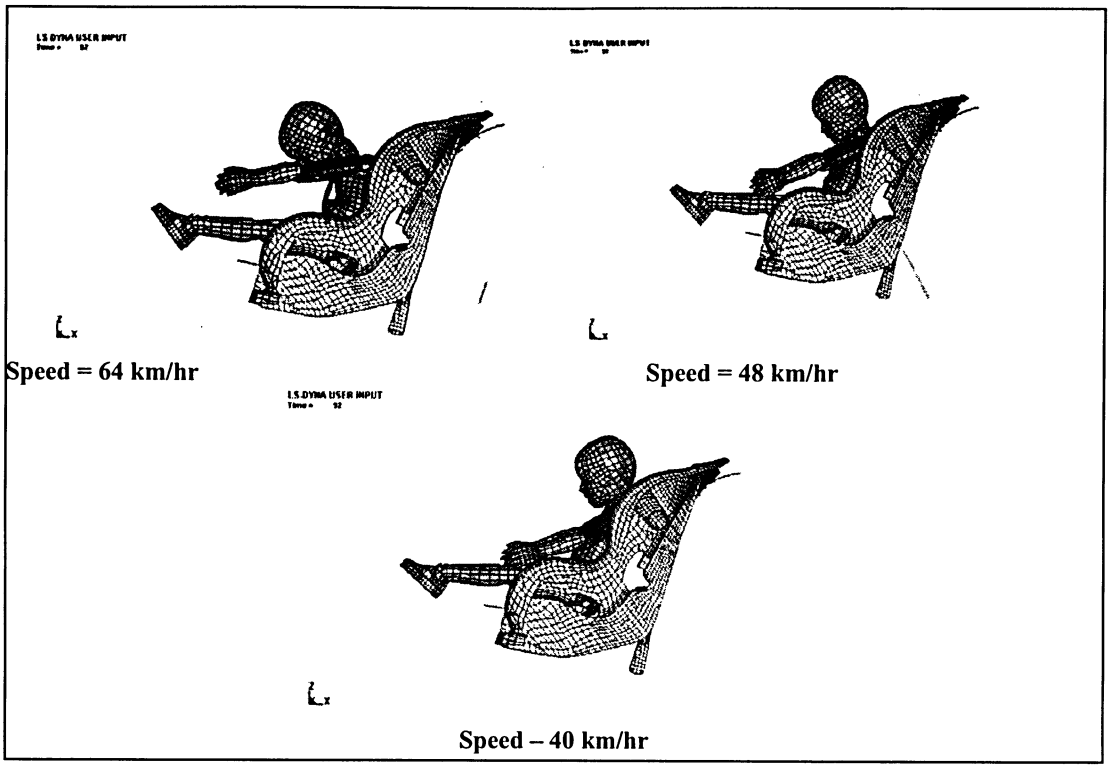

Figure 5.3 Schematic comparison of deflection profile for a 3 year old child model at 92ms after collision - "Fixed pole-rigid support" Impact scenario – 64, 48, 40 km/hr Speeds

5.3 Anchored Bolts - Steel Base Plate

This type of traffic support design is considered to be the most conventional steel pole system currently used in North America. The system is designed with a breakaway base built on top of a concrete foundation, and with anchor bolts embedded into the foundation as specified in the Canadian Highway Bridge Design Code [18]. This system is more favorable over the more conventional systems because it is designed to shear away during a severe vehicle collision. The breakaway point is designed to occur before the critical injury potential is reached in order to protect the occupants of the vehicle. The major disadvantage of such a system is the damage potential that the breakaway design can

inflict in a busy downtown intersection where mere minutes in delays to the intersection from fallen wires and lights can cause local business significant loss in revenue. The other disadvantage is the collateral damage to surrounding property such as buildings and/or injury or death to the civilians in a busy downtown area.

The results of the anchored base analysis are presented in Table 5.3. A total of 10 simulations were analyzed in order to investigate the child dummy response and are summarized in the following paragraphs of this chapter. The effects of steel vs. aluminum pole materials were first analyzed, followed by the effects of thickness variations to the shell section for the aluminum poles under investigation.

Table 5.3 Maximum values from time history results for anchored bolts system – Steel base simulation

		Anchored Base Simulation - 10 Runs Total								
Description	H.A.- 'X'	H.A. -'Z'	C.A. -'X'	C.A.-'Z'	R.U.N.F.	R.L.N.F.	R.U.N.M	R.L.N.M.	HIC 15	HIC 36
Limitation (NHTSA)			55	55	2120	2120	27	68	570	570
Sled Test.	-34	45	-63	-39	1300	1300	35	104	175	324
					STEEL POLE					
64 km/hr -3.05mm	-27.5	30.5	-26.7	-25.4	944	1144	34.6	103.8	75.2	225.4
% of Limit			49%	46%	45%	54%	128%	153%	13%	40%
48km/hr-3.05mm	-27.82	28.8	-27.3	-21.8	950.4	805.8	30.4	102.6	80.6	241.5
% of Limit			50%	40%	45%	38%	113%	151%	14%	42%
40km/hr-3.05mm	-20.5	16.6	-23.2	-14.2	670	565	23.6	75.7	34.5	102.7
% of Limit (NHTSA)			42%	26%	32%	27%	87%	111%	6%	18%
					ALUMINIUM POLE					
64km/hr -6.35mm	-27.1	32.9	-29.2	-27.7	1015	1103	29.2	96.4	89.1	266.4
% of Limit			53%	50%	48%	52%	108%	142%	16%	47%
64km/hr -5.05mm	-26.6	35.7	-27.5	-24.9	995	1096	28.3	92.5	95.2	281.9
% of Limit			50%	45%	47%	52%	105%	136%	17%	49%
64km/hr -4.80mm	-22.2	28.1	-22	-23.4	767	820	23.1	69.8	48.8	143
% of Limit			40%	43%	36%	39%	86%	103%	9%	25%
64km/hr -3.05mm	-20.7	18.8	-21.7	-21.1	733	645	20.4	69.5	43.3	128.1
% of Limit			39%	38%	35%	30%	76%	102%	8%	22%
48km/hr -4.80mm	-29.1	27.3	-26.5	-31.5	930	810	29.9	111.3	67.3	194.7
% of Limit			48%	57%	44%	38%	111%	164%	12%	34%
48km/hr -3.05mm	-18	17.5	-18.6	-16.7	581	523	18.2	63.8	32.8	93.7
% of Limit			34%	30%	27%	25%	67%	94%	6%	16%
40km/hr -4.80mm	-23.4	15.2	-22.9	-15.9	672	540	23.3	76.6	33.5	98.1
% of Limit			42%	29%	32%	25%	86%	113%	6%	17%

	STEEL POLE			ALUMINIUM POLE		
Vel. - Thickness	M.I.E.	T.0.V	T.M.H.X.	M.I.E.	T.0.V	T.M.H.X.
64km/hr -6.35mm				14.5	N/A	75
64km/hr -5.05mm				19.8	N/A	70
64km/hr -4.80mm				32.7	N/A	70
64km/hr -3.05mm	50.9	N/A	90	75.9	N/A	70
48km/hr -4.80mm				21.5	110	112
48km/hr -3.05mm	30.2	112	113	47.4	N/A	90
40km/hr -4.80mm				16.7	118	120
40km/hr -3.05mm	21.9	124	120			

H.A.- 'X'= Head Acceleration 'X' (g)
H.A. -'Z'= Head Acceleration 'Z' (g)
C.A. -'X'= Chest Acceleration 'X' (g)
C.A. -'Z'= Chest Acceleration 'Z' (g)
R.U.N.F= Resu. Upper Neck Force (N)
R.L.N.F= Resu.Lower Neck Force (N)
R.U.N.M= Res.Upper N. Moment (N·m)
R.L.N.M.=Resu.Lower N. Moment (N·m)
HIC 15= Head Injury Criteria 15ms
HIC 36= Head Injury Criteria 36ms
M.I.E=Max.Internal Energy (kJ)
(for Pole and Support System)
T.0.V.=Time of 0 Velocity (ms)
T.M.H.X.=Time of Max H.A.-'X' (ms)

5.3.1 Results for Steel and Aluminum Traffic Poles

Figure 5.4 illustrates the internal energy absorbed for the 64 km/hr stele pole simulation. From this figure it is evident that the absorbed energy for the pole and support system, including bolts, nuts, and steel base plate, begins to level out at approximately 58 ms. This pattern is directly related to the point in time when the anchored bolts of the support system begin the fracture causing the steel pole to completely shear away at a final time of approximately 64 ms. This pattern illustrates the designed shearing behavior of the anchored base support system. From the analysis of the results one can clearly observe that the critical HIC values are well below the theoretical threshold as originally predicted. The HIC 36 value is observed to be at 40% (225.4) of the 570 recommended limit by the NTHSA. The neck injury values are slightly above their limit for the upper and lower neck moments, however one cannot clearly state the effect of the injuries to the neck region since the Neck Injury Criteria is currently not available from the NHSTA as a reference for a 3-year-old child dummy. One can only assume that injury to this area is likely, one cannot predict to what extent. The important feature of the results is that severe injuries to the head are highly unlikely and that the chance of survival is very high.

From Figure 5.5 one can observe that the total absorbed energy for the 48 and 40 km/hr simulations takes on a different pattern than for the 64 km/hr simulation. For these cases, the absorbed energy continues to grow with time until the point is reached where the vehicle is close to the 0 velocity point, after which the vehicle starts to take on a negative velocity from the original trajectory. The internal energy for the 48 km/hr simulation is approximately 41% less than the 64 km/hr simulation, however the HIC values are in fact

slightly higher because the vehicle was brought completely to rest as opposed to the steel pole 64 km/hr condition described above. The 48 km/hr and 40 km/hr simulations are still below the critical HIC value of 570, and the design is valid in terms of survival for a 3-year child due to a head injury based only on a finite element analysis.

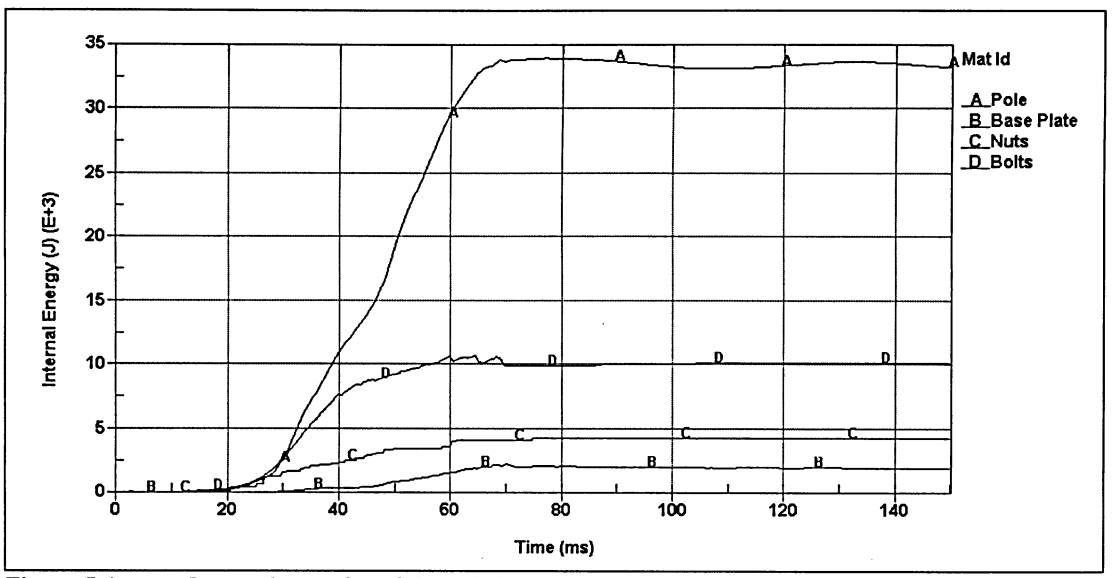

Figure 5.4 Internal energies of the pole/support system – (Anchored base – Steel pole – 64 km/hr)

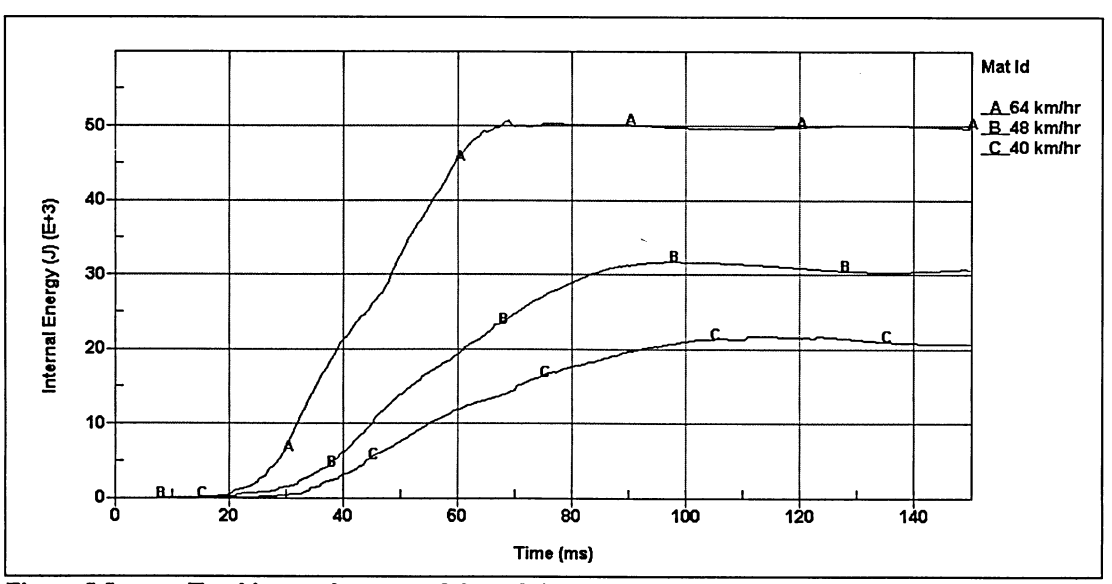

Figure 5.5 Total internal energy of the pole/support system – (Anchored base – Steel pole – 64, 48, 40 km/hr)

5.3.2 Aluminum Pole

The aluminum pole considered in this study follows similar patterns to the results from the steel pole discussed above. In addition to velocity variations, the effects of shell thickness for the laminar pole were also varied and analyzed in this section. This was undertaken because the pole of 3.05 mm thickness completely failed during impact velocity of 64 km/hr as per the schematic illustration in Figure 5.6.

Before discussing the effects of the traffic pole shell thickness, the effect of impact velocity was studied for 64, 48 and 40 km/hr. Similar trends were also observed for the 64 km/hr simulation in terms of internal energy absorption, as the 4.80 mm thick pole sheared away during impact after approximately 60 ms of simulation.

The HIC value for aluminum pole impacted at 64 km/hr speed was observed to be significantly lower at 144 as compared to the steel pole simulation recorded at 225.4. The HIC value of the aluminum pole impacted at 48 km/hr was recorded at 194.7 compared to 241.5 experienced for the steel pole simulation. The 40 km/hr aluminum pole simulation also out performed the steel pole by having critical HIC values lower by approximately 10% of the HIC value. To further understand the increase in performance of the aluminum pole, it is important to consider the internal energy absorbed by the system.

Figure 5.7 illustrates the time history graphs for the absorbed energy of the aluminum pole support system. The total energy absorbed by the aluminum pole compared to the

steel pole is slightly less because of higher deformation and flexibility characteristics of the pole material compared to the steel pole. As the aluminum pole structure got over-stressed, it continued to absorb the impact by balancing the kinetic energy of the crash against its strain energy and less with its internal energy compared to the steel pole. This extra flexibility in the aluminum pole has created greater shock absorption and has effectively lowered the injury risk criteria for the 3-year old child dummy model. This characteristic can be further observed from deflection time history profile of Figure 5.8 for the steel vs. aluminum design configurations for 48 and 40 km/hr impact speeds. The total body deflection is in average approximately 400 mm greater for the aluminum pole than that for the steel pole system.

In the case of thickness variation of the laminar pole shell, the amount of absorbed energy increases with decrease in the shell thickness. This energy decrease is directly attributed to the greater degree of deformation of the pole shell and crushing potential brought upon by a decrease in the pole thickness. As mentioned earlier, the pole completely fails at 3.05 mm during the 64 km/hr impact speed. In the case of 48 km/hr impact, the 3.05mm thick aluminum pole stays upright and effectively absorbs the energy and creates a favorable dummy response having the injury reference criteria well below the injury threshold limitation. In the case of pole shell thickness greater than 5.05 mm, the pole deforms less than the steel pole, thus increases the injury potential over the conventional 3.05 mm thick steel pole scenario.

In conclusion, the aluminum pole, namely the 4.80 mm pole shell thickness scenario, would be the preferred deign for the anchor bolts-steel base support system as it offers the lowest response in terms of injury criteria provided by the NHTSA. The steel material design is also satisfactory for use, however the results need to be further verified and validated with real life testing procedures before definite recommendations can be made based on current finite element analysis.

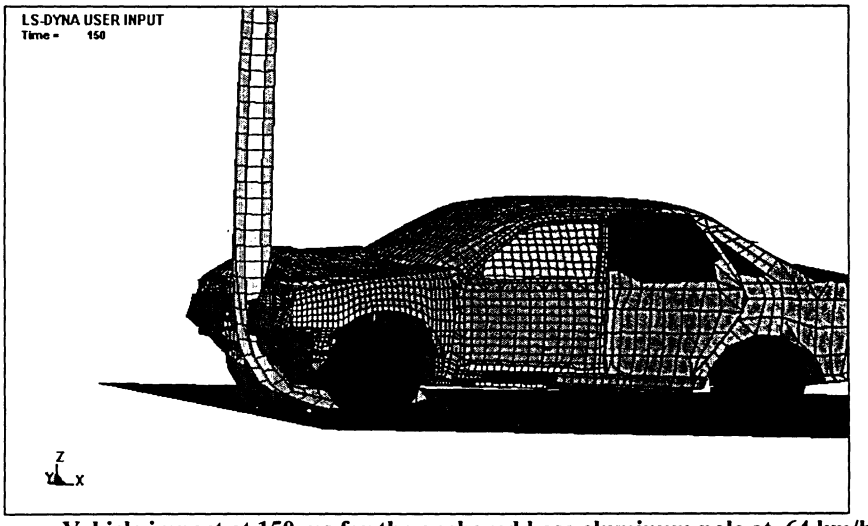

Figure 5.6 Vehicle impact at 150 ms for the anchored base aluminum pole at 64 km/hr speed

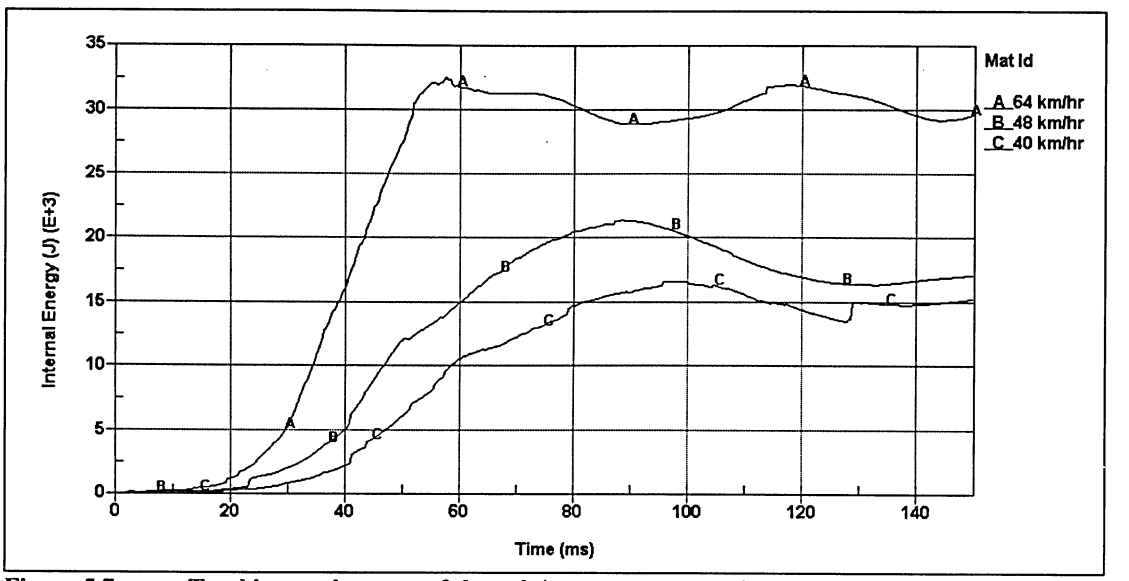

Figure 5.7 Total internal energy of the pole/support system – (Anchored base – 4.80mm thick - Aluminium pole – 64, 48, 40 km/hr)

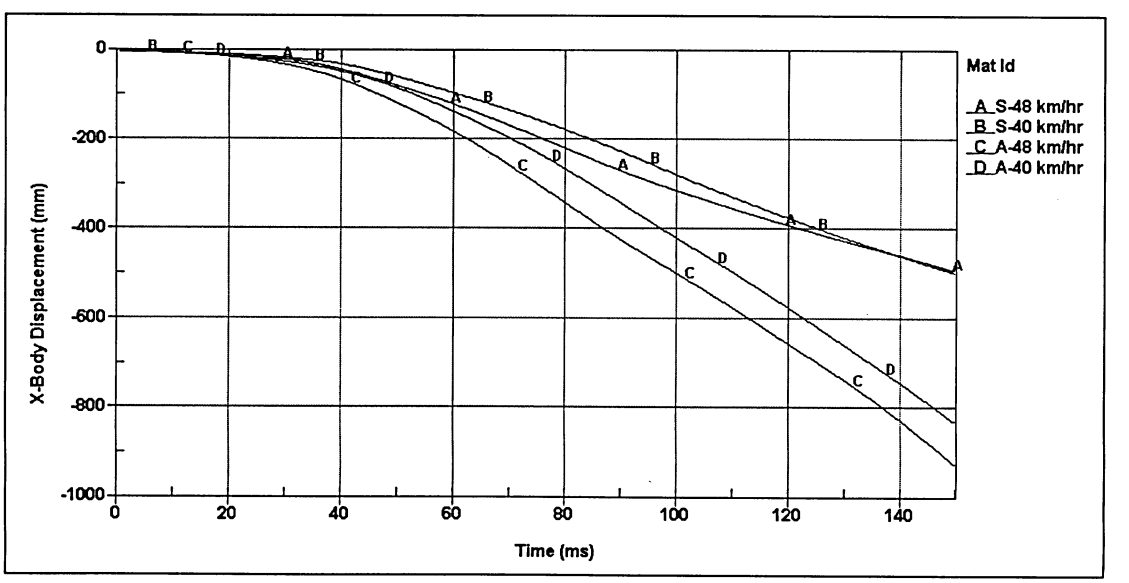

Figure 5.8 Deflection time history for steel ('S') and aluminium poles ('A')

5.4 Anchored Bolts/Springs – Steel Base Plate Condition

Similar to anchored bolts system of section 5.3, springs were used in this study to investigate the potential for any significant improvement in energy absorption characteristics to the base support system of the pole structure. A total of 6 simulations were analyzed, 3 runs for steel and 3 for aluminum, at 64, 48, and 40 km/hr velocities, respectively.

Based on Table 5.4, the results clearly indicate that the introduction of the springs/bolts base system creates a much stiffer response and a less desirable structure in terms of energy absorption compared with the conventional anchored bolts system. The majority of the results in terms of injury impact response results have all increased for both the steel and aluminum poles.

Referring to the energy absorption characteristics of this system in comparison to the standard anchored bolts system of section 5.3, we can clearly observe from the maximum values of Table 5.4 and Table 5.3 that the spring/bolts support system has absorbed less energy during the impact and in turn has created greater damage within the vehicle. The absorbed energy for the steel pole base plate-anchored bolts are 50.9, 30.2, and 21.9 kJ respectively, and are much less for the steel pole springs/bolts system at 32.3, 14.6, and 9.7 kJ respectively. This increase in stiffness can be further observed through the deflection time history profile illustrated between the anchored base and the springs/bolts system shown in Figure 5.9. From the figure, it becomes clear that the springs/bolts system (solid lines) lags the flexibility compared to the more conventional anchored base

system (light lines). Only the aluminum pole for the springs/bolts system comes close in deflection and resembles the flexibility of a steel pole system for the anchored base system. The spring system is approximately 300 mm stiffer in terms of deflection compared to the anchored system. This increase in rigidity creates a less favorable effect in terms of the occupant injury response as outlined per the results.

The anchored bolts system is very effective based on the current results and in terms of structural effectiveness between the support and pole interaction. The bolts are usually secondary in terms of energy absorption next to the pole, and this characteristic can be observed from Figure 5.4 of the previous section. The nuts and the base plate do not affect the results to a significant degree because their energy absorption and flexibility is quite low in comparison, however their interaction within the system contributes significantly to the overall effectiveness of the anchored bolts base support system.

Table 5.4 Maximum values from time history results for the springs/bolts base simulation

		Spring Base Simulation - 6 Runs Total								
Description	**H.A.- 'X'**	**H.A. -'Z'**	**C.A. -'X'**	**C.A.-'Z'**	**R.U.N.F.**	**R.L.N.F.**	**R.U.N.M**	**R.L.N.M.**	**HIC 15**	**HIC 36**
Limitation (NHTSA)			**55**	**55**	**2120**	**2120**	**27**	**68**	**570**	**570**
Sled Test.	**-34**	**45**	**-63**	**-39**	**1300**	**1300**	**35**	**104**	**175**	**324**
					STEEL POLE					
64 km/hr -3.05mm	-23.7	36	-29.7	-27.8	1127	1080	29.6	91.9	117.9	349.9
% of Limit			**54%**	**51%**	**53%**	**51%**	**110%**	**135%**	**21%**	**61%**
48km/hr-3.05mm	-29.1	-20.2	-42.1	-19	1243	1199	32.4	106.3	194.4	579.1
% of Limit			**77%**	**35%**	**59%**	**57%**	**120%**	**156%**	**34%**	**102%**
40km/hr-3.05mm	-24.7	27.8	-69.4	-16.3	935	1156	26.9	90.7	76.7	229.2
% of Limit			**126%**	**30%**	**44%**	**55%**	**100%**	**133%**	**13%**	**40%**
					ALUMINIUM POLE					
64km/hr -4.80mm	-26.9	34.4	34.6	-27.7	1074	1019	29.5	89	108.7	320.7
% of Limit			**-63%**	**50%**	**51%**	**48%**	**109%**	**131%**	**19%**	**56%**
48km/hr -4.80mm	-26.4	39.3	-34.3	-19.2	1206	1088	29.8	106.5	121.7	451
% of Limit			**62%**	**35%**	**57%**	**51%**	**110%**	**157%**	**21%**	**79%**
40km/hr -4.80mm	-25.9	30.6	-31	-15.3	1001	880	29.2	99.6	98.2	262.2
% of Limit			**56%**	**28%**	**47%**	**42%**	**108%**	**146%**	**17%**	**46%**

	STEEL POLE			ALUMINIUM POLE		
Vel. - Thickness	**M.I.E.**	**T.0.V**	**T.M.H.X.**	**M.I.E.**	**T.0.V**	**T.M.H.X.**
64km/hr -4.80mm				26.2	N/A - 8.4 mps	65
64km/hr -3.05mm	32.3	N/A - 8.1 mps	77			
48km/hr -4.80mm						
48km/hr -3.05mm	14.6	94	107	21.1	97	111
40km/hr -4.80mm						
40km/hr -3.05mm	9.7	96	108	11.4	96	106

H.A.- 'X'= Head Acceleration 'X' (g)
H.A. -'Z'= Head Acceleration 'Z' (g)
R.U.N.F= Resu. Upper Neck Force (N)
R.L.N.F= Resu.Lower Neck Force (N)
R.U.N.M= Res.Upper N. Moment (N·m)
R.L.N.M.=Resu.Lower N. Moment (N·m)
HIC 15= Head Injury Criteria 15ms
HIC 36= Head Injury Criteria 36ms
M.I.E= Max.Internal Energy (kJ)
(for Pole and Support System)
T.0.V.= Time of 0 Velocity (ms)
T.M.H.X.= Time of Max H.A.-'X' (ms)

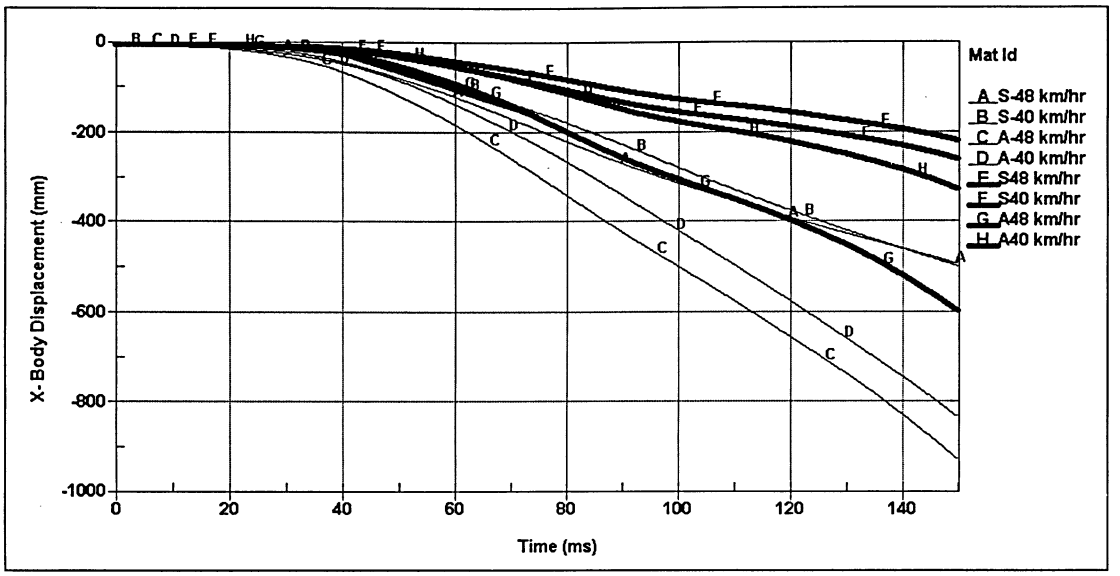

Figure 5.9 Deflection comparison profile for anchored base vs. springs/bolts base system (Light Lines: Anchored base system), (Solid Lines: Springs/Bolts system)

5.5 Anchored Bolts/Dampers - Steel Base Plate

The damper/bolts condition is a similar concept to the springs/bolts system, and contains a rubber material surrounding the bolts that lies between nuts and the base plate of the support system. This system was designed to increase the energy dissipation in the support system during a collision with minimized resistance in its reaction to the impulse.

The results from the bolts/damper system follow a similar pattern to that of the previous section and absorb more energy compared to the spring system. Similar to the results discussed for the springs/bolts system, the dampers/bolts system does not perform as favorable as the anchored base system, Table 5.5 and 5.2. This pattern is attributed to the fact that the rubber material surrounding the bolts creates less flexibility within and adds some kickback to the system, but is not as severe as the springs/bolts condition.

From Figure 5.10 of this section it is evident that the energy absorption is related to the base support type and generally deceases in value from anchored to damper to spring base systems for the pole structure designs under consideration. The energy absorption related to each base support type influences the severity of the injury response for the child occupant, but is not the main factor that contributes to the severity of the injury. This pattern however fluctuates and is not clearly correlated to the injury response for vehicle impact speed of 48 km/hr and greater. This is more evident for the aluminum pole simulation where the internal energy for the damper base system is actually greater than the anchored base system, and contradicts the previously observed logic between energy absorption and injury criteria.

To further investigate this contradiction, Table 5.6 of this section illustrates the deflection amongst different designs currently under review. From this table it becomes evident that the anchored base system deforms with a highest value in terms of average body deflection, followed by the damper system, and lastly the spring system. This deflection pattern is related to the level of injury observed for the three systems under consideration. As previously mentioned, the anchored base system has the most favorable results in terms of child safety and has the best deflection and energy absorption characteristics compared to the three base system designs under consideration.

The above noted characteristics, namely energy and deflection, also influence the time that the child dummy occupant reaches maximum head accelerations and zero velocity

times. In reference to Tables 5.3, 5.4, and 5.5 one can observe that the time to reach the zero velocity and maximum head acceleration for the anchored support system is significantly improved, and occurs on average between 10 to 25 ms later than the spring and damper systems. This pattern is a critical consideration that designers try to address while designing safe roadside structures. It becomes beneficial to extend the time to reach the maximum injury criteria and to extend the time to completely stop a vehicle between design improvements for a particular scenario. Normally, the severity of the injury, along with energy absorption and flexibility are directly related to the time that a vehicle completely stops, and in conjunction correlate to the occupant injury response. However, designers are also careful not to expose occupants to prolonged injury response in terms of time duration, and especially during the maximum response values, because the Head Injury Criterion is directly related to the time duration of maximum response.

Based on the results form the dampers/bolts base system, it becomes clearly evident that the dampers performed more favorable in terms of injury criteria compared to the spring system, however, the results are not as favorable as compared to the more conventional anchored base system most commonly used on North American roads.

Table 5.5 Maximum values from time history results for the damper/bolts base simulation

		Damper Base Simulation - 6 Runs Total								
Description	**H.A.- 'X'**	**H.A. -'Z'**	**C.A. -'X'**	**C.A.-'Z'**	**R.U.N.F.**	**R.L.N.F.**	**R.U.N.M**	**R.L.N.M.**	**HIC 15**	**HIC 36**
Limitation			**55**	**55**	**2120**	**2120**	**27**	**68**	**570**	**570**
Sled Test.	**-34**	**45**	**-63**	**-39**	**1300**	**1300**	**35**	**104**	**175**	**324**
					STEEL POLE					
64 km/hr -3.05mm	-23.5	33.7	-24	-30.9	1057	979	27.9	94.3	101	291.4
% of Limit			**44%**	**56%**	**50%**	**46%**	**103%**	**139%**	**18%**	**51%**
48km/hr-3.05mm	-24	29.9	-32.3	-20.9	945	855	29.2	98.3	119.2	347.6
% of Limit			**59%**	**38%**	**45%**	**40%**	**108%**	**145%**	**21%**	**61%**
40km/hr-3.05mm	-25.2	24.6	-27.4	-16.2	825	683	24.9	88.1	57.3	171.7
% of Limit			**50%**	**29%**	**39%**	**32%**	**92%**	**130%**	**10%**	**30%**
					ALUMINIUM POLE					
64km/hr -4.80mm	-26	36.9	-27.3	-30.5	1116	1084	27.7	95.7	113.6	337.5
% of Limit			**50%**	**55%**	**53%**	**51%**	**103%**	**141%**	**20%**	**59%**
48km/hr -4.80mm	-28.3	34.5	-34.3	-20.3	1129	1046	31.1	110.2	138	406.9
% of Limit			**62%**	**37%**	**53%**	**49%**	**115%**	**162%**	**24%**	**71%**
40km/hr -4.80mm	-24.2	24.8	-27.7	-15.3	842	704	23.7	88.2	55.6	165.1
% of Limit			**50%**	**28%**	**40%**	**33%**	**88%**	**130%**	**10%**	**29%**

	STEEL POLE			**ALUMINIUM POLE**		
Vel. - Thickness	**M.I.E.**	**T.0.V**	**T.M.H.X.**	**M.I.E.**	**T.0.V**	**T.M.H.X.**
64km/hr -4.80mm				37.3	N/A - 7.99mps	78
64km/hr -3.05mm	42.4	N/A-7.8mps	78			
48km/hr -4.80mm				22.3	101	115
48km/hr -3.05mm	30.3	102	116			
40km/hr -4.80mm						
40km/hr -3.05mm	18.4	105	118	14	104	118

H.A.- 'X'= Head Acceleration 'X' (g)
H.A. -'Z'= Head Acceleration 'Z' (g)
R.U.N.F= Resu. Upper Neck Force (N)
R.L.N.F= Resu.Lower Neck Force (N)
R.U.N.M= Res.Upper N. Moment (N·m)
R.L.N.M.=Resu.Lower N. Moment (N·m)
HIC 15= Head Injury Criteria 15ms
HIC 36= Head Injury Criteria 36ms
M.I.E= Max.Internal Energy (kJ)
(for Pole and Support System)
T.0.V.= Time of 0 Velocity (ms)
T.M.H.X.= Time of Max H.A.-'X' (ms)

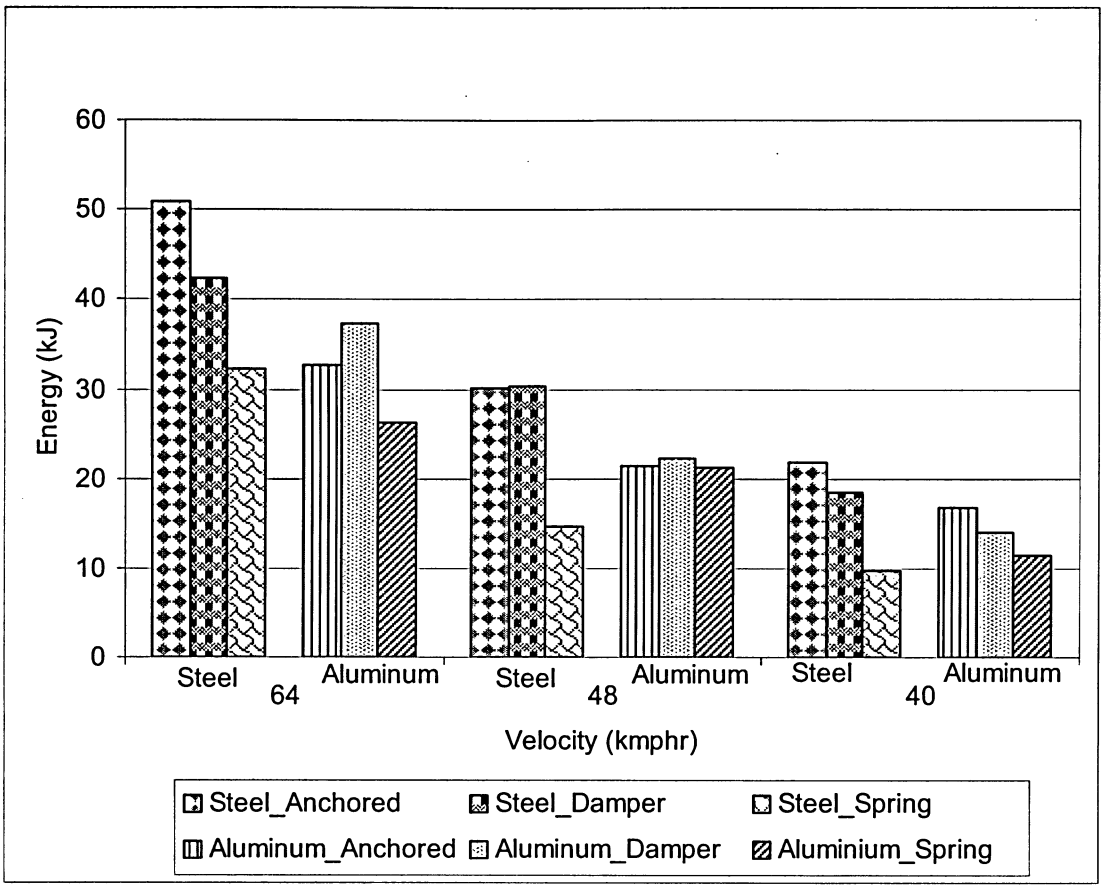

Figure 5.10 **Energy absorption comparisons between anchored, damper, and spring base supports for steel and aluminum poles, respectively**

Table 5.6 **Traffic pole body deflections**

	Pole Deflection (mm)					
	Steel pole			Aluminium pole		
	Anchored Support	Damper Support	Spring Support	Anchored Support	Damper Support	Spring Support
48 km/hr	491	427	256	926	755	595
40 km/hr	495	373	215	831	602	324

5.6 Fixed Support

This section of the results focuses on the effects of introducing a fixed support system for the steel and aluminum materials currently under investigation. This situation is considered in this study because many cities including the City of Toronto have poles with the fixed system still in use.

Based on the results from Table 5.7 it becomes evident that the fixed base support system in not a very favorable situation and should be avoided at all costs. The HIC results for both the steel and aluminum poles are similar in pattern and are over the NHTSA limit by roughly an average of 9%, including the lower neck moments exceeding the acceptable values by approximately 73% of the limit.

To further understand the effects of the fixed base system in terms of steel and aluminum pole materials, one must observe the effects of internal energies for this system in conjunction with the deflection profiles. From Figure 5.11 one can observe that the steel pole system has absorbed more energy than the aluminum pole system. The steel pole system in this section has greater absorption characteristics and deforms less in terms of average body motion, however it has greater internal deformation and energy absorption of the crash impulse. On the other hand, the aluminum pole system has greater flexibility and balances the crash impulse to a greater degree with its strain energy from the impact compared with the steel pole. This can be further observed from figure 5.12 noting the schematic illustration of the deflection comparisons between the steel and aluminum poles. The scenario on the left illustrates that the steel pole after the impact deforms less

and has greater internal damage as opposed to the aluminum pole that has more extensive deformation and has less internal damage.

Based on the results from this section, it becomes evident that the fixed pole system does not offer effective protection to the child occupant during a frontal 64 km/hr collision. It would be recommended to further investigate the fixed base system using field experiments to validate the design and determine whether the old designs are up to date in terms of satisfying the current standards.

In the next section, the fixed base design is modified with a solid rubber base cylinder section in order to minimize the forces experienced within the vehicle during a frontal collision.

Table 5.7 Maximum values from time history results of the fixed base simulation

		Fixed Base Simulation - 2 Runs Total								
Description	H.A.-'X'	H.A. -'Z'	C.A. -'X'	C.A.-'Z'	R.U.N.F.	R.L.N.F.	R.U.N.M	R.L.N.M.	HIC 15	HIC 36
Limitation			55	55	2120	2120	27	68	570	570
Sled Test.	-34	45	-63	-39	1300	1300	35	104	175	324
STEEL POLE										
64 km/hr -3.05mm	-28.9	47	-39.6	-29.1	1415	1309	33.8	117.5	206.1	610.6
% of Limit			72%	53%	67%	62%	125%	173%	36%	107%
ALUMINIUM POLE										
64km/hr -4.80mm	-29.4	48.4	-41	-30.2	1372	1371	30.2	117.7	210	629.9
% of Limit			75%	55%	65%	65%	112%	173%	37%	111%

	STEEL POLE			ALUMINIUM POLE		
Vel. - Thickness	M.I.E.	T.0.V	T.M.H.X.	M.I.E.	T.0.V	T.M.H.X.
64km/hr -3.05mm	68.5	115	98			
64km/hr- 4.80mm				62	105	80

H.A.-'X'= Head Acceleration 'X' (g)
H.A. -'Z'= Head Acceleration 'Z' (g)
C.A. -'X'= Chest Acceleration 'X' (g)
C.A. -'Z'= Chest Acceleration 'Z' (g)
R.U.N.F= Resu. Upper Neck Force (N)
R.L.N.F= Resu.Lower Neck Force (N)
R.U.N.M= Res.Upper N. Moment (N·m)
R.L.N.M.=Resu.Lower N. Moment (N·m)
HIC 15= Head Injury Criteria 15ms
HIC 36= Head Injury Criteria 36ms
M.I.E= Max.Internal Energy (kJ)
(for Pole and Support System)
T.0.V.=Time of 0 Velocity (ms)
T.M.H.X.=Time of Max H.A.-'X' (ms)

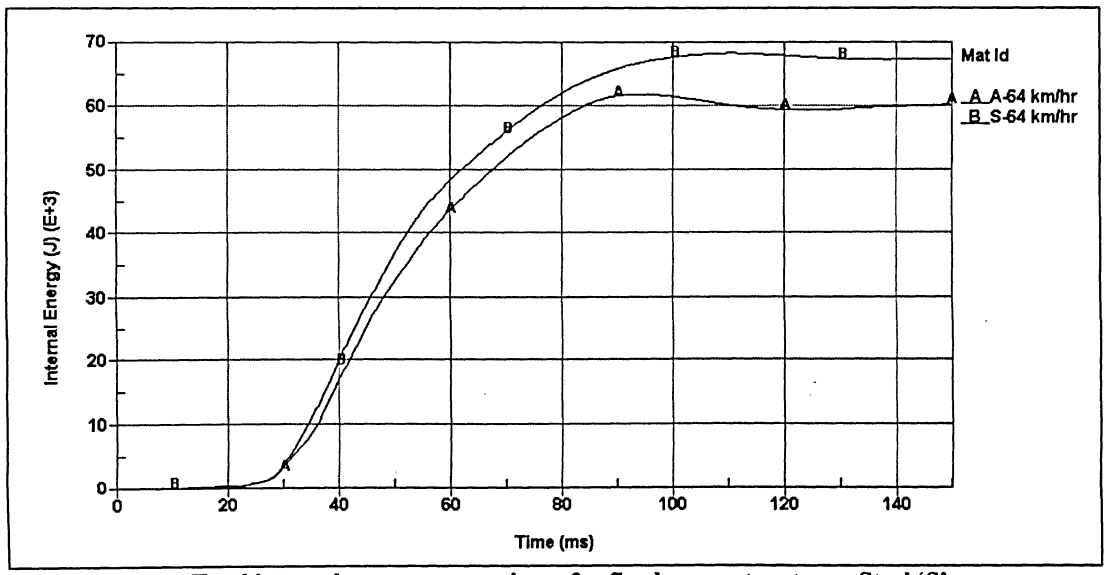

Figure 5.11 Total internal energy comparisons for fixed support system – Steel 'S' vs. Aluminum 'A' poles

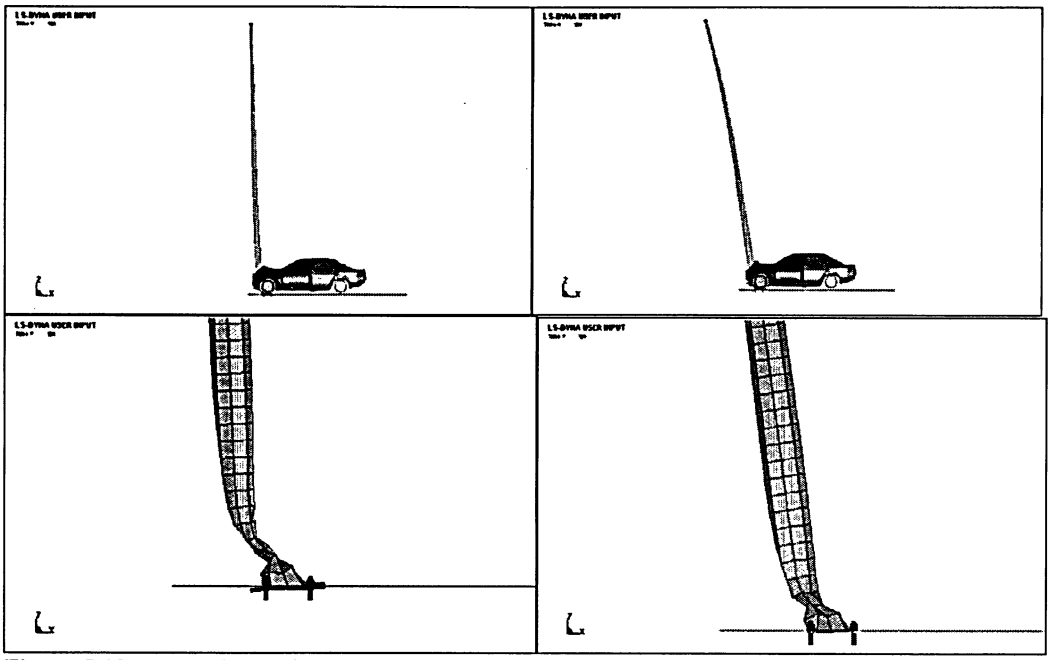

Figure 5.12 Deformation and deflection comparison between steel (left) and aluminum (right) traffic poles

5.7 Rubber Base – Fixed Support

In this section the design under consideration is composed of a steel pole attached to a solid rubber base pole via a fixed connection, and is connected to the ground via a base pate and a fixed support system. The rubber base provided is set at approximately 600 mm in height is order to absorb the impact force while in contact with the vehicles front end and the bumper system.

This design was performed to study the effects of having a more flexible material involved when a fixed support is introduced into the pole design system. The results

from Table 5.8 clearly indicate that rubber cylinder made of very flexible material caused the injury response of child dummy to increase. Based on the results one can clearly observe that very little internal energy is absorbed by the rubber-steel pole fixed support system, namely 28.3 kJ as opposed to the 68.5 and 62 kJ absorbed by the steel and aluminum systems for the standard fixed base system described in the previous section. This pattern clearly becomes evident while studying the total energy absorbed in a graphical format based on Figure 5.13. In this figure one can observe the energy differences between the various poles and the support systems.

To further investigate this characteristic, Figure 5.14 provides the internal energy absorbed for the pole materials only as opposed to the rubber support system previously considered. From this figure one can observe that the rubber solid support of the pole absorbs less energy as compared to the whole pole system previously described in Figure 5.13. Graph C in Figure 5.14 represents the steel portion of the pole that is attached to the rubber section. The steel portion is shown to absorb more energy compared to the rubber support and is not in direct contact with the impacting vehicle. Graph D in this figure indicates the low magnitude of the energy absorbed by the rubber support during impact. Also, one can observe that the peak internal energy is approximately 5 kJ and is reached during the 74 ms point of impact. The maximum energy of 5 kJ is held constant until the 80 ms point, which also represents the time that the vehicle has reached the zero velocity mark. After 80 ms from the start of impact, the internal energy starts to decrease until it reaches a value of 0.8 kJ at the 150 ms from the start of impact.

After the 80 ms point after impact, it becomes quite evident that the elastic characteristics, based on the results of the rubber material, force the pole to spring back to its original shape. There is little damage to the rubber section and the internal deformations are quite minor compared to the steel and aluminum poles, Figure 5.15. For the steel and aluminum sections, the deformations are permanent and the absorbed energy slightly decreases after the maximum point is reached as per Figure 5.14. In terms of occupant safety, this characteristic is of significance because the energy absorbed by the pole decreases the vehicle's own internal energy and in turn creates a more favorable environment for the occupants. Figure 5.15 schematically illustrates the differences in shell deformation between the rubber support, steel pole, and aluminum pole structures for the fixed support system impacted at a speed of 64 km/hr. From this figure the rubber solid support is shown to exhibit very little internal deformation, followed by the aluminum pole and lastly the steel pole.

In conclusion, the rubber base material is not a desirable alternative to the conventional steel and aluminum pole designs because the material does not absorb the impact energy well and causes greater damage within the impacting vehicle. This damage should always be minimized in order to reduce the injury potential to the occupants and therefore a more suitable design needs to be considered.

Table 5.8 Maximum values from time history results of the fixed rubber base simulation

		Rubber Base Simulation - 3 Runs Total								
Description	H.A.- 'X'	H.A. -'Z'	C.A. -'X'	C.A.-'Z'	R.U.N.F.	R.L.N.F.	R.U.N.M	R.L.N.M.	HIC 15	HIC 36
Limitation			55	55	2120	2120	27	68	570	570
Sled Test.	-34	45	-63	-39	1300	1300	35	104	175	324
RUBBER BASE										
64 km/hr -Solid	-39.5	65.5	-68.5	-36.9	1780	2022	41.1	136.5	641.9	1871
% of Limit			125%	67%	84%	95%	152%	201%	113%	328%
48km/hr-Solid	-27.7	39.5	-38.1	-27.7	1223	1103	32.4	108.5	136.3	538.9
% of Limit			69%	50%	58%	52%	120%	160%	24%	95%
40km/hr-Solid	-25	33.1	-30	-20.2	1120	960	32.1	98.3	118.3	349.8
% of Limit			55%	37%	53%	45%	119%	145%	21%	61%

	RUBBER BASE		
Vel. - Thickness	M.I.E.	T.0.V	T.M.H.X.
64km/hr -Solid	28.3	80	100
48km/hr -Solid	14.1	85	110
40km/hr -Solid	9.5	84	104

H.A.- 'X'= Head Acceleration 'X' (g)
H.A. -'Z'= Head Acceleration 'Z' (g)
R.U.N.F= Resu. Upper Neck Force (N)
R.L.N.F= Resu.Lower Neck Force (N)
R.U.N.M= Res.Upper N. Moment (N·m)
R.L.N.M.=Resu.Lower N. Moment (N·m)
HIC 15= Head Injury Criteria 15ms
HIC 36= Head Injury Criteria 36ms
M.I.E= Max.Internal Energy (kJ)
(for Pole and Support System)
T.0.V.= Time of 0 Velocity (ms)
T.M.H.X.= Time of Max H.A.-'X' (ms)

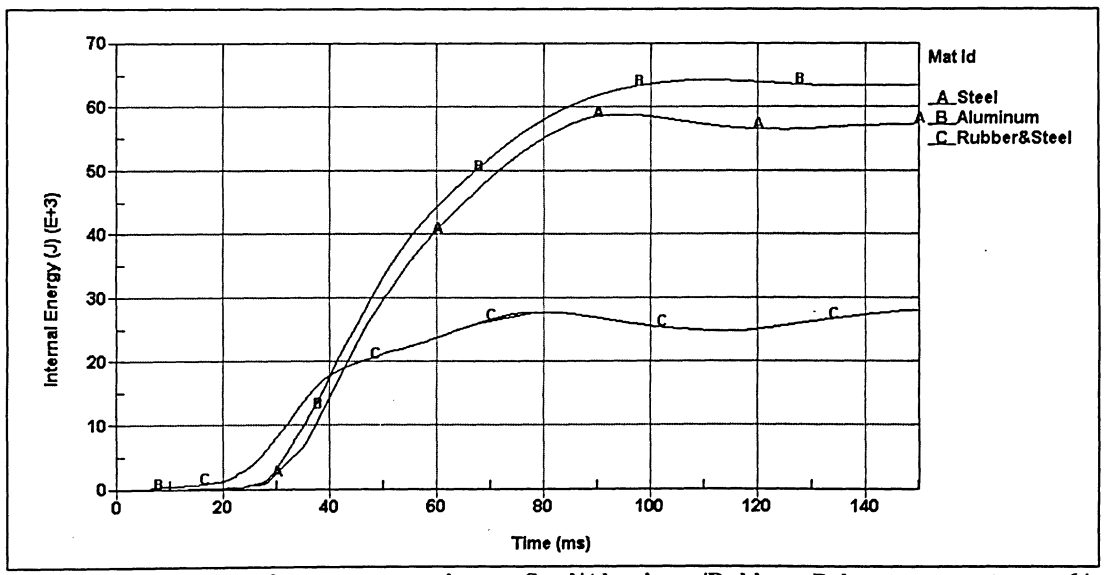

Figure 5.13 Internal energy comparisons – Steel/Aluminum/Rubber - Pole support systems – 64 km/hr impact speed

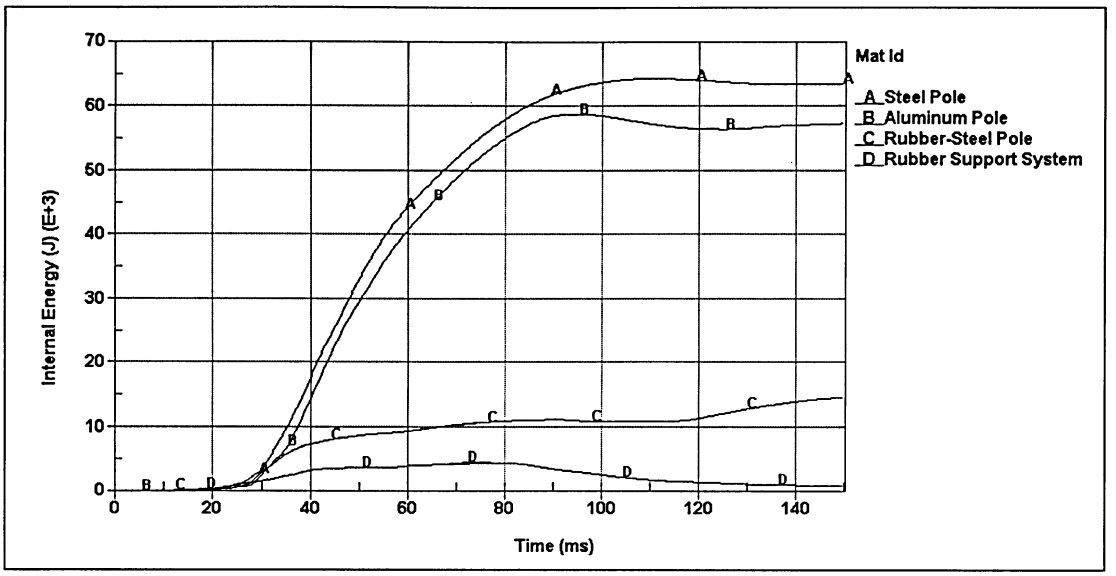

Figure 5.14 Internal energy comparisons for pole materials only – Steel/Aluminum/Rubber-Steel for 64km/hr

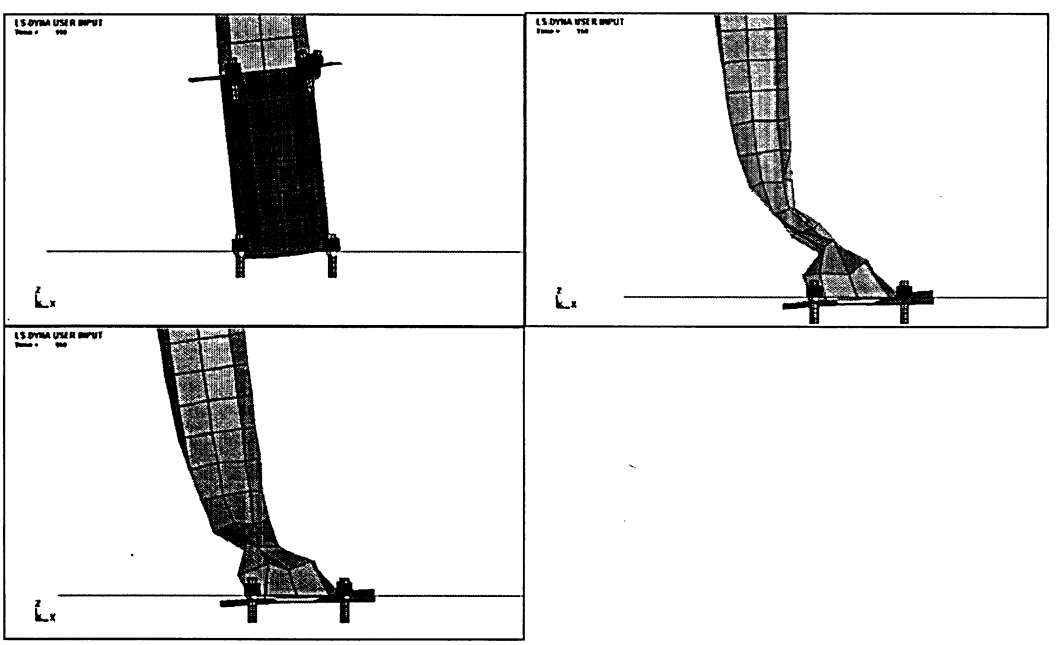

Figure 5.15 Schematic views of rubber support system (Top Left), steel (Top Right), and aluminum (Bottom) poles after 150 ms of 64 km/hr impact speed

5.8 Traffic Pole Embedded Into Soil Support

In this section, the effect of embedding a pole directly into the soil is investigated for a clay and sand soils. The soil is represented by spring elements, surrounding the embedded pole portions that are defined to act in compression only as described in the previous chapters. The objective of this section is to provide traffic poles strong enough during minor impacts and under service loading, and yet to remain flexible enough to avoid serious injury to the occupants within the vehicle.

5.8.1 Pole Embedded in Clay Soil

A total of 9 simulations were performed as per Table 5.9. The first part of this analysis focused on determining the appropriate thickness for the steel and aluminum poles used in this study. The shell thickness for the aluminum pole of 4.20 mm offered little lateral resistance to the extreme forces experienced during the impact and in turn failed completely during the simulation of 150 ms. The section had to be increased to 5.05 mm so that the most desirable protection against the lateral forces experienced during the impact is achieved. The 5.05 mm aluminum pole was observed to be highly deformable through the soil base support, and did not fall down after the impact. The steel pole also failed at its original studied thickness of 3.05 mm and had to be increased to 4.05 mm in order to provide desirable results. Figure 5.16 illustrates the internal energy absorbed by the steel pole for three different shell thickness, namely: 4.05, 4.20, and 5.05 mm. The

4.05 mm shell absorbed the greatest amount of internal energy, and offered most favorable results in terms of child injury response.

In the next part of analysis of this section, the steel and aluminum pole materials are directly compared against their respected impact velocities. For comparison purposes, the steel pole thickness was set at 5.05 mm in order to keep parameters consistent and to analyze the effect of material embedment for a clay soil type.

Based on the results from Table 5.9, the aluminum pole offered the greatest protection in terms of occupant injury response. The injury criteria values were below their limit and the results alone are favorable. However, when observing the impact scenario, one can observe that the pole twisted and rotated significantly under the impact condition and influenced the effectiveness of the springs which are meant to represent the clay soil under consideration. The steel pole had less significant rotation and twist and in turn offered more realistic results. From Table 5.9, the vehicle velocity for the aluminum pole at the end of 150 ms of impact was observed at 19 km/hr and 11km/hr for the 64 and 48 km/hr simulations, respectively. This characteristic indicates that the springs were not effective during the impact and provided less than the required design resistance for the 1.2 m deep clay soil type. Despite the instability of the aluminum pole configuration, the simulations were further analyzed with respect to the remaining soil conditions in order to generally study the effects of the embedment depths and soil type with respect to aluminum material properties. The aluminum pole results were required in order to

reinforce, if applicable, the characteristics of the steel pole with respect to the effects of varying soil conditions.

Although the injury response criteria for the steel pole is more severe compared to the aluminum pole, the steel material would still be recommended for use based on the limitations provided by the NHSTA. However, the author of this thesis questions the effectiveness of the method currently employed to study the effect of embedding poles in soils represented by springs. There are no validations currently available to date using vehicles and child dummy models with this method and more up to date field tests need to be performed in order to offer confidence with this method. The author recommends modeling the complex characteristics of the soil material using more advanced finite element techniques that can represent the various soil parameters most effectively and should be the focus of future studies.

Table 5.10 summarizes the results for the aluminum and steel poles in reference to embedded depths vs. impact velocity. From the table it becomes quite evident that the severity of the injury response increases with each increase in embedment depth. The actual difference between the 1.8 m and 1.2 m embedment depths in terms of injury criteria for the steel pole is approximately 50 for HIC 36 limiting parameter, Figure 5.17. The majority of the injury reference values appear to be in satisfactory levels in terms of the NHTSA posted injury limit for a 3-year old child dummy. Only the lower neck moment appears to exceed this criterion, however the rest of the neck injury parameters

seem to be below their respected limits. This patterns indicates that the risk of injury to the neck region is likely, but is not considered sever and life threatening.

Table 5.9 Maximum values from time history results for embedded pole into clay soil – 1.2m deep

		Clay 1.2m - 9 Runs Total								
Description	**H.A.- 'X'**	**H.A. -'Z'**	**C.A. -'X'**	**C.A.-'Z'**	**R.U.N.F.**	**R.L.N.F.**	**R.U.N.M**	**R.L.N.M.**	**HIC 15**	**HIC 36**
Limitation			**55**	**55**	**2120**	**2120**	**27**	**68**	**570**	**570**
Sled Test.	**-34**	**45**	**-63**	**-39**	**1300**	**1300**	**35**	**104**	**175**	**324**
					STEEL POLE					
64 km/hr -5.05mm	-27.6	37.1	-27.6	-31.54	1143	1110	21.9	99.1	116.7	349.2
% of Limit			**50%**	**57%**	**54%**	**52%**	**81%**	**146%**	**20%**	**61%**
64km/hr-4.20mm	-26.6	31.2	-23.9	-30.5	1053	1002	18.7	87.7	106	315.3
% of Limit			**43%**	**55%**	**50%**	**47%**	**69%**	**129%**	**19%**	**55%**
64km/hr-4.05mm	-25.3	30.5	-21.6	-30.1	1021	1000	20.1	83.5	95.7	284.6
% of Limit			**39%**	**55%**	**48%**	**47%**	**74%**	**123%**	**17%**	**50%**
48km/hr-5.05mm	-23.4	38.1	-24.3	-22.1	1154	951	23.3	75.8	122.5	367.1
% of Limit			**44%**	**40%**	**54%**	**45%**	**86%**	**111%**	**21%**	**64%**
48km/hr-4.20mm	-17.6	22.3	-19.7	-20.6	743	725	16.3	65.3	46	136.9
% of Limit			**36%**	**37%**	**35%**	**34%**	**60%**	**96%**	**8%**	**24%**
40km/hr-5.05mm	-18.9	21.3	-19.6	-12.5	749	963	19.2	64.5	42.5	126.8
% of Limit			**36%**	**23%**	**35%**	**45%**	**71%**	**95%**	**7%**	**22%**
					ALUMINIUM POLE					
64km/hr -5.05mm	-19.1	20.4	-16.1	-21.7	747	648	15.5	63.2	47.3	141.4
% of Limit			**29%**	**39%**	**35%**	**31%**	**57%**	**93%**	**8%**	**25%**
48km/hr -5.05mm	-12.2	-10.2	-11	-15.6	400	430	12.2	46	18.7	52.5
% of Limit			**20%**	**28%**	**19%**	**20%**	**45%**	**68%**	**3%**	**9%**
40km/hr -5.05mm	-10.1	8.8	-9.7	-11.7	324	334	10.7	35.5	10.4	29.5
% of Limit			**18%**	**21%**	**15%**	**16%**	**40%**	**52%**	**2%**	**5%**

	STEEL POLE			ALUMINIUM POLE		
Vel. - Thickness	**M.I.E.**	**T.0.V**	**T.M.H.X.**	**M.I.E.**	**T.0.V**	**T.M.H.X.**
64 km/hr -5.05mm	59.4	N/A - 3.1mps	70	75.3	N/A-5.3mps	72
64km/hr-4.20mm	84.6	N/A - 3.0mps	72			
64km/hr-4.05mm	90	N/A - 3.9mps	73			
48km/hr-5.05mm	19.7	N/A - 1.0mps	90	33.2	N/A-3.6mps	77
48km/hr-4.20mm	30.1	N/A -1.4mps	91			
40km/hr-5.05mm	9	N/A - 1.2mps	80	20.1	N/A - 2.6mps	68

H.A.- 'X'= Head Acceleration 'X' (g)
H.A. -'Z'= Head Acceleration 'Z' (g)
R.U.N.F= Resu. Upper Neck Force (N)
R.L.N.F= Resu.Lower Neck Force (N)
R.U.N.M= Res.Upper N. Moment (N·m)
R.L.N.M.=Resu.Lower N. Moment (N·m)
HIC 15= Head Injury Criteria 15ms
HIC 36= Head Injury Criteria 36ms
M.I.E= Max.Internal Energy (kJ)
(for Pole and Support System)
T.0.V.= Time of 0 Velocity (ms)
T.M.H.X.= Time of Max H.A.-'X' (ms)

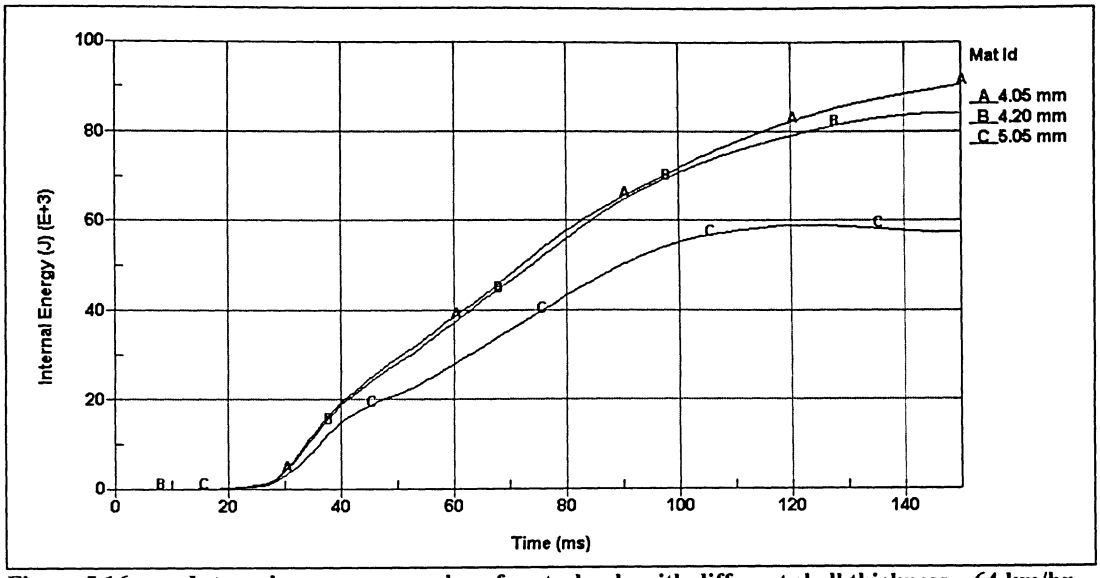

Figure 5.16 Internal energy comparison for steel pole with different shell thickness – 64 km/hr impact speed - 1.2m clay embedment depth

Table 5.10 Maximum values from time history results - Clay soil comparison for different embedment lengths

		Clay Comparison Table								
Description	H.A.-'X'	H.A. -'Z'	C.A. -'X'	C.A.-'Z'	R.U.N.F.	R.L.N.F.	R.U.N.M	R.L.N.M.	HIC 15	HIC 36
Limitation			55	55	2120	2120	27	68	570	570
Sled Test.	-34	45	-63	-39	1300	1300	35	104	175	324
					STEEL POLE					
64 km/hr - 1.8m	-26.4	38.4	-28.1	-31.3	1212	1129	20.6	99.7	133	399
64 km/hr - 1.5m	-27	37.75	-27.85	-31.42	1177.5	1119.5	21.25	99.4	124.85	374.1
64 km/hr - 1.2m	-27.6	37.1	-27.6	-31.54	1143	1110	21.9	99.1	116.7	349.2
48km/hr-1.8m	-23.9	31.7	-25.6	-22.6	1025	868	21	73.8	98.9	292.6
48km/hr-1.5m	-21.7	30	-24.8	-22.8	898	915	20.8	72.1	77	228.5
48km/hr-1.2m	-23.4	38.1	-24.3	-22.1	1154	951	23.3	75.8	122.5	367.1
40km/hr-1.8m	-18	17.9	-20.4	-13.8	689	664	20.1	64.9	34.7	103.3
40km/hr-1.5m	-18	17.7	-19	-12.6	655	641	19.2	65.2	31.8	94.8
40km/hr-1.2m	-18.9	21.3	-19.6	-12.5	749	963	19.2	64.5	42.5	126.8
					ALUMINIUM POLE					
64km/hr - 1.8m	-18.9	22.6	-16.1	-21.5	811	616	14.9	62.9	58.7	172.5
64km/hr - 1.5m	-20.3	22.1	-13.8	-23.9	779	674	15.9	68.6	50.9	151.4
64km/hr - 1.2m	-19.1	20.4	-16.1	-21.7	747	648	15.5	63.2	47.3	141.4
48km/hr - 1.8m	-13.1	-10	-12.8	-16.1	405.1	463	13.8	45	18.7	53.6
48km/hr - 1.5m	-13.2	-11.8	-11.7	-19	430	516	14.6	47.6	33.4	92.8
48km/hr - 1.2m	-12.2	-10.2	-11	-15.6	400	430	12.2	46	18.7	52.5
40km/hr - 1.8m	-10.1	8.6	-10.2	-12	332.5	345	10.6	34.7	10.7	29.3
40km/hr - 1.5m	-10.5	9	-11.7	-14.4	349	380	11.7	37.4	10.7	30.3
40km/hr - 1.2m	-10.1	8.8	-9.7	-11.7	324	334	10.7	35.5	10.4	29.5

	STEEL POLE			ALUMINIUM POLE		
Vel. - Thickness	M.I.E.	T.0.V	T.M.H.X.	M.I.E.	T.0.V	T.M.H.X.
64 km/hr - 1.8m	60.9	N/A-2.0mps	82	74.4	N/A-5.0mps	70
64 km/hr - 1.5m	60.5	N/A-2.5mps	72	75.9	N/A-5.6mps	79
64 km/hr - 1.2m	59.4	N/A - 3.1mps	70	75.3	N/A-5.3mps	72
48km/hr - 1.8m	19.3	N/A-.9mps	85	35	N/A-3.1mps	63
48km/hr - 1.5m	19.3	N/A-.9mps	79	35	N/A-3.1mps	70
48km/hr - 1.2m	19.7	N/A - 1.0mps	90	33.2	N/A-3.6mps	77
40km/hr - 1.8m	19.3	N/A-.9mps	85	35	N/A-3.1mps	63
40km/hr - 1.5m	8.9	N/A-1.1mps	90	20.2	N/A-2.9mps	76
40km/hr - 1.2m	9	N/A - 1.2mps	80	20.1	N/A - 2.6mps	68

H.A.- 'X'= Head Acceleration 'X' (g)
H.A. -'Z'= Head Acceleration 'Z' (g)
R.U.N.F= Resu. Upper Neck Force (N)
R.L.N.F= Resu.Lower Neck Force (N)
R.U.N.M= Res.Upper N. Moment (N·m)
R.L.N.M.=Resu.Lower N. Moment (N·m)
HIC 15= Head Injury Criteria 15ms
HIC 36= Head Injury Criteria 36ms
M.I.E= Max.Internal Energy (kJ)
(for Pole and Support System)
T.0.V.= Time of 0 Velocity (ms)
T.M.H.X.= Time of Max H.A.-'X' (ms)

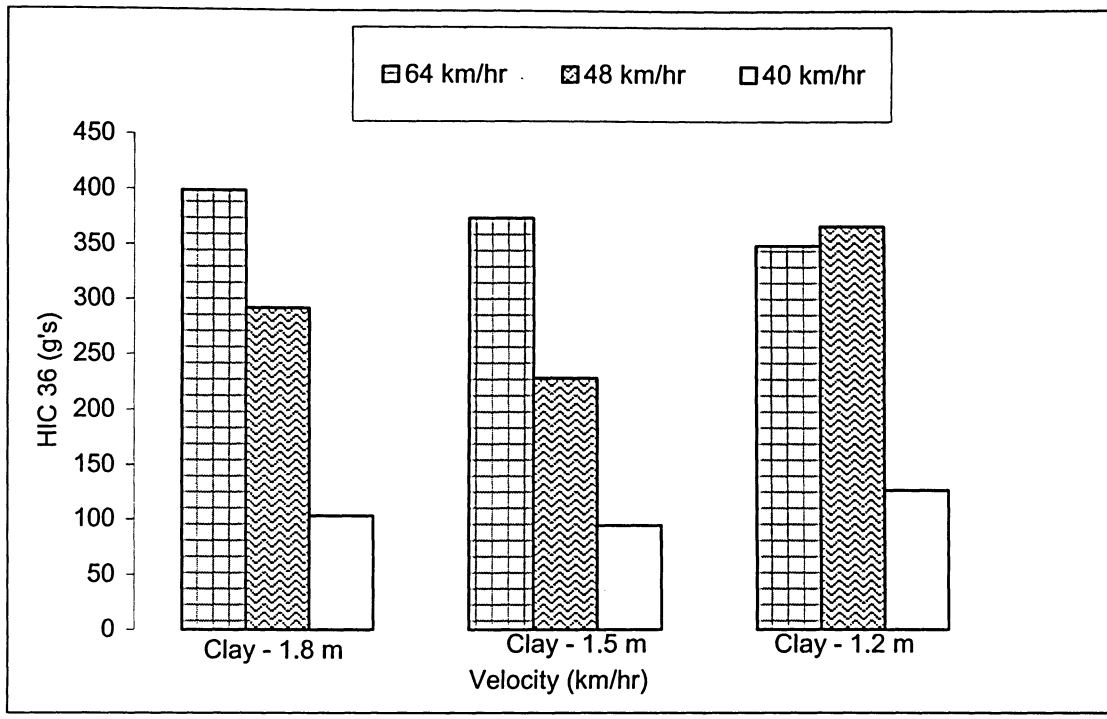

Figure 5.17 HIC 36 comparison for clay soil – Embedded pole Depths vs. Velocity – Steel pole

5.8.2 Pole Embedment in Sandy Soil

One of the disadvantages of the clay soil type is that the soil has poor drainage characteristics, and during a rain event, swells and absorbs the water internally. This characteristic is not favorable in terms of required performance and can cause the soil to act much stiffer than anticipated during cold weather conditions when the water tends to freeze. To overcome these disadvantages, the sandy soil as described in chapter 3 of this thesis in considered for the impact analysis. Sand has very good drainage properties and provides fairly consistent performance throughout the weather extremes. One disadvantage of the sandy soil is the increase in lateral bearing resistance compared to the clay soil type. Thus, this section of the thesis investigates the influence of the increased

lateral resistance for a sandy soil in terms of occupant injury response compared to the clay soil previously discussed.

Table 5.11 of this section summarizes the results for the sandy soil versus embedment depths for the steel and aluminum poles. From this figure we can observe that the results are very similar to the clay soil described in Table 5.10. The injury parameters are similar in range for both soil types. The slight difference is in the absorbed energy for the pole and support system for the sandy soil condition. It is observed that the sandy soil system absorbs less energy due to a stiffer response induced from the properties of the soil. The graphical comparison of the results for the clay and sandy soil types are not reported herein because the results vary between the two soils with no clear patterns observed.

Table 5.11 Maximum values from time history results – Sandy soil comparison for different embedment lengths

		Sand Comparison Table								
Description	H.A.- 'X'	H.A. -'Z'	C.A. -'X'	C.A.-'Z'	R.U.N.F.	R.L.N.F.	R.U.N.M	R.L.N.M.	HIC 15	HIC 36
Limitation			55	55	2120	2120	27	68	570	570
Sled Test.	-34	45	-63	-39	1300	1300	35	104	175	324
STEEL POLE										
64 km/hr - 1.8m	-25.4	37.4	-27.5	-31.3	1165	1052	20	97.8	124	369.5
64 km/hr - 1.5m	-29.7	36.4	-27.4	-31	1188	1029	22.8	98.8	137.2	410.4
64 km/hr - 1.2m	-26.6	35.6	-27.7	-30.9	1141	1062	21	99.5	113.4	337.9
48km/hr - 1.8m	-23.1	37.3	-26.7	-22	1140	975	22.1	75.4	142.2	423
48km/hr - 1.5m	-21.1	29.2	-25.3	-21.9	892	866	22.1	71.4	71.9	214.3
48km/hr - 1.2m	-20.1	28.3	-25.3	-21.5	917	834	22.7	72.1	81.2	240.2
40km/hr - 1.8m	-18.1	18	-19.9	-15.6	659	655	19.1	67.3	30.4	90.9
40km/hr - 1.5m	-16.9	17.1	-18.9	-13.2	617	611	17.6	64.7	25.8	77.13
40km/hr - 1.2m	-16.2	18.3	-18.7	-17.8	637	644	18.7	62.8	29.5	87.5
ALUMINIUM POLE										
64km/hr - 1.8m	-16.9	16.3	-17.3	-21.3	610	547	16.3	61.4	37.7	106.8
64km/hr - 1.5m	-18.6	19.8	-16.2	-21.2	702	605	15.2	63.5	39.1	117.2
64km/hr - 1.2m	-20.3	20.7	-17.9	-21.7	789	647	16.8	65.6	49.8	146.8
48km/hr - 1.8m	-12.8	-11.1	-12	-18.3	413	497	13.7	45.4	33.5	93.6
48km/hr - 1.5m	-12.8	-11.56	-12.1	-18.7	428	511	13.8	46.2	30.4	83.6
48km/hr - 1.2m	-12.6	-11.2	-11.9	-18.6	413	494	14.2	45.3	33.2	95.07
40km/hr - 1.8m	-9.9	-7.4	-10.1	-11.6	372	352	10.7	36.6	9.7	27.1
40km/hr - 1.5m	-10.1	8.9	-10.6	-13	391	336	10.5	35	9.6	27.4
40km/hr - 1.2m	-10.7	-7.4	-12.1	-12.8	339	341	13.4	38.6	5.7	16.9

	STEEL POLE			ALUMINIUM POLE		
Vel. - Thickness	M.I.E.	T.0.V	T.M.H.X.	M.I.E.	T.0.V	T.M.H.X.
64 km/hr - 1.8m	60.2	N/A-2.1mps	68	74	N/A-5.0mps	92
64 km/hr - 1.5m	60.7	N/A-1.9mps	72	74.4	N/A-5.0mps	76
64 km/hr - 1.2m	61.7	N/A-2.3mps	83	74.9	N/A-5.0mps	75
48km/hr - 1.8m	18.8	N/A-.7mps	90	36.3	N/A-4.0mps	70
48km/hr - 1.5m	19.3	N/A-.9mps	80	36.7	N/A-4.0mps	71
48km/hr - 1.2m	19.5	N/A-.8mps	83	35.7	N/A-4.0mps	70
40km/hr - 1.8m	8.5	N/A-1.1mps	89	20.2	N/A-2.4mps	67
40km/hr - 1.5m	8.7	N/A-1.1mps	83	19.9	N/A-2.5mps	66
40km/hr - 1.2m	9.2	N/A-1.1mps	83	20.3	N/A-2.9mps	77

H.A.- 'X'= Head Acceleration 'X' (g)
H.A. -'Z'= Head Acceleration 'Z' (g)
R.U.N.F= Resu. Upper Neck Force (N)
R.L.N.F= Resu.Lower Neck Force (N)
R.U.N.M= Res.Upper N. Moment (N·m)
R.L.N.M.=Resu.Lower N. Moment (N·m)
HIC 15= Head Injury Criteria 15ms
HIC 36= Head Injury Criteria 36ms
M.I.E= Max.Internal Energy (kJ)
(for Pole and Support System)
T.0.V.= Time of 0 Velocity (ms)
T.M.H.X.= Time of Max H.A.-'X' (ms)

5.8.3 Injury Response Comparison – Soil Support vs. Anchored Steel Base Support

In this section of the thesis the results from the soil and anchored bolts systems are compared in terms of injury response and pole support conditions. For the soil condition in comparison, the 1.5 m embedment depth steel pole 5.05 mm thick for a sandy soil is presented as the representative system. For comparison and evaluation purpose, the 4.80 mm aluminum pole from the anchored bolts base system is also chosen to represent the most favorable occupant injury response scenario. All results of the injury time history injury response for the above scenarios in comparison are presented in the Appendix section of this thesis.

The results in comparison are summarized in Table 5.12 and indicate that the anchored bolts support condition provided a more desirable system in terms of occupant safety. In terms of critical injury parameters, and the overall performance, the aluminum pole anchored base system offers a more favorable occupant injury response. The maximum HIC36 values for the 64 and 48 km/hr impact speeds are recorder as 143 and 194.7, respectively, for the anchored base as opposed to 410.4 and 214.3 g's recorded for the sandy soil condition. Only lower neck values were recorded above their respected limits for both the anchored base and soil-pole systems. Generally, the lower neck injury criterion was observed to be higher in most scenarios performed in this thesis, including the sled tests and the finite element analysis taken during the validation stages for the 3-year-old child dummy model.

Figure 5.18 presents the energy absorbed for the anchored bolts system for the aluminum pole in comparison to the embedded pole for a 1.5 m sandy soil support condition. From this figure, one can observe that the internal energy of the system for the sandy soil condition is quite unique and is related to the impact velocity of the vehicle. For the 64 km/hr velocity, the internal energy is quite high and absorbs approximately 60.7 kJ of internal energy as compared to the 32.7 kJ absorbed by the anchored bolts system. For the 48 and 40 km/hr scenarios, the absorbed energy reduces significantly down to 21.5 and 16.7kJ, respectively. This dramatic increase in internal energy absorption and subsequent increase in the occupant injury response is related to the stiffness characteristics of the springs and the subsequent increase in their value as the pole deflects through the soil during an impact. For the lower velocity speeds, namely the 48 and 40 km/hr, the balance of impact energy is more defined and does not increase with such a high rate as compared with the 64 km/hr velocity, Figures 5.19 and 5.20. From Figure 5.20, one can observe that at speeds lower than 64 km/hr, the kinetic energy reaches its peak at a later time and the curve characteristic has a more defined shape. The energy does not experience such violent and sudden transitions in shape throughout the time history graph, and the lines appear to be smoother in shape. The combination between the kinetic and internal energy indicates that the occupant experiences less violent forces as the vehicle undergoes through various transition stages of energy transfer involved during a vehicle collision. The slope of the internal and kinetic energy for the 64 km/hr pole system is much steeper and greater in value compared to the values recorded at lower speeds.

To further understand the difference in performance between the velocity variations considered for the sandy soil condition, one must consider the deformation vs. time history in Figure 5.21, and note that vehicle deforms to a greater degree for the 64 km/hr run. This increase in lateral pole displacement continues to increase until the lateral resistance of the soil is increased to the point where the resistance is much greater than the resistance provided by the soil during lower velocity speeds, and the vehicle is brought to rest at a more violent rate, which was also described in the previous paragraph of this section. This in turn means that when the vehicle actually starts to slow down, it will slow down at a much greater rate causing the HIC values and the occupant injury response to increase dramatically as is shown in Table 5.12. This observation is exactly in agreement with Chapter 4 of this thesis, which states, "*In graphical terms, HIC is related to the quantity $\Delta V/\Delta t$ that represents the slope curve on a velocity time history graph. As a general rule of thumb, larger slopes will result in larger values of the HIC.*" Figure 5.22 clearly indicates that on average, the 64 km/hr impact speed has a much greater slope in terms of the velocity time history graph as compared to the lower velocity speeds, which was expected.

Referring to the time history graphs for the head acceleration values in the 'X' direction, Figures 5.23 and 5.24, the anchored base support condition had a more gradual increase to its maximum value compared with the sandy soil condition that took on a much steeper slope for the 48 km/hr impact speed. The other defining characteristic between the curves is the duration of maximum loading, which is clearly greater for the sandy soil condition as opposed to the anchored system shown in Figures 5.25 and 5.26. For the 64

km/hr simulation, the shearing effect of the anchored bolts can be observed from the time lag in maximum values compared with the 48 km/hr velocity, Figure 5.24.

To summarize the paragraphs presented above, the sandy soil is a less desirable system because the time history graphs have a greater increase in value over time, a higher occupant injury response, and a longer time of duration for the maximum occupant response compared to the anchored base system.

Figures 5.27 and 5.28 schematically compare the two support types described above in terms of child occupant response, and the following patterns can be observed:

- For the first 92 ms of the simulation both support types exhibited similar limb deflections and extensions.
- During 120 ms of impact the anchored base support condition exhibits greater child limb extension and deflection, as compared to the sandy soil condition. The child occupant starts to travel in the negative 'X' direction for the anchored base support and the head extends further down as opposed to the sandy soil condition. The extensions for the sandy soil condition are further up in the 'Z' direction as opposed to straight out since the vehicle starts to ride up the pole while it deflects through the soil.
- At 150 ms of impact, the strength of the 'g' force is not as extreme for the anchored base simulation and the majority of the limb extension is attributed to

the fact that the vehicle is bouncing back from the impact. The head is not as extended as compared with the 120 ms point in time. For the sandy soil condition the 'g' force is still active as the vehicle continues to slow down and the limbs are even further extended in the 'Z' direction. This pattern clearly represents the longer time duration of injury exposure observed from the time history graphs outlined in the previous paragraphs of this section.

The schematic representation of the child dummy during the impact further reinforces previously made observations, and clearly illustrates that the injury response will increase the longer the occupants are exposed to extreme forces. Normally, the head can sustain high accelerations if the loading is relatively short and lesser accelerations if the time duration is relatively long which was outlined in chapter 4 of this thesis, and is illustrated in the results and schematic figures presented in this chapter.

The major advantage of the anchored bolts base system compared to the soil embedment support system is that the interaction between the strain and stress exhibited between the anchor bolts, pole, support, and the vehicle is just right. The vehicles occupants experience relatively high forces just for a fraction of the time, which in turn represents a desirable occupant response in terms of injury during the vehicle impact. On the contrary, the sandy soil condition creates greater deflection for the pole structure during the impact, which in return creates extended time duration of critical forces, as the vehicle takes longer to slow down. This pattern influences the injury potential of the

child dummy occupant and creates a less favourable response as compared to the anchored base system scenario.

Table 5.12 Maximum values from time history results – Sand (Steel) vs. Anchored bolts (Aluminum Pole) comparison

Sand vs. Anchored Bolts Comparison Table										
Description	H.A.- 'X'	H.A. -'Z'	C.A. -'X'	C.A.-'Z'	R.U.N.F.	R.L.N.F.	R.U.N.M	R.L.N.M.	HIC 15	HIC 36
Limitation			55	55	2120	2120	27	68	570	570
Sled Test.	-34	45	-63	-39	1300	1300	35	104	175	324
SANDY SOIL - STEEL POLE – 5.05mm										
64 km/hr - 1.5m	-29.7	36.4	-27.4	-31	1188	1029	22.8	98.8	137.2	410.4
48km/hr - 1.5m	-21.1	29.2	-25.3	-21.9	892	866	22.1	71.4	71.9	214.3
40km/hr - 1.5m	-16.9	17.1	-18.9	-13.2	617	611	17.6	64.7	25.8	77.13
ANCHORED BASE – ALUMINUM POLE – 4.80mm										
64km/hr	-22.2	28.1	-22	-23.4	767	820	23.1	69.8	48.8	143
48km/hr	-29.1	27.3	-26.5	-31.5	930	810	29.9	111.3	67.3	194.7
40km/hr	-23.4	15.2	-22.9	-15.9	672	540	23.3	76.6	33.5	98.1

	STEEL POLE			ANCHORED BASE – AL. POLE		
Velocity	M.I.E.	T.0.V	T.M.H.X.	M.I.E.	T.0.V	T.M.H.X.
64 km/hr -	60.7	N/A-1.9mps	72	32.7	N/A	70
48km/hr -	19.3	N/A-.9mps	80	21.5	110	112
40km/hr -	8.7	N/A-1.1mps	83	16.7	118	120

H.A.- 'X'= Head Acceleration 'X' (g)
H.A. -'Z'= Head Acceleration 'Z' (g)
R.U.N.F= Resu. Upper Neck Force (N)
R.L.N.F= Resu.Lower Neck Force (N)
R.U.N.M= Res.Upper N. Moment (N·m)
R.L.N.M.=Resu.Lower N. Moment (N·m)
HIC 15= Head Injury Criteria 15ms
HIC 36= Head Injury Criteria 36ms
M.I.E= Max.Internal Energy (kJ)
(for Pole and Support System)
T.0.V.= Time of 0 Velocity (ms)
T.M.H.X.= Time of Max H.A.-'X' (ms)

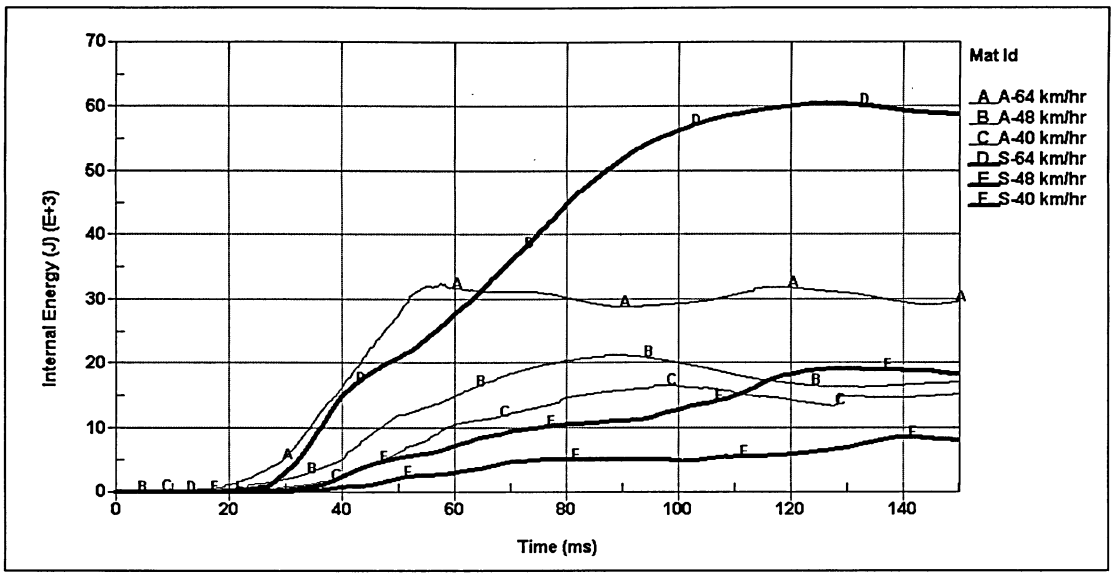

Figure 5.18 Internal energy comparison – Anchored base aluminium pole system 4.80 mm (light lines) vs. Steel pole 5.05 mm embedded in 1.5 m of sand (solid lines)

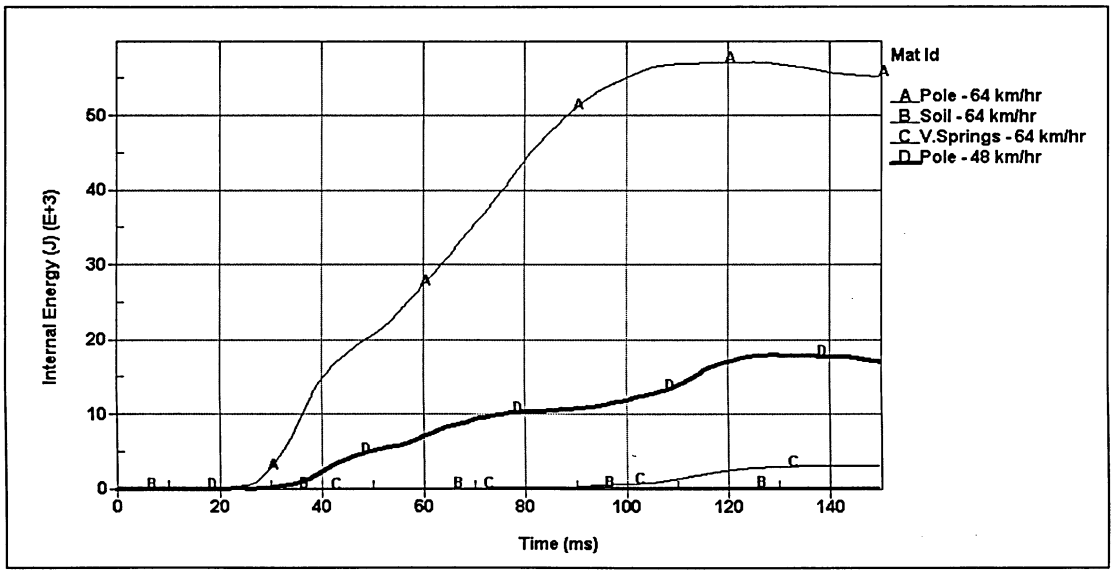

Figure 5.19 Internal energies for sandy soil 1.5 m – 5.05 mm steel pole – 64 km/hr (light lines) and 48 km/hr (solid lines)

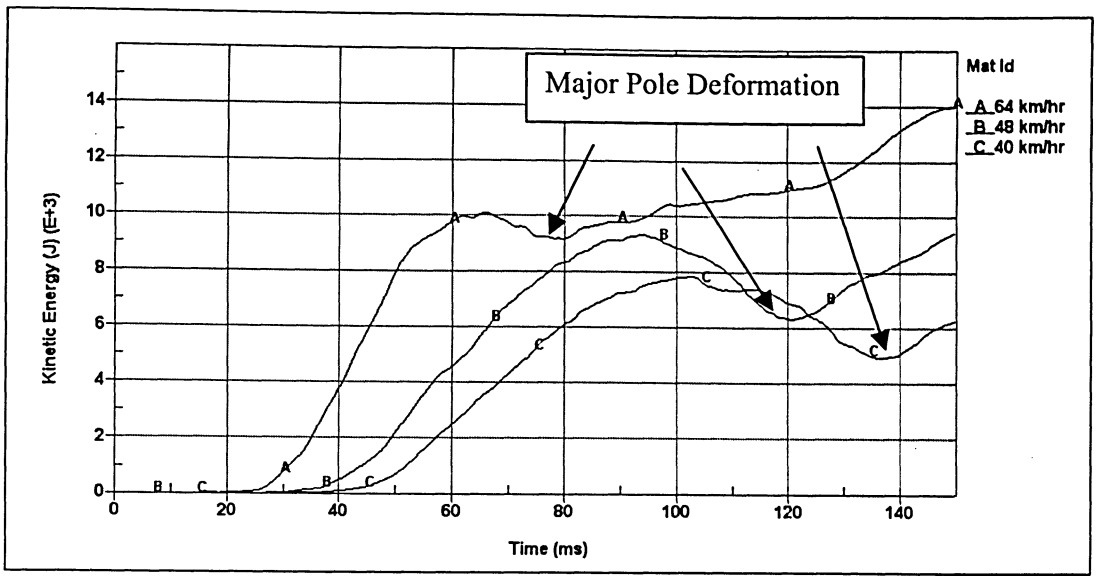

Figure 5.20 Kinetic energies comparison for sandy soil 1.5 m – Steel pole 5.05 mm shell thickness

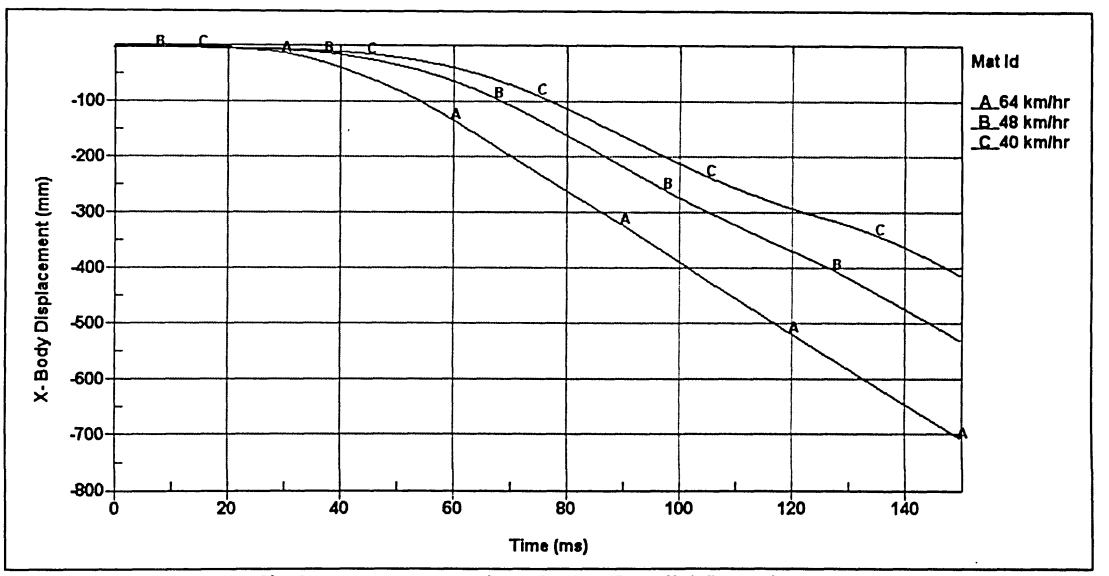

Figure 5.21 X-Body displacement comparison for sandy soil 1.5m pole support system – Steel pole 5.05 mm shell thickness

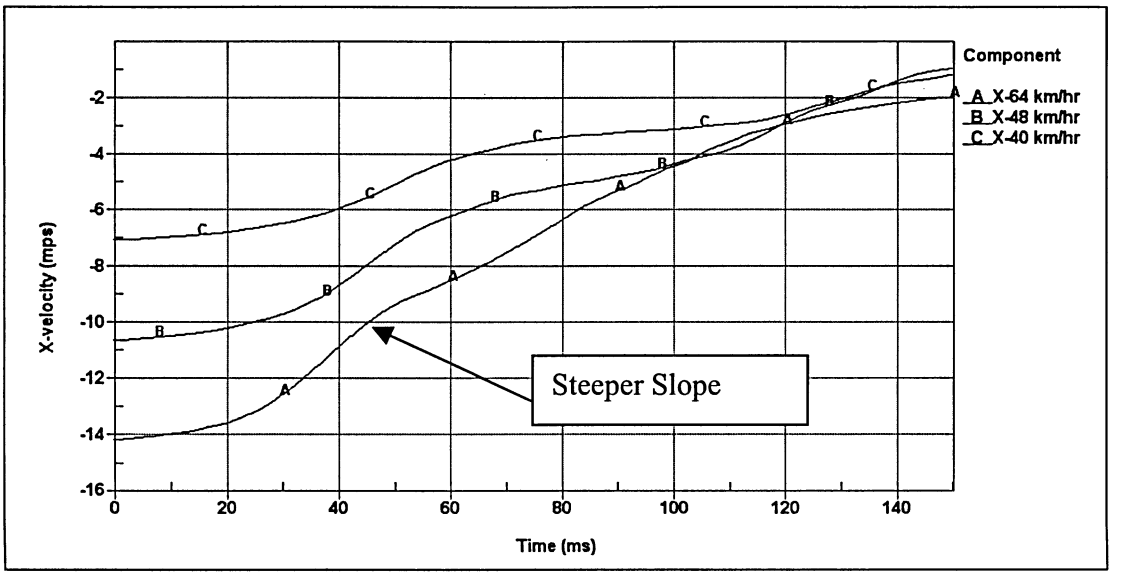

Figure 5.22 Velocity comparison for sandy soil 1.5 m pole support system – Steel pole 5.05 mm shell thickness

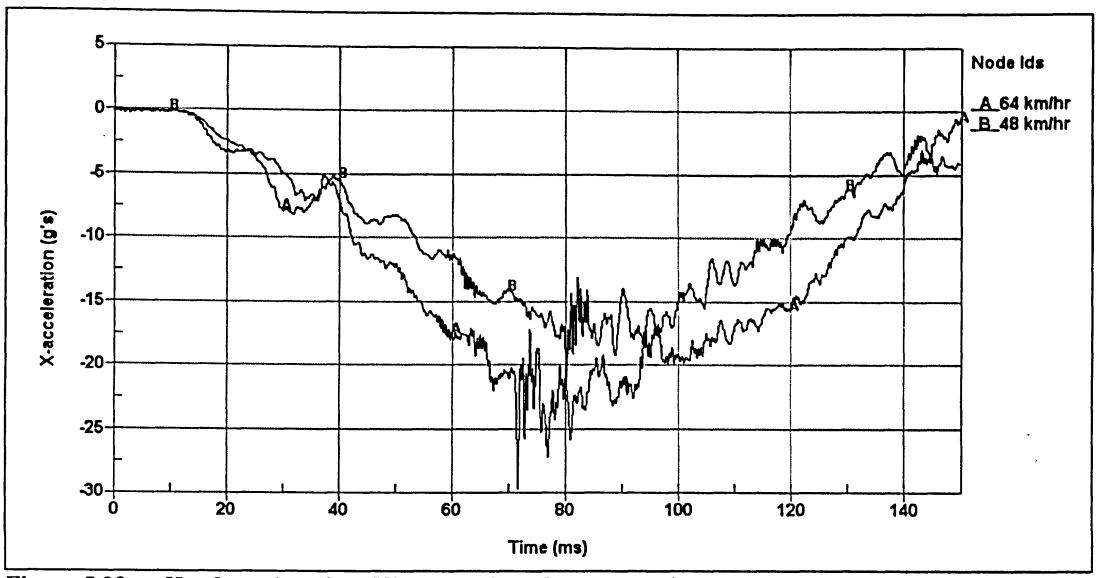

Figure 5.23 Head acceleration 'X' comparison for sandy soil 1.5m pole support system – Steel pole 5.05 mm shell thickness

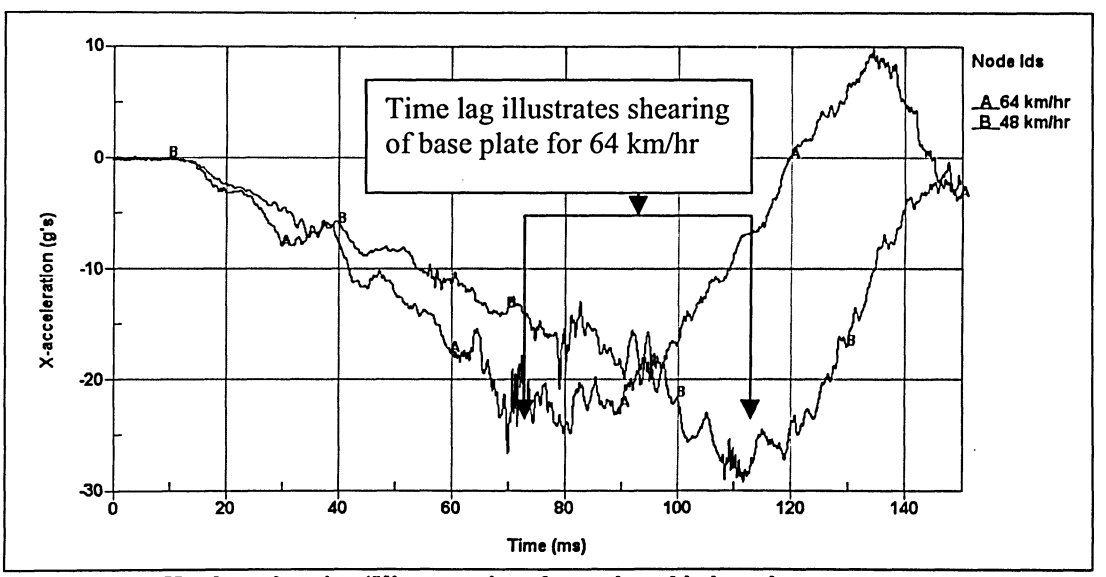

Figure 5.24 Head acceleration 'X' comparison for anchored bolts pole support system – Aluminum pole 4.80 mm shell thickness

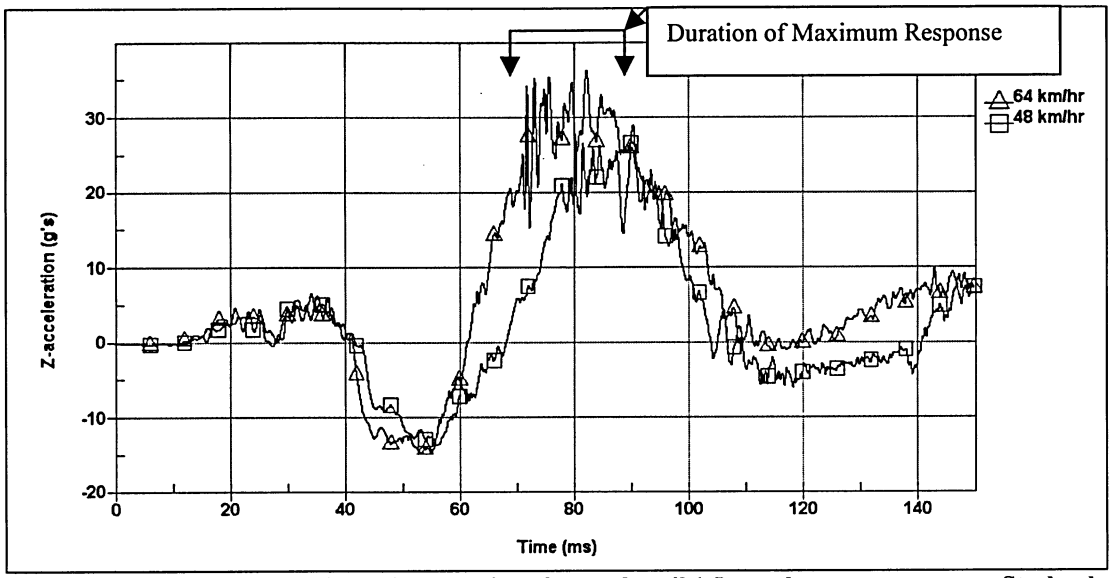

Figure 5.25 Head acceleration 'Z' comparison for sandy soil 1.5 m pole support system – Steel pole 5.05 mm shell thickness

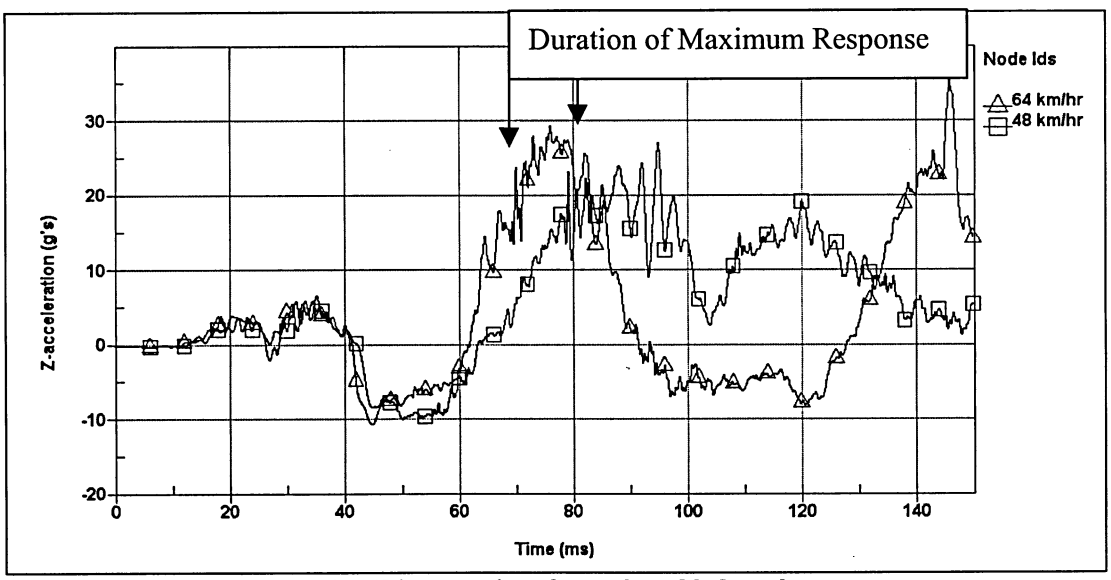

Figure 5.26 Head acceleration 'Z' comparison for anchored bolts pole support system – Aluminum pole 4.80 mm shell thickness

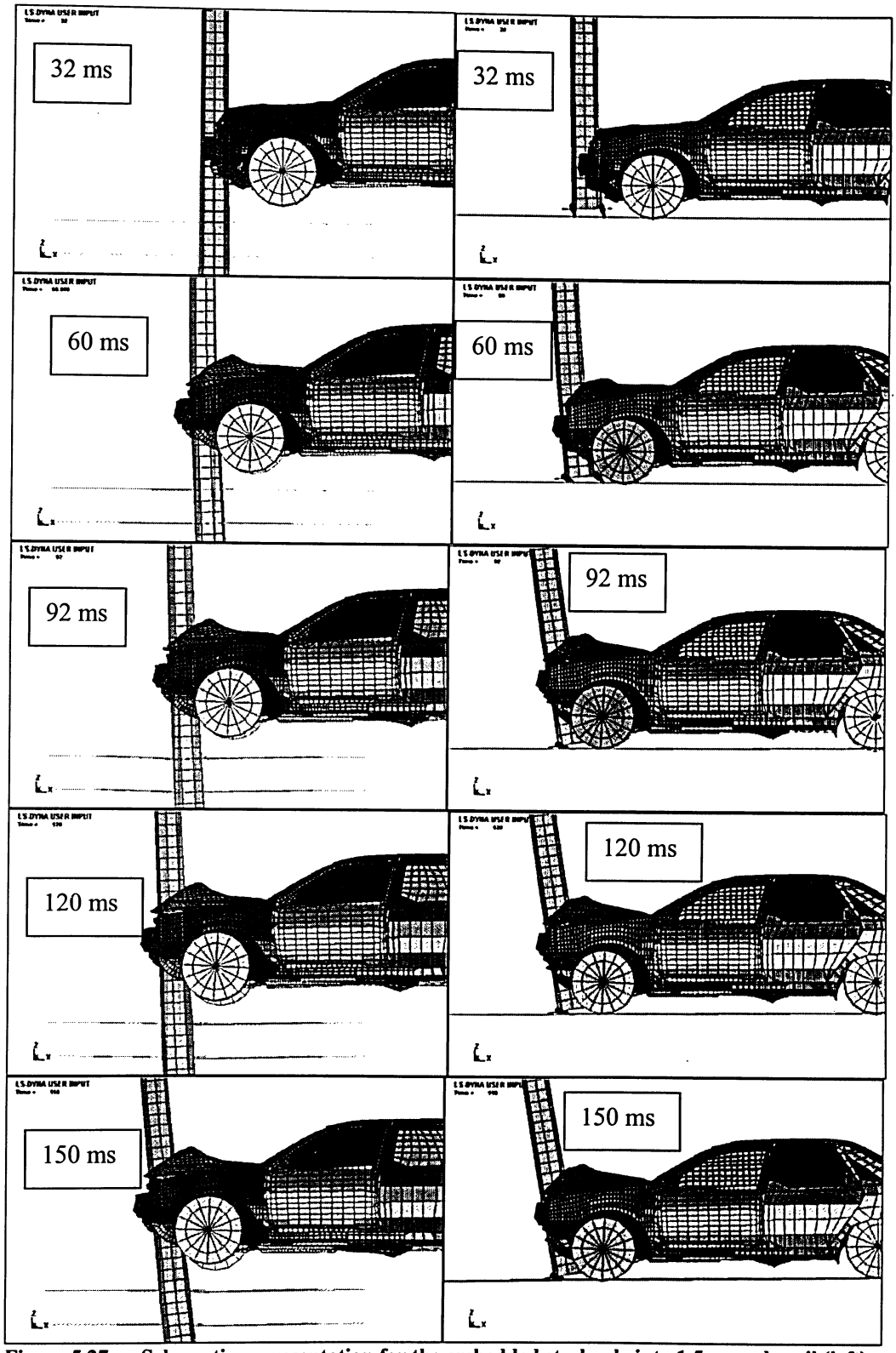

Figure 5.27 Schematic representation for the embedded steel pole into 1.5m sandy soil (left) vs. anchored base plate aluminium pole support system (right) for 48 km/hr impact speed

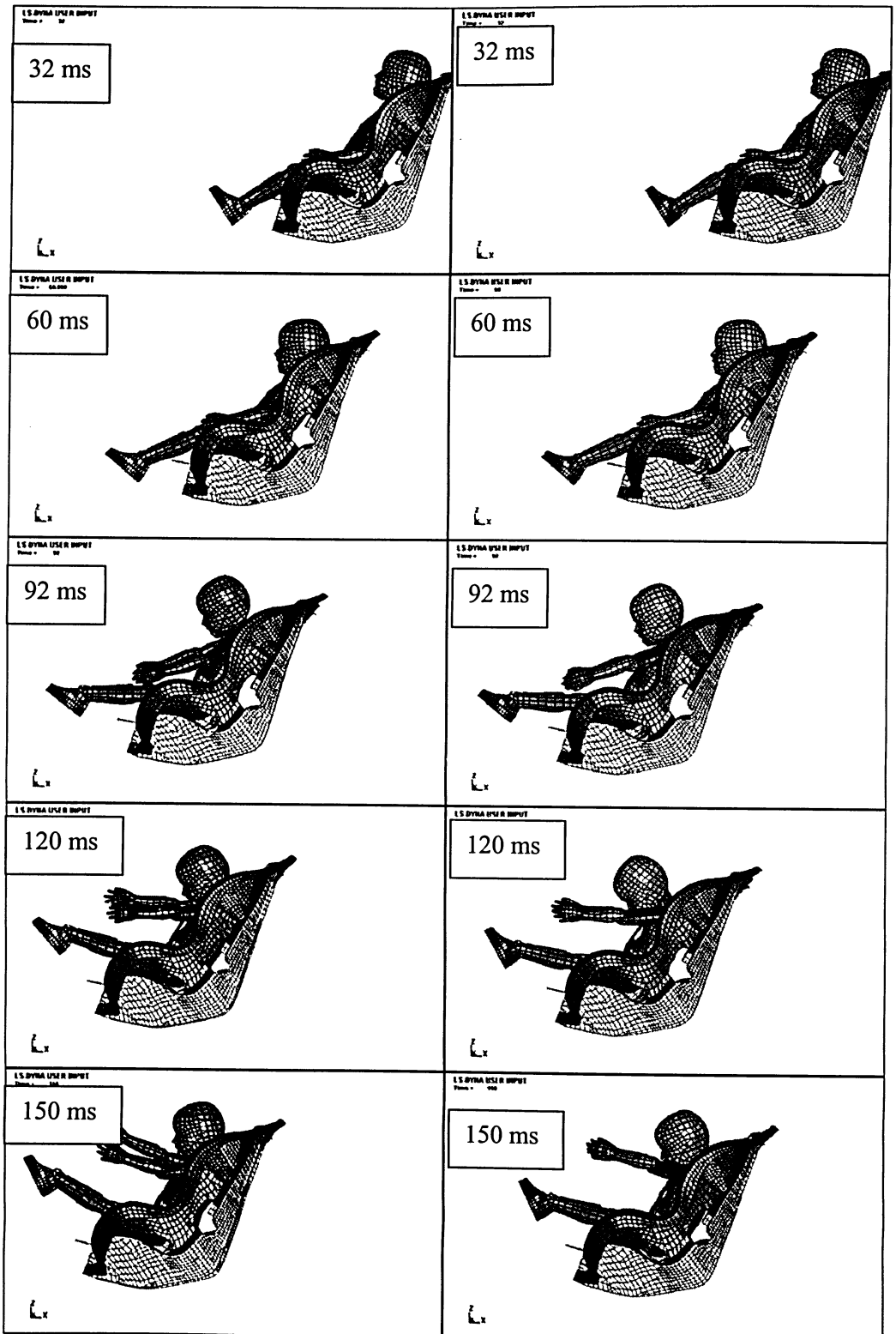

Figure 5.28 Schematic representation of the child dummy during Impact – Embedded steel pole 1.5 m sandy soil (left) vs. Anchored base plate aluminium pole (right) for 48 km/hr impact speed

5.9 Summary of Findings

Each of the design simulations presented above have their defining characteristics that help aid in the understanding of the vast complexity involved during a vehicle collision. The critical patterns observed help to further understand the potential improvements to the existing systems for traffic infrastructure. The material properties involved during the design stages are considered crucial in terms of effectiveness for each scenario considered with respect to crashworthiness. From the results presented in this chapter, especially from the results presented in the last section, the patterns observed clearly illustrate the importance of the stress/strain relationship of a material type. Clearly, the effectiveness of each system depended on the total stress/strain characteristic of each design with respect to the support conditions considered.

The aluminum pole offered a more favorable response in terms of overall effectiveness because it offered more favorable strain against the applied stress compared to the steel pole. The rubber base pole system had the lowest Young's modulus as per Table 5.13, and offered high strains under applied stresses. However, this high yield strain resulted in thick sections during design to effectively stay upright under minor collisions, and to remain effective during service loading, and increased the child dummy injury response.

Table 5.13 - Material properties considered for this study

	Steel	Aluminium	Rubber
Density: ρ = kN/m^3	78.3	27	10.63
Young's Modulus: E = GPa	207	69	2.46
Yield Stress: σ = MPa	215	240	24.7
Poisson's Ratio: υ =	0.28	0.33	0.323

The effect of impact velocity and support type is interrelated, and needs to be further examined on a case-by-case basis. In terms of the most desirable occupant response based on the finite element analysis presented in this thesis, the anchored shear base type of a pole support system is recommended as being the effective crashworthy system in suburban areas where damage to the surrounding area is minimized. However, in cases where damage to the surrounding environment is crucial, support conditions need to be carefully designed to reflect the respected surrounding site conditions. The soil support system would be recommended in such circumstances, such as critical urban areas where damage to the surrounding environment needs to be minimized. The soil support can be masked with the use of flowerbeds and/or sodded islands, which would work together with the desired ambiance, and yet will remain crashworthy for the posted speeds.

CHAPTER 6

CONCLUSIONS AND RECOMMENDATIONS

6.1 General

Statistics indicate that child restraint systems (CRS) need to be combined with other mechanisms to increase their effectiveness during vehicle collisions. Currently, resources are being invested towards designing energy absorbing mechanisms that will absorb the kinetic energy more effectively during a vehicle collision, and will thus minimize the injury potential. The main objective of the enclosed research focused on minimizing child injuries experienced during frontal vehicle to barrier collision by improving the safety and energy absorption of laminar traffic poles. By using the available finite element models, the crash scenario was reconstructed in order to effectively analyze and further understand that various parameters affecting injury development. The main goal of this thesis was to understand what could be done to minimize injury and/or lessen the severity during a vehicle collision with a traffic pole involving a child occupant.

6.2 Conclusion

In conclusion, based on current finite element analysis, the anchored base support system proved to be effective in terms of crashworthiness for a child dummy compared to all other system analyzed in this thesis. The embedded pole/soil system also provided

desirable crashworthy results, however, the effectiveness is questionable since the soil properties are vastly simplified with the use of vertical and horizontal springs.

Based on the current finite element analysis the following recommendations can be made in terms of designing crashworthy traffic pole structures:

- Avoid highly non-deformable objects such as trees and rigid traffic poles. It is recommended to mandate traffic protection devices in all areas with poor energy absorbing characteristics that resemble non-deformable objects. If such traffic protection structures are not available due to site conditions, the posted speeds shall not be greater than 40 km/hr for these sections of the road.
- Overall, the aluminum pole material is a more desirable option in terms of occupant injury response during a vehicle impact since the pole has greater flexibility and balances the crash impulse to a greater degree with its strain energy.
- The stress strain relationship plays a crucial role during a vehicle impact. The material properties of a particular pole type need to be designed in order to effectively absorb the impact energy by balancing the kinetic energy of the crash against the materials strain and internal energies.
- It becomes beneficial to extend the time to reach the maximum injury criteria and to extend the time to completely stop a vehicle. However, one must be careful not to expose to occupants to prolonged injury response in terms of time duration, and especially during the maximum response values.

- Each collision needs to be studied on a case-by-case basis since the impact scenario is a highly complex mechanism.
- Very flexible elastic material types should be avoided because such materials do not absorb the impact energy well and cause greater internal vehicle damage.

It is also important to note that the finite element analysis currently employed to study crashworthiness based on a 3-year-old child dummy are only approximate in form. The results need to be validated using field tests to verify their accuracy. Based on the analysis and results from this study, recommendations should be used from this report as guidelines only.

6.3 Recommendations for Future Research

Based on the research conducted in this thesis, the following points are recommended for further investigation:

- The 3-year old child dummy model used in future research should be further designed and validated for finite element analysis in all directions of the impact scenario.
- More advanced techniques are recommended in the finite element modeling of the soil in order to account for the diversity and vastness of the soil properties.

- More complex finite element models of the vehicle should be considered in future studies as the computational power becomes more advanced and available in order to improve the accuracy of the results.
- Outdated existing traffic infrastructure that might pose a high risk to motorists such as wooden poles and fixed steel structures should be analyzed using appropriate methods in order to evaluate their in-service performance.
- It is recommended that the results presented above need to be validated using field testing procedures in order to effectively develop vehicle and human occupant models that will respond accurately for all deigns considerations, all impact scenarios, and will represent the vast majority of the population exposed to hazards.
- Currently, finite element models are being developed to represent the human tissues, including muscles, organs and bone matter. These models are being developed in order to study the occupant safety and are recommended for future crashworthiness research once these models become validated for use.

REFERENCES

1. Sachs, M. K., and Tombrello, S. M. "*Car Seat Safety: Buckling Up Isn't Always Enough.*" Gerber Pediatric Basics, Volume 90 (2000), pp. 10-24.
2. National Center for Statistics and Analysis (NCSA), "*Traffic Safety Facts 2000*" DOT HS 809 324, NHTSA, March 2002.
3. Weber, K. "*Rear-Facing Restraint for Small Child Passengers.*" UMTRI Research Review, Volume 24 (1995), pp. 590-593.
4. Fact Monster. Total U.S. Population. January 2003. <http://www.factmonster.com/ipka/A0004997.htm>.
5. CIA – The World Factbook, Canada, January 2003, <http://www.cia.gov/cia/publications/factbook/goes/ca.html>.
6. Turchi, R., Altenhof, W., Kapoor, T. and Howard, A.., "*An investigation into the head and neck injury potential of three-year-old children in forward and rearward facing child safety seats.*" Woodhead Publishing Ltd, IJCrash (2004), Vol. 9, No.4, pp. 419-431.
7. Eppinger, R, Sun, E., and Saul, R., "*Development of Improved Injury Criteria for the Assessment of Advanced Automotive Restraint Systems – II.*" National Highway and Traffic Safety Administration, 1999.
8. Eppinger, R, Sun, E, and Saul, R., "*Supplement: Development of Improved Injury Criteria for the Assessment of Advanced Automotive Restraint Systems – II.*" National Highway and Traffic Safety Administration, 2000.
9. Lesire, P., Gran, R., and Hummel, T., " *The Crest Project Accident Data Base.*" European CREST Project (2002), pp. 347-356.

10. Trosseille, X., "*Child Restraint System for Cars.*" European Commission, Directorate General Research C-RTD, CREST Project SMT4-CT95-2019 (2000).

11. Merriam-Webster Online Dictionary, January 2006, < http://www.m-w.com/dictionary/crashworthiness>.

12. Technical Services – Forensic Engineering, February 2006, <http://www.e-z.net/~ts/crash.htm, FMVSS 213>.

13. FMVSS 213: " *Child Restraint Systems." Federal Motor Vehicle Safety Standards Part 571"*, Standard 213, Washington D.C., 2001.

14. LS-DYNA Version 970 5434a, Livermore Software Technology Corporation (LSTC), January 2005.

15. Sennah, K., Emam, A., Howard, A., and Hale, I., "*Multi-body Dynamic Simulations of Forward Facing Child Occupants Under Varying Crash Pulses*", Proceedings of the Canadian Multidisciplinary Road Safety Conference XIII, Banff, Alberta, June 8-11, 2003.

16. Elmarakbi, A. Sennah, K., "*Evaluation of Fiber Reinforced Polymer (FRP) Traffic Light Pole Involved in Vehicle Collision*". Proceedings of the Canadian Multidisciplinary Road Safety Conference XV, Fredericton, NB, (June 5-8. 2005).

17. Sennah, K., Samaan, E., and Siriya, P., "*Crashworthiness of Motor Vehicle and Luminaire support in Side Impact*", Proceedings of the Canadian Multidisciplinary Road Safety Conference XIII, Banff, Alberta, June 8-11, 2003.

18. CSA International, "Canadain Highway Bridge Design Code of 2000", CSA International, Standards Council of Canada, December 2000.

19. White Sun of the Dessert, August 2006, <www.desertsun.co.uk/blog/?cat=14>.

20. Klinich D.K, Augustem G., Backaitis, S., and Klainberger, M., "*Tehchniques for Developing Child Dummy Protection Reference Values,* Child Injury Protection Team – Event Report, NRD-20, October 1996.

21. Weber, K. "*Rear-Facing Restraint for Small Child Passengers.*" UMTRI Research Review, Volume 24 (1995), pp. 590-593.

22. CREST, "Child Restraint System for Cars" European Commission, Directorate General Research C-RTD, CREST Project SMT4-CT95-2019.

23. Ross, H.E., Sickling, D.L., Zimmer, R.A., and Michie, J.D., "*NCHRP Report 350, Recommended Procedures for Safety Performance Evaluation of Highway Features*, Natioanl Academy Press, 1993.

24. Hallquist, O. J., "*LS-DYNA Theoretical Manual*" Livermore Software Technological Corporation, Livermore CA., May 1998.

25. SAE J 211/1 "*Instrumentation for Impact Test – Part 1 – Electronic Instrumentation, Society of Automotive Engineers*, Warrendale PA., (2003).

26. FMVSS 213: " *Child Restraint Systems." Federal Motor Vehicle Safety Standards Part 571"*, Standard 213, Washington D.C., 2001.

27. LS-DYNA, "*Model of the Hybrid III 3 year old child dummy – version 2.3B2 – Users Manual"*, First Technology Safety Systems, Plymouth MI., 2000.

28. P.A. Du Bois, "*Crashworthiness Engineering Course Notes*", Livermore Software Technology Corporation, (2004).

29. Matlock, H. (1970). "*Correlations for design of laterally loaded piles in soft clay: Preprints, Second Annual Offshore Technology Conference."* Paper No. 1204, 577-588, 1977.

30. Braja M. D., "*Foundation Engineering – Fourth Edition*" Brooks/Cole Publishing, (1999), p. 11.

31. Ray, H. M., "*Evaluation human Risk in side impact collisions with roadside objects.*", Paper No. 00-0520, Transportation Research Board, 79th Annual Meeting, January 9-13, 2000., Washington, D.C., pp. 1-16.

APPENDIX

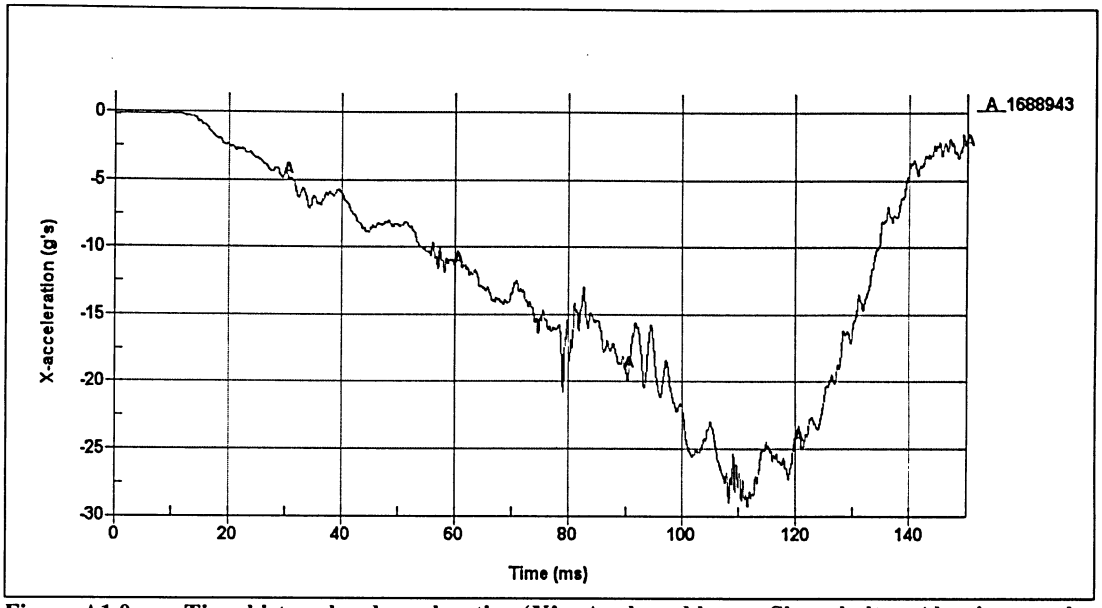

Figure A1.0 Time history head acceleration 'X' – Anchored base – Shear bolts – Aluminum pole 4.80mm – 48 km/hr

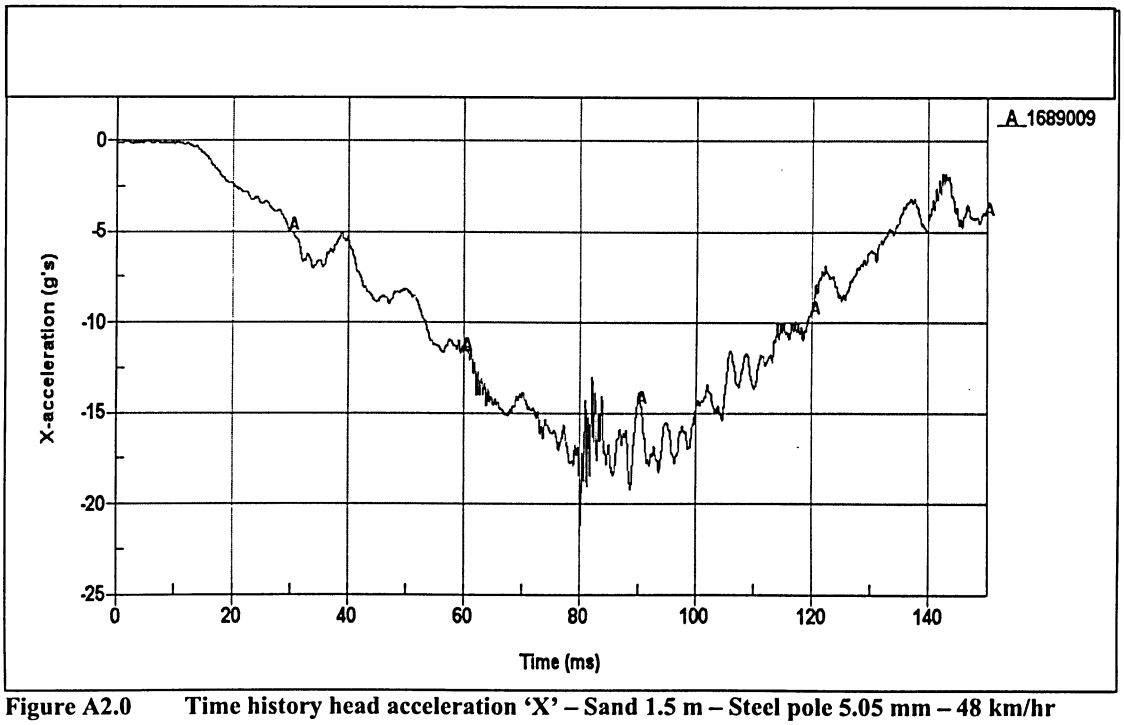

Figure A2.0 Time history head acceleration 'X' – Sand 1.5 m – Steel pole 5.05 mm – 48 km/hr

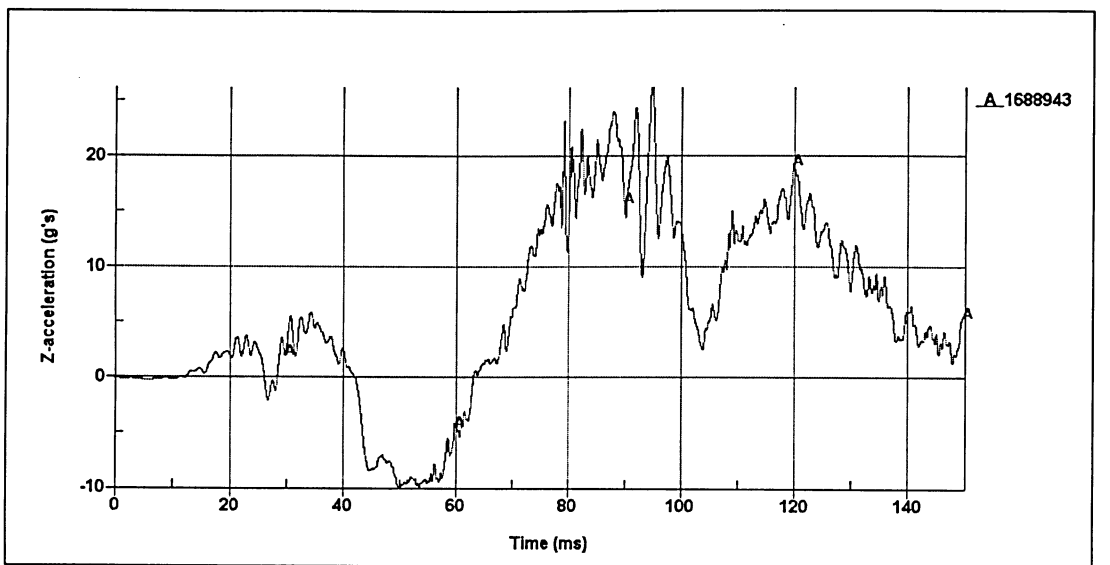

Figure A3.0 Time history head acceleration 'Z' – Anchored base – Shear bolts – Aluminum pole 4.80 mm – 48km/hr

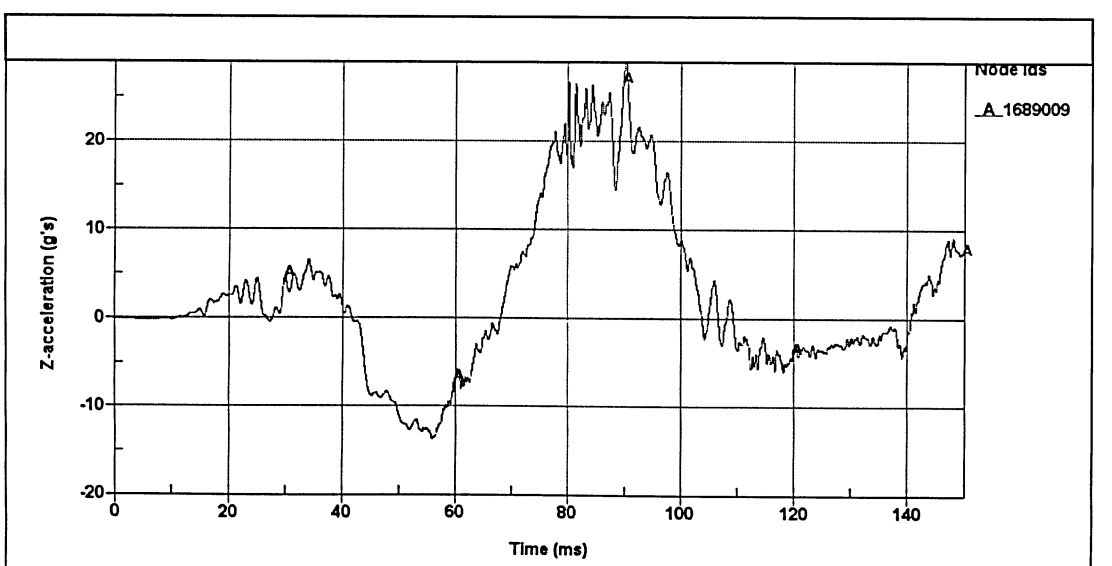

Figure A4.0 Time history head acceleration 'Z' – Sand 1.5 m – Steel pole 5.05 mm – 48 km/hr

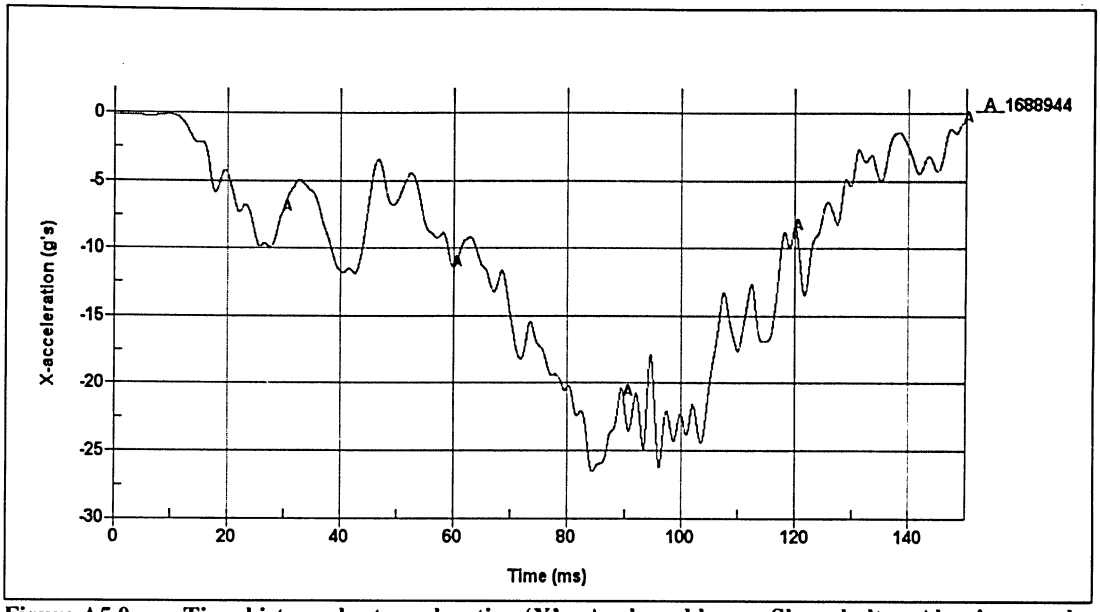

Figure A5.0 Time history chest acceleration 'X' – Anchored base – Shear bolts – Aluminum pole 4.80 mm – 48 km/hr

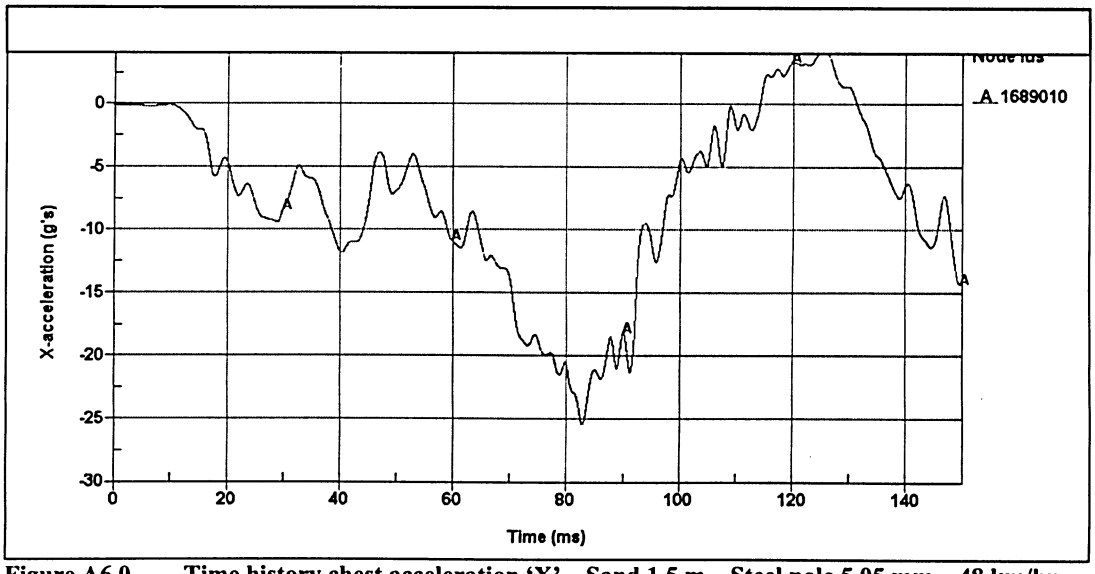

Figure A6.0 Time history chest acceleration 'X' – Sand 1.5 m – Steel pole 5.05 mm – 48 km/hr

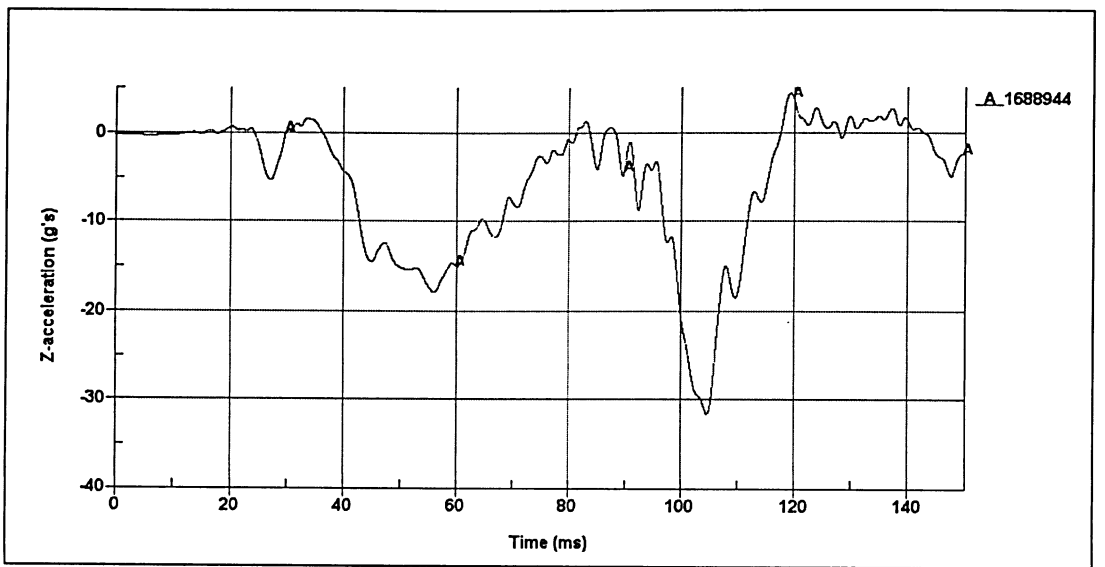

Figure A7.0 Time history chest acceleration 'Z' – Anchored base – Shear bolts – Aluminum pole 4.80 mm – 48 km/hr

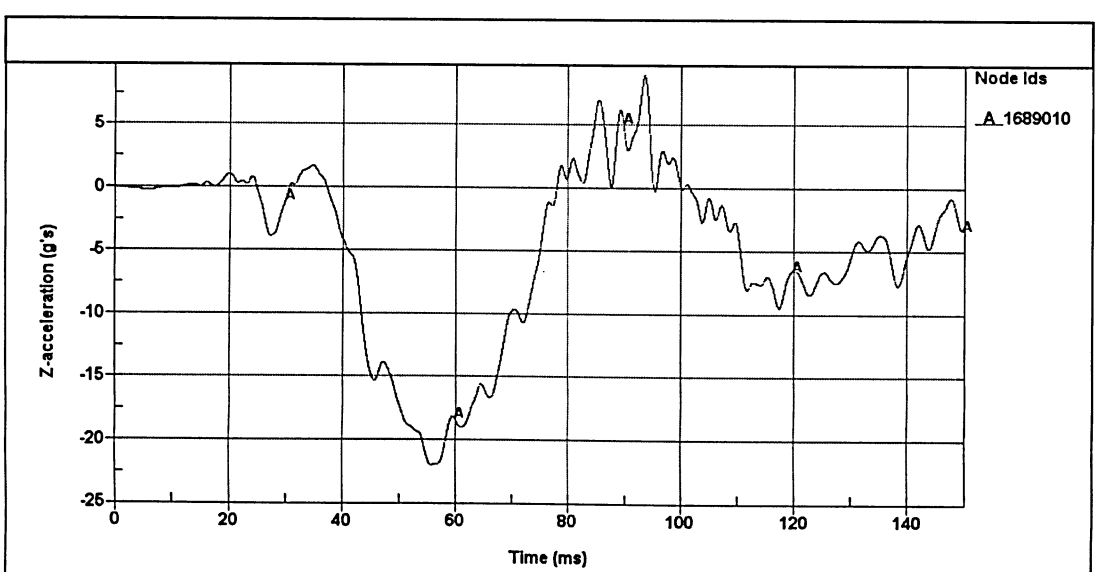

Figure A8.0 Time history chest acceleration 'Z' – Sand 1.5 m – Steel pole 5.05 mm – 48 km/hr

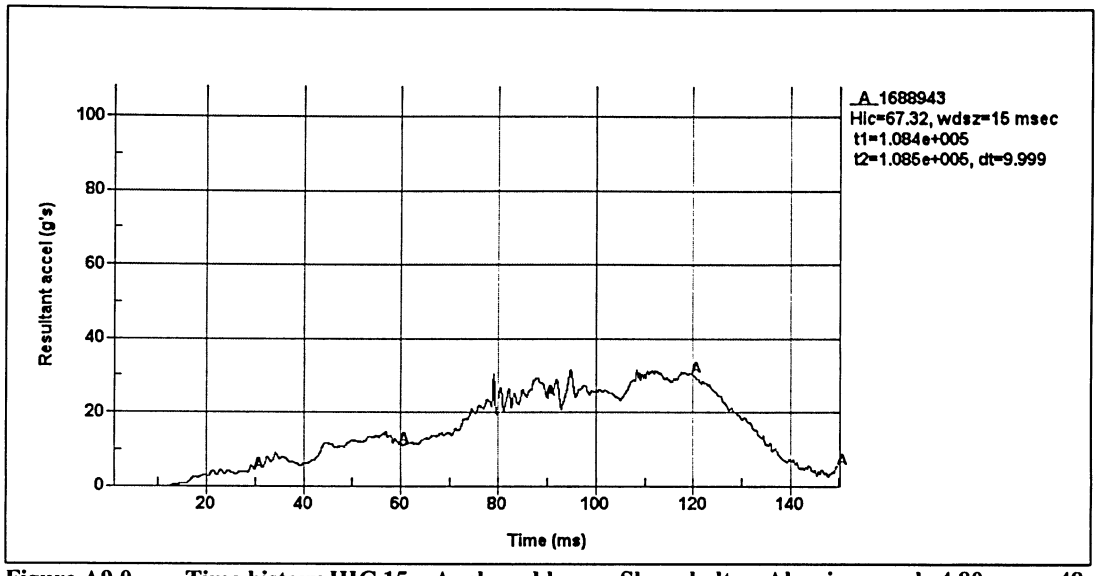

Figure A9.0 Time history HIC 15 – Anchored base – Shear bolts – Aluminum pole 4.80 mm – 48 km/hr

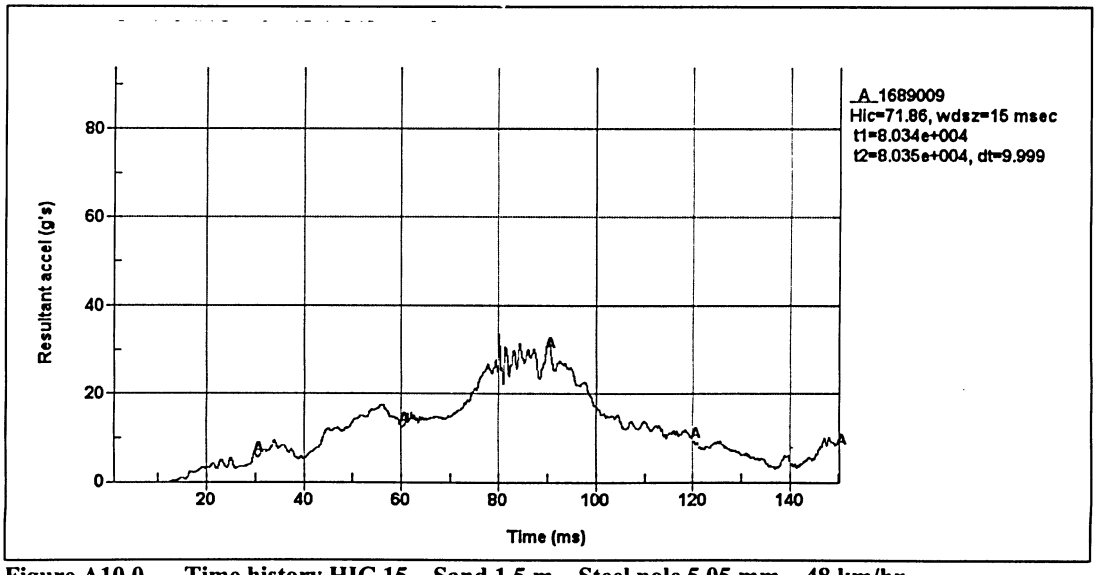

Figure A10.0 Time history HIC 15 – Sand 1.5 m – Steel pole 5.05 mm – 48 km/hr

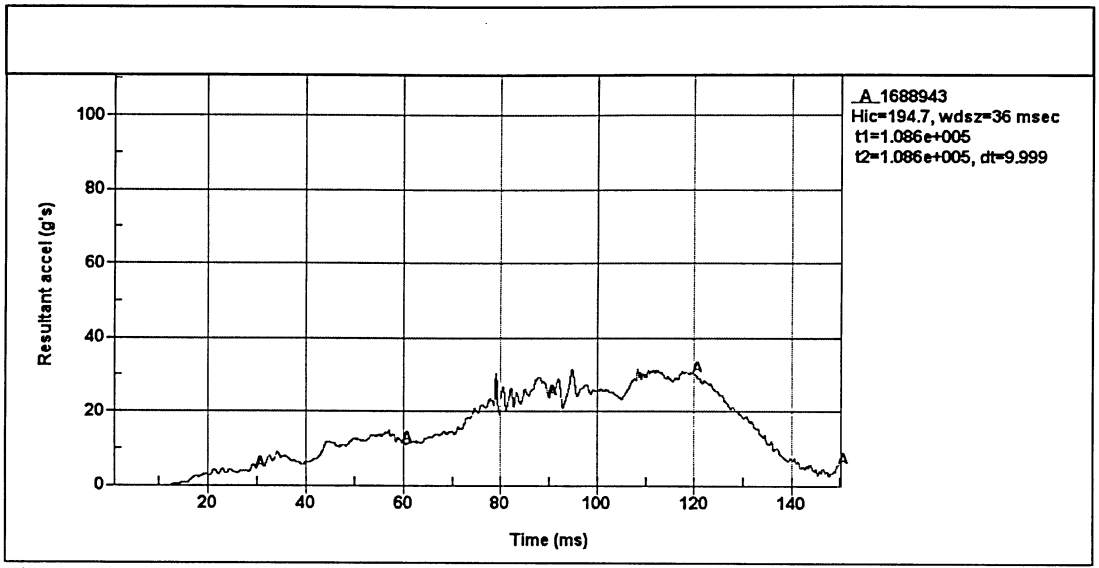

Figure A11.0 Time history HIC 36 – Anchored base – Shear bolts – Aluminum pole 4.80 mm – 48 km/hr

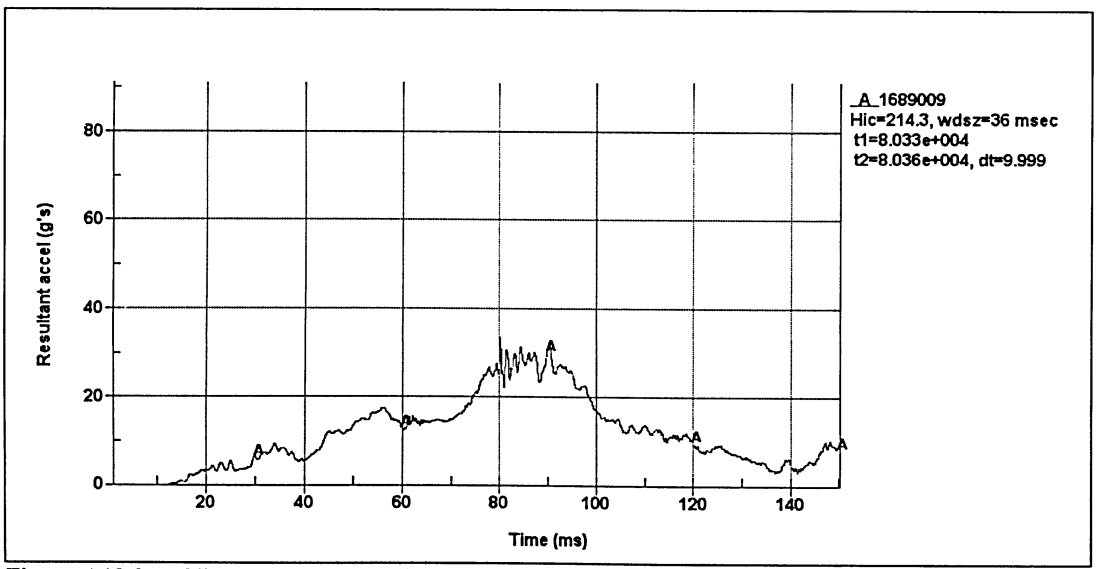

Figure A12.0 Time history HIC 36 – Sand 1.5 m – Steel pole 5.05 mm – 48 km/hr

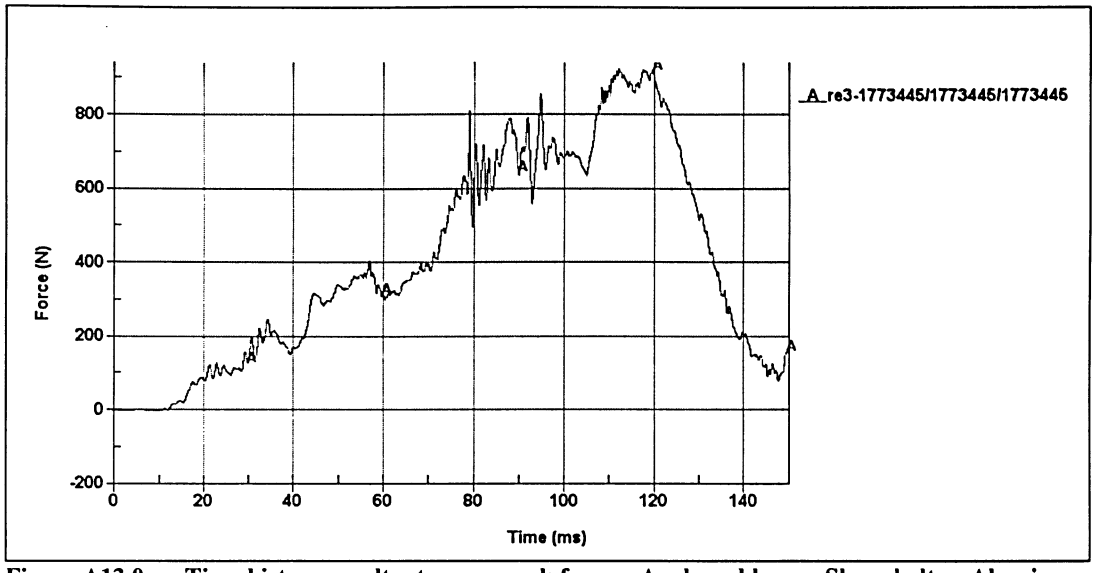

Figure A13.0 Time history resultant upper neck force – Anchored base – Shear bolts – Aluminum pole 4.80 mm – 48 km/hr

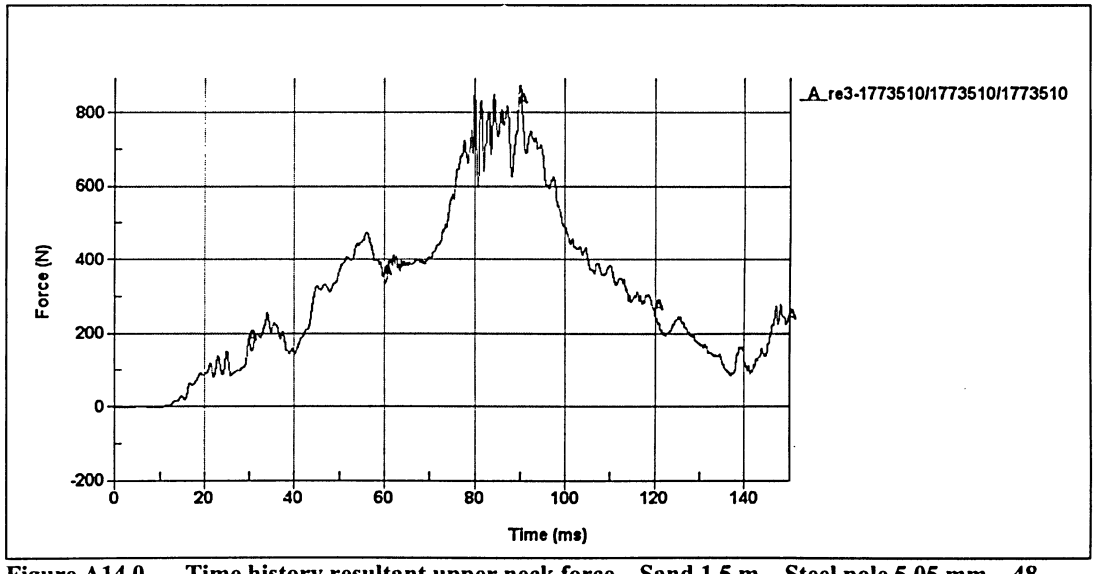

Figure A14.0 Time history resultant upper neck force – Sand 1.5 m – Steel pole 5.05 mm – 48 km/hr

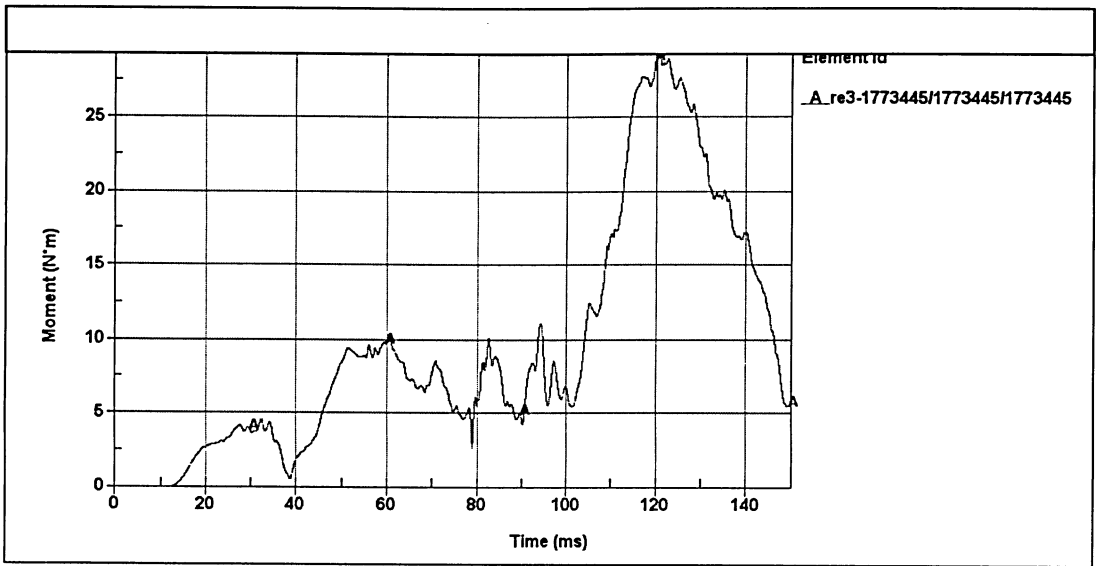

Figure A15.0 Time history resultant upper neck moment – Anchored base – Shear bolts – Aluminum pole 4.80 mm – 48 km/hr

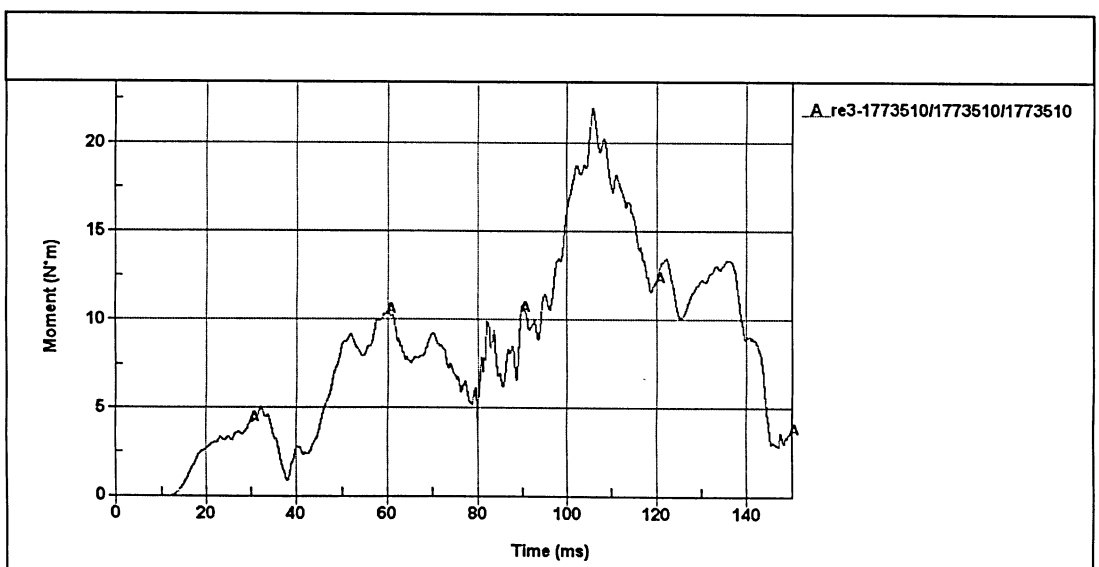

Figure A16.0 Time history resultant upper neck moment – Sand 1.5 m – Steel pole 5.05 mm – 48 km/hr

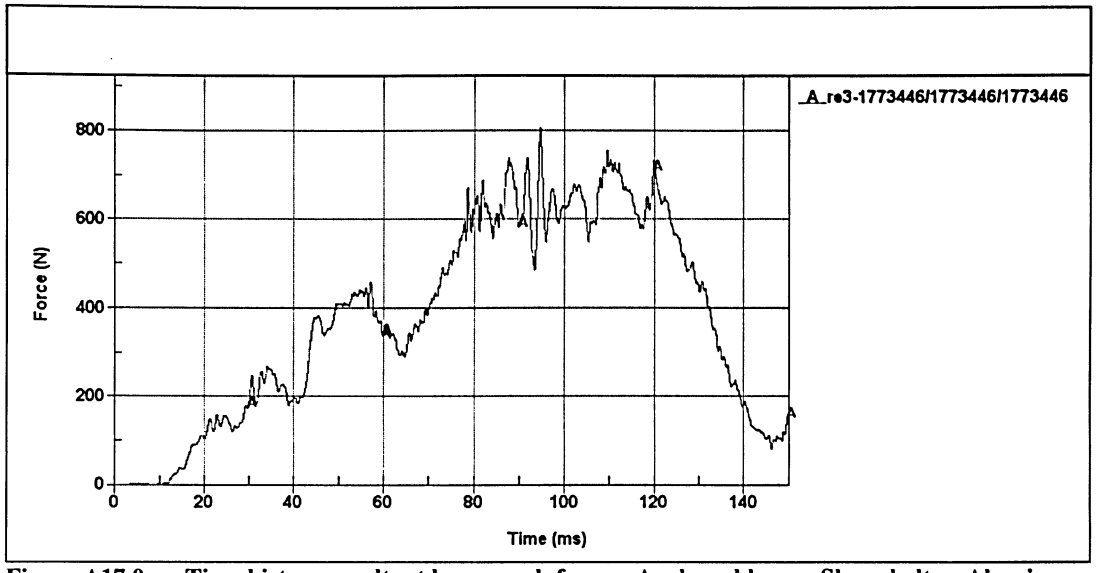

Figure A17.0 Time history resultant lower neck force – Anchored base – Shear bolts – Aluminum pole 4.80 mm – 48 km/hr

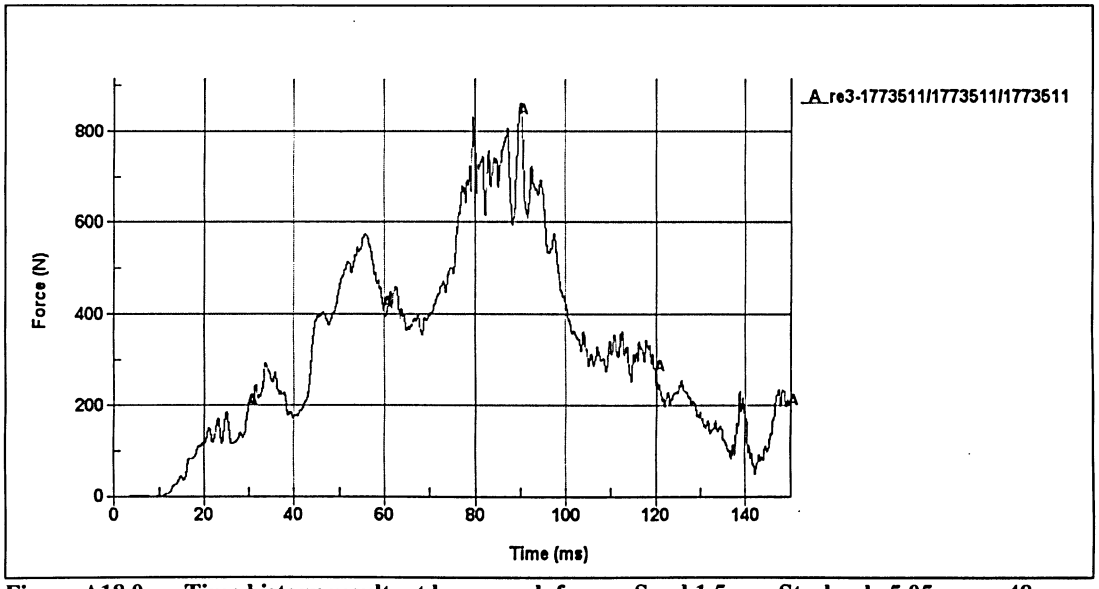

Figure A18.0 Time history resultant lower neck force – Sand 1.5 m – Steel pole 5.05 mm – 48 km/hr

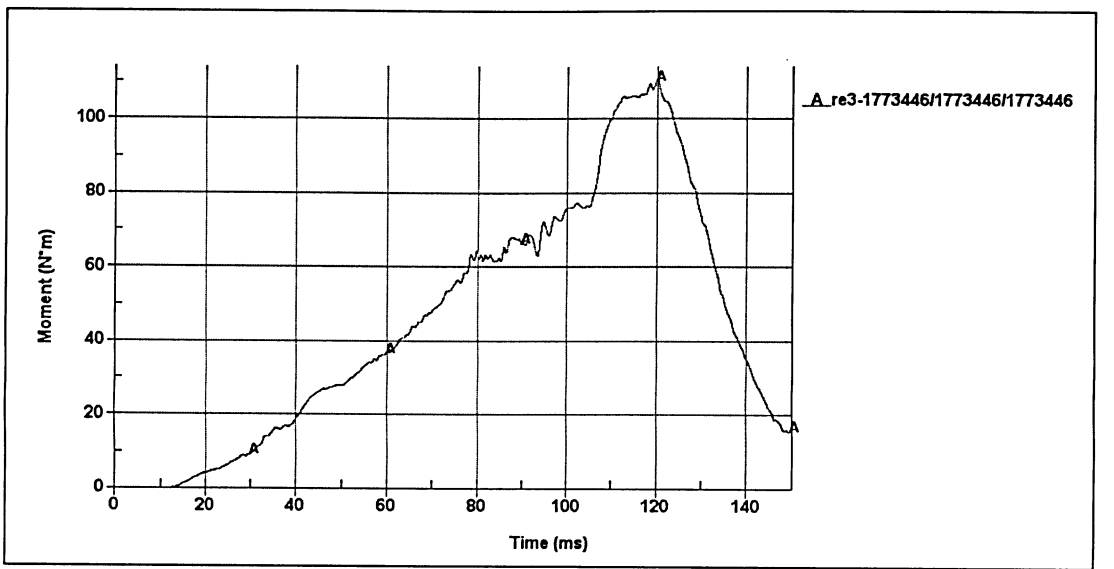

Figure A19.0 Time history resultant lower neck moment – Anchored base – Shear bolts – Aluminum pole 4.80 mm – 48 km/hr

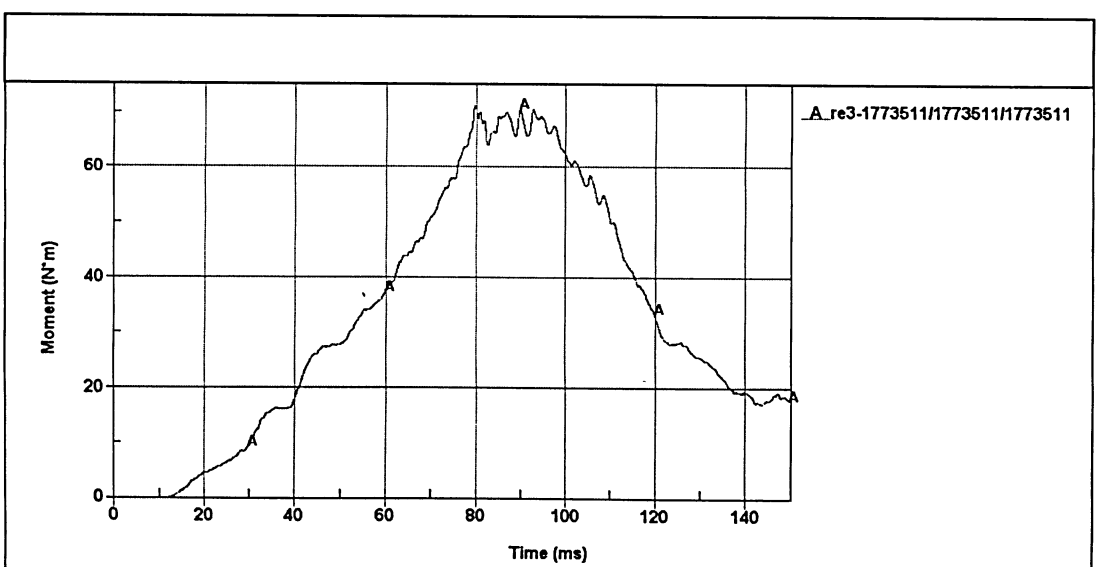

Figure A20.0 Time history resultant lower neck moment – Sand 1.5 m – Steel pole 5.05 mm – 48 km/hr